The Arabidopsis SHORTROOT network coordinates shoot apical meristem development with auxin dependent lateral organ initiation

Authors:

Elmehdi Bahafid[1], Imke Bradtmöller[1], Ann Marlene Thies[1], Thi Thuy Oanh Nicole Nguyen[1], Crisanto Gutierrez[2], Bénédicte Desvoyes[2], Yvonne Stahl[1], Ikram Blilou[3], Rüdiger Simon[1*]

Affiliation:

[1]Institute for Developmental Genetics, Heinrich Heine University, Building 26.14.00.071, 40225 Düsseldorf, Germany

[2]Centro de Biologia Molecular Severo Ochoa, CSIC-UAM, Cantoblanco, Madrid, Spain.

[3]Laboratory of Plant Cell and Developmental Biology, Division of Biological and Environmental Sciences and Engineering, 4700 King Abdullah University of Science and Technology, Ibn Al Haytham Bldg.2, room 3274, Thuwal 23955-6900, Kingdom of Saudi Arabia

*to whom correspondence should be addressed, at ruediger.simon@hhu.de

Author contributions:

Elmehdi Bahafid, Yvonne Stahl, Ikram Blilou and Rüdiger Simon initiated and designed the project. Elmehdi Bahafid conducted all experiments and data analyses. Imke Bradtmöller, Ann Marlene Thies and Thi Thuy Oanh Nicole Nguyen performed part of the cloning and the imaging. Crisanto Gutierrez and Benedicte Desvoyes provided the PlaCCI reporter and discussed results.

Abstract

Unlike animals, plants have the capacity to produce new organs post-embryonically throughout their entire life cycle. This is due to stem cells present in the shoot and the root apical meristems (SAM and RAM, respectively). In the SAM, stem cells are located in the central zone (CZ) where they divide slowly. Stem cell daughters are displaced laterally and enter the peripheral zone (PZ). Here, their mitotic activity increases, and lateral organ primordia (LOP) are formed. How the spatial arrangement of these different domains is initiated and controlled during SAM growth and development, and how sites of LOP are determined in the PZ is not yet completely understood.

In the RAM, the GRAS family transcription factor SHORTROOT (SHR) acts as a master regulator of signalling pathways that maintain the root stem cell niche and control formation of ground tissue layers. We hypothesized that SHR could perform a similar role in the SAM, and found that SHR, together with its target transcription factors SCARECROW (SCR), SCARECROW-LIKE23 (SCL23) and JACKDAW (JKD), controls shoot meristem size by regulating cell division rates, and promotes formation of lateral organs. SHR, SCR, SCL23 and JKD are expressed in very distinct patterns in the SAM. Where these expression domains overlap, they can physically interact to activate expression of the key cell cycle regulator *CYCLIND6;1* (*CYCD6;1*) and thereby promote the formation of new cell layers.
In the PZ, upregulation of *SHR* expression at sites of organ initiation depends on the phytohormone auxin, acting through the auxin response factor MONOPTEROS (MP) and auxin response elements in the *SHR* promoter. In the CZ, the SHR-target SCL23 physically interacts with WUS, a key regulator of stem cell maintenance, and both SCL23 and WUS expression are subject to negative feedback regulation from stem cells through the CLAVATA signalling pathway. Together, our findings illustrate how SHR-dependent transcription factor complexes act in different domains of the shoot meristem to mediate cell division and auxin dependent organ initiation in the PZ, and coordinate this activity with stem cell maintenance in the CZ of the SAM.

Introduction

In multicellular organisms, stem cells are the source of all tissues and organs. In contrast to animals where organs are formed during embryogenesis, plants form organs only postembryonically, and they can continuously produce new organs throughout their life span. This process depends on the activity of pluripotent stem cells embedded in their shoot and root apical meristems (SAM and RAM, respectively).

In the SAM, stem cells are located in the central zone (CZ) at the tip of the meristem. Directly underneath lies the organizing center (OC), which is required for stem cell maintenance. The stem cells in the CZ have a low mitotic activity, but after cell division, descendants are continuously displaced towards the peripheral zone (PZ). Here, they start to divide faster and provide founder cells for lateral organ primordia (LOP) that will develop at the meristem flank (Reddy *et al.*, 2004). How the communication between these distinct functional domains is coordinated to balance stem cell proliferation in the center with organ formation at the periphery of the SAM is still not completely understood. This is in contrast to the RAM where the gene networks regulating the spatial arrangement of the different tissue types are well known. In the RAM, a member of the plant-specific GRAS transcription factor (TF) family, SHORT-ROOT (SHR) has a key regulatory role in the maintenance of the root stem cell niche identity and tissue patterning (Pysh *et al.*, 1999, Lee *et al.*, 2008, Long *et al.*, 2015b, Helariutta *et al.*, 2000, Nakajima *et al.*, 2001). Plants lacking functional SHR show a ‘short root´ phenotype, with roots carrying fewer ground tissue layers (Di Laurenzio *et al.*, 1996, Scheres *et al.*, 1995, Pysh et al., 1999). *SHR* is transcribed in the stele, and SHR protein moves one cell layer outward where it interacts with the GRAS domain TFs SCARECROW (SCR) and SCARECROW LIKE 23 (SCL23), and with the BIRD/INDETERMINATE DOMAIN TF JACKDAW (JKD) (Long et al., 2015b, Long *et al.*, 2017, Nakajima et al., 2001, Cui *et al.*, 2007). The resulting multimeric complex promotes asymmetric cell division (ACD) of the Cortex-Endodermis Initial/daughter (CEI/CEID) by directly activating the expression of the key cell cycle regulator *CYCLIND6;1* (*CYCD6;1*) to instruct development of distinct endodermis and cortex cell layers (Long *et al.*, 2015a, Long et al., 2015b, Long et al., 2017, Di Laurenzio et al., 1996, Helariutta et al., 2000, Nakajima et al., 2001). SCR and SHR are required for the maintenance and specification of the QC, as *shr* and *scr* mutants show abnormal QC cells (Sabatini et al., 2002, Petersson et al., 2009). *SHR*, *SCR* and *SCL23* are also expressed in leaves and the SAM, but their function was mainly studied in leaves (Wysocka-Diller *et al.*, 2000, Gardiner *et al.*, 2011, Wang *et al.*, 2011, Cui *et al.*, 2014). Here, we asked whether patterning in the SAM involves the SHR signaling pathway in a mechanism similar to the RAM..

In the SAM, stem cell maintenance depends on the homeodomain transcription factor WUSCHEL (WUS) (Laux *et al.*, 1996, Zhang *et al.*, 2017). *WUS* transcripts are limited to the

97 OC, but WUS protein moves via plasmodesmata from the OC to the CZ to directly activate the
98 transcription of the secreted signalling peptide CLAVATA3 (CLV3) in stem cells (Mayer *et al.*,
99 1998, Yadav *et al.*, 2011, Daum *et al.*, 2014). In turn, CLV3 acts to limit *WUS* expression to
100 the OC via a system of receptor-like kinases and co-receptors: CLAVATA1 (CLV1),
101 CLAVATA2 (CLV2), CORYNE (CRN) and BARELY ANY MERISTEM1-3 (BAM1-3)
102 (Bleckmann & Simon, 2009, Clark *et al.*, 1997, Fletcher *et al.*, 1999, Nimchuk *et al.*, 2015,
103 Ohyama *et al.*, 2009). The resulting WUS-CLV3 negative feedback circuit controls stem cell
104 homeostasis in the SAM (Brand *et al.*, 2000, Schoof *et al.*, 2000). Recently it was shown that
105 WUS interacts in the OC with the GRAS family transcription factors HAIRY MERISTEM 1 and
106 2 (HAM1/2) to restrict CLV3 activation to the apical domain of the CZ (Han *et al.*, 2020).

107 Formation of lateral organ primordia at the meristem flanks is preceded by establishment of a
108 local maximum of the plant hormone auxin (Benková *et al.*, 2003, Heisler *et al.*, 2005, Vernoux
109 *et al.*, 2011a). This auxin maximum is generated by the auxin efflux carrier PIN-FORMED1
110 (PIN1) through polar auxin transport (Friml *et al.*, 2004, Gälweiler *et al.*, 1998). The
111 transcriptional auxin read-out is carried out by the Auxin/Indole-3-acetic acid (Aux/IAA)
112 repressor proteins that under low auxin conditions dimerize with auxin response factors (ARFs)
113 and repress their activity (Mockaitis & Estelle, 2008). ARFs bind DNA at the promoters of their
114 target genes via an auxin response element (AuxRE) (Boer *et al.*, 2014). An increase in auxin
115 levels triggers the formation of a complex between Aux/IAA and TIR1/AFB leading to the
116 degradation of Aux/IAA and the release of the ARFs, which can now regulate expression of
117 auxin response genes (Paque & Weijers, 2016). Auxin-dependent lateral organ initiation is
118 mediated by AUXIN RESPONSE FACTOR 5/MONOPTEROS (ARF5/MP) (Berleth & Jürgens,
119 1993, Hardtke & Berleth, 1998). MP plays a crucial role in the initiation of flower primordia as
120 the strong *mp* allele lacks roots and a weak allele cannot produce flowers and forms a naked
121 inflorescence stem (Yamaguchi *et al.*, 2013). MP directly induces the expression of its target
122 gene *LEAFY (LFY),* a plant-specific transcription factor that plays a key role in flower primordia
123 initiation and in primordium fate specification (Schultz & Haughn, 1991, Weigel *et al.*, 1992,
124 Yamaguchi et al., 2013, Wu *et al.*, 2015). Transcript levels of *SHR* and *SCR* are strongly
125 reduced in *mp* mutant embryos (Möller *et al.*, 2017) suggesting that MP regulates expression
126 of *SHR* and *SCR* during embryonic development.

127 We here started to unravel how organ initiation at the periphery is coordinated with stem cell
128 behaviour in the center of the SAM. We show that SHR, SCR, SCL23 and JKD act in the SAM
129 in different expression domains with complementary and overlapping patterns, and together,
130 they cover all the functional domains of the SAM. Interestingly, the overlapping region of the
131 four TFs coincides with the expression of *CYCLIND6;1 (CYCD6;1).* We find that mutants for
132 genes in the SHR gene regulatory network show reduced meristem sizes and delay cell cycle
133 progression due to an extended G1 phase. We demonstrate that auxin via MP promotes

expression of *SHR* and *SCR* in the PZ, where SHR acts upstream of *LFY* to promote flower primordia formation. In the meristem centre, members of the SHR network directly interact with the CLV3-WUS circuit. Together, our study shows how mobile TFs of the SHR network establish a balance between stem cell maintenance and lateral organ initiation, by controlling cell division rates and cell fate in different domains within the SAM in an auxin dependent manner.

140 ## Results

141 ### *SHR* and *SCR* coordinate shoot meristem size and primordia initiation

142 In order to identify SHR and SCR regulatory roles in shoot meristem development, we first
143 analyzed the phenotypes of null mutant alleles of *SHR* (*shr-2*) and *SCR* (*scr-3* and *scr-4*). All
144 mutants displayed a small rosette, dwarfed shoot phenotype and initiated fewer flowers
145 compared to wild type (WT) (Fig. 1A-D; Suppl Fig. 1A-D). To assess the function of *SHR* and
146 *SCR* in the SAM, we measured meristem sizes and the average time interval between the
147 initiation of successive lateral organs (plastochron). Plastochrons were increased in the
148 mutants (*shr-2, scr-3* and *scr-4*) compared to WT, indicating a significant delay in the initiation
149 of lateral organs in the mutants (Fig. 1M; Suppl Fig. 1A'-D'). Next, we determined meristem
150 size using confocal microscopy by imaging the meristem of mutants and WT (Fig. 1E-H) and
151 measuring the surface area of the SAM excluding organ primordia as a proxy for meristem
152 size. We found that the meristem is significantly reduced in the mutants (Fig. 1N), and
153 hypothesized that SHR and SCR may serve to coordinate meristem size with lateral organ
154 primordia initiation during SAM development. To better understand the cause for the reduction
155 in SAM size, we analyzed both cell number and area on the meristem surfaces. Analysis of
156 average cell surface areas showed no differences between mutants and WT (Suppl Fig. 1E),
157 however, cell numbers were reduced in all mutants (Fig. 1O). We next investigated if there
158 were any significant differences in cell proliferation rate between WT, *shr-2*, *scr-3* and *scr-4* at
159 the SAMs. We used the plant cell cycle marker *PlaCCI* (Desvoyes *et al.*, 2020) (Fig. 1I-L), an
160 imaging tool combining the three reporters *pCDT1a:CDT1a-eCFP*, *pHTR13:HTR13-mCherry*
161 and *pCYCB1;1:NCYCB1;1-YFP*, which individually mark the G1, S + G2 and mitotic (M)
162 phases, respectively. In shoot meristems (excluding organ primordia) of *shr-2*, *scr-3* and *scr-*
163 *4*, the percentage of cells in G1 marked with CDT1a-CFP was significantly increased compared
164 to WT (Fig. 1P; Suppl Fig. 1F), indicating delayed progression through the cell cycle. We
165 conclude that *SHR* and *SCR* promote cell cycle progression in the meristem by controlling the
166 G1 phase, which could account for the observed reduction in SAM size and delay in organ
167 initiation in the PZ of *shr* and *scr* mutants.

168 ### SHR and SCR promote auxin signalling in the SAM

169 Since organ initiation sites are determined by auxin accumulation and signaling (Vernoux *et*
170 *al.*, 2011b), we asked if auxin accumulation is affected by loss of *SHR* or *SCR* functions, which
171 would explain the observed delayed lateral organ initiation in *shr* and *scr* mutants (Fig. 1M).
172 We introduced the auxin transcriptional output reporter *pDR5v2:3xYFP-N7* (Heisler et al.,
173 2005) into the *shr-2* and *scr-4* mutants and assessed the number of domains with auxin output

174 maxima compared to WT (Fig. 2A-C, arrowheads). We found that the average number of *DR5*
175 positive domains in SAMs of *shr-2* and *scr-4* was significantly reduced (Fig. 2D), indicating that
176 SHR and SCR functions are required to establish auxin maxima in the SAM.

177 To closely evaluate how the distribution of auxin was affected in the SAM during the loss of
178 SHR and SCR activities, we further evaluated auxin levels in the different meristem domains
179 using the R2D2 auxin input sensor (Liao *et al.*, 2015). R2D2 is a degron-based ratiometric
180 auxin reporter consisting of an auxin-dependent degradation domain II (DII) of an Aux/IAA
181 protein fused to Venus, and a mutant auxin nondegradable domain II (mDII) fused to tdTomato.
182 The ratio of the fluorescence intensities between Venus and tdTomato represents a proxy for
183 the level of auxin in every cell, with high ratios indicating low auxin levels and vice versa. We
184 observed that the domains of low auxin in meristems of *shr-2* and *scr-4* mutants were
185 expanded and sometimes extended beyond lateral organ boundaries into primordia (Fig. 2E-
186 G, arrowheads). Altogether, these results show that SHR and SCR functions are required to
187 maintain the proper distribution of auxin within the SAM. This safeguards the regular
188 generation of auxin maxima in the peripheral zone, which is a prerequisite for organ initiation.

189 **SHR and SCR expression in shoot and flower meristems**

190 To unravel the precise expression patterns of SHR and SCR in the meristem, we made use of
191 previously established translational reporter lines which functionally complement the
192 corresponding *shr* or *scr* mutants (Long et al., 2017). Using confocal microscopy, we imaged
193 *pSHR:YFP-SHR* transgenic plant meristems and studied SHR expression in the inflorescence
194 meristems at 36 DAG. YFP-SHR was detected in initiating flower primordia, in floral organ
195 primordia and in diverse flower organs (Fig. 3A). The transcriptional reporter *pSHR:ntdTomato*
196 (Möller et al., 2017) shows expression from P1 onwards in the third meristematic cell layer (L3)
197 and, weakly, in the L2 of older primordia (Fig. 3C; Suppl Fig. 2A). No *SHR* expression was
198 observed in the center of the SAM or floral meristems (Fig. 3A, left inset), or stem cell domains
199 (Fig. 3A, right inset, asterisks). The translational reporter *pSHR:YFP-SHR* (Fig. 3A and D)
200 revealed that SHR protein localized throughout L3 cells and appeared to be preferentially
201 confined to the nuclei in L2 cells and also in L1 cells, where *SHR* is normally not expressed
202 (Fig. 3C). Based on the combined observation of *SHR* transcriptional activity and the SHR
203 protein localization, we conclude that SHR, similar to its activity in RAM, acts as a mobile
204 transcription factor moving from the inner cell layers to the outermost cell layers of the organ
205 primordia to mediate proper SAM development. We then evaluated the expression of *SCR* in
206 the shoot meristem. A transcriptional reporter for *SCR* (*pSCR:H2B-YFP*) was previously
207 described to be expressed in the QC and the root endodermis (Xu *et al.*, 2006). In the SAM,
208 we found fluorescent signal only in differentiated vasculature of the shoot, and in a patchy

209 pattern in some flower primordia (Suppl Fig. 2B, inset). Since the transcriptional *SCR* reporter
210 might lack control elements that contribute to the native *SCR* expression pattern, we used a
211 translational reporter line, *pSCR:SCR-YFP* that was previously shown to complement all *scr*
212 mutant phenotypes (Long et al., 2017). We observed SCR-YFP fluorescence in the nuclei of
213 L1 cells in the central zone of the SAM and further extended into the deeper meristem layers
214 specifically of the peripheral zone and lateral organ primordia (Fig. 3B, inset). Notably, SCR-
215 YFP was lacking in the deeper regions of the meristem center and the rib meristem. In lateral
216 organ primordia, *SCR* expression starts from the L1 and L2, and extends into deeper regions
217 during further development. Stronger expression was found in the boundary region that
218 separates lateral organ primordia from the remainder of the SAM (Fig. 3E). Thus, SHR and
219 SCR proteins are found in partially overlapping domains during lateral organ primordia
220 development. Importantly, *SHR* is missing from the SAM center, where *SCR* is expressed in
221 the L1 (compare Fig. 3A, right inset, with Fig. 3B, inset).

222 SHR and SCR form protein complexes in the SAM

223 SHR and SCR localize in an overlapping domain during lateral organ development (Fig. 3D
224 and E), and SCR and SHR co-localized predominantly in nuclei of cells in the L1 and L3 of
225 lateral organ primordia (Fig. 4A and C). Previous *in vivo* FRET-FLIM studies demonstrated
226 direct interaction between SHR and SCR in the RAM (Long et al., 2017). We now investigated
227 if SHR and SCR also interact in the SAM. For FRET-FLIM studies, we used YFP-SHR as
228 fluorescent donor and SCR-RFP as acceptor. Reductions in the fluorescence lifetime of YFP
229 due to resonance energy transfer to RFP are recorded as a quantitative readout for FRET,
230 indicative of interaction between YFP-SHR and SCR-RFP. We used SAMs at 36 DAG for
231 FRET measurements between YFP-SHR and SCR-RFP in lateral organ primordia, petal
232 primordia and sepal primordia. As a negative control for non-interacting proteins, we used
233 SAMs from plants coexpressing *pSCR:SCR-YFP* with *pSCR:SCR-RFP*, since SCR proteins
234 do not homodimerize (Long et al., 2017) (Fig. 4B and D). The YFP-SHR donor-only sample
235 showed a fluorescence lifetime of 2.75 ± 0.02ns (Fig. 4E), which significantly decreased by
236 approximately 0.3 ± 0.03ns in cells where SCR-RFP was coexpressed (Fig. 4E), whereas
237 samples with SCR-RFP and SCR-YFP coexpression showed no significant changes in mean
238 fluorescence lifetime compared to the SCR-YFP donor-only control (Fig. 4F). These results
239 show that the SCR and SHR proteins physically interact in the SAMs of Arabidopsis.

240 A SHR-SCR heteromer regulates expression of *SCR* in lateral organ primordia

241 We next tested if SHR regulates *SCR* expression. We compared the SCR protein localization
242 using the *pSCR:SCR-YFP* reporter line in WT and the *shr-2* mutant background. SCR protein

243 levels remained unaffected in the central zone of the SAM, where *SHR* is normally not
244 expressed (Fig. 5B, C and G). However, in the lateral organ primordia, SCR protein level was
245 strongly reduced in *shr-2* compared to WT (Fig. 5D, E and H). Analysis of *SCR* transcript levels
246 by qRT-PCR corroborated a significant decrease in *shr-2* mutants shoot meristems (Fig. 5I).
247 We conclude that SHR acts as a transcriptional activator of *SCR* in the SAM, but that *SCR*
248 expression in the meristem center is SHR-independent. Importantly, the expression pattern of
249 *pSHR:ntdTOMATO* does not entirely overlap with the expression pattern of *pSCR:SCR-YFP*,
250 indicating that SHR acts as a mobile protein also in the SAM (Suppl Fig. 6A,D). We then tested
251 if SCR restricts movement of SHR protein by nuclear retention in the SAM or lateral organ
252 primordia. Analysis of SAMs coexpressing *pSHR:SHR-YFP* and *pSCR:SCR-RFP* showed that
253 SHR-YFP is enriched in the nuclei of cells coexpressing SCR-RFP at the lateral organ
254 primordia (Fig. 5A inset and F). This enrichment could indicate that SCR entraps SHR in the
255 nuclei, thus restricting its further intercellular movement.

256 **Roles of *JKD* in the SAM**

257 The BIRD-family transcription factor JACKDAW (JKD) can interact with SHR and SCR and
258 form multiprotein complexes (Long et al., 2015b, Long et al., 2017, Welch *et al.*, 2007), here
259 we investigated if JKD also affects SAM development. SAM sizes of *jkd-4* mutants were
260 increased compared to WT, due to a significant rise in cell number (Fig. 6A-D, and Suppl Fig.
261 3A). For expression studies, we used the transcriptional reporter *pJKD:YFP-RFP* and the
262 translational *pJKD:JKD-YFP* reporter that has been previously shown to complement the *jkd-*
263 *4* mutant phenotype (Long et al., 2017). *JKD* was found to be expressed only in some cells of
264 the peripheral zone of the SAM, and in the abaxial regions of flower primordia (Fig. 6E-F and
265 I). The expression patterns of both transcriptional and translational reporter lines were mostly
266 identical (Fig. 6E-F), indicating that *JKD* RNA and protein are found in the same cells, and that
267 JKD protein is not mobile. The JKD expression domain expands from few cells at the abaxial
268 side of P1 into a ring-like abaxial domain in sepals, and at later stages, in stamen and carpel
269 primordia (Fig. 6G and I). Based on the observed JKD expression (Fig 6E-F and I), we asked
270 if JKD localization directly correlates with early sepal development. To do this, we used the
271 strong *lfy-12* mutant where flower meristems fail to produce proper flower organs but instead
272 generate mostly sepal-like organs (Weigel et al., 1992), and the *clv3-9* mutant, which has an
273 excessively enlarged SAM and flowers with additional organs (Schlegel *et al.*, 2021). JKD was
274 confined to sepal primordia of *clv3-9* mutants and to the sepal-like organs of *lfy-12* mutants
275 like in WT (Suppl Fig. 3C-D). We tested for potential molecular interactions of JKD with SCR
276 in the SAM *in vivo* using FRET-FLIM. SAMs coexpressing *pJKD:JKD-YFP* and *pSCR:SCR-*
277 *RFP* (Fig. 6J) showed significant fluorescence lifetime reductions of up to 0.17 ± 0.02ns,
278 compared to the JKD-YFP donor-only which exhibited a lifetime of 3.02 ± 0.03ns (Fig. 6H). We

279 conclude that SHR-SCR can form multimeric complexes with JKD in the SAM periphery, in
280 floral organ primordia and in floral organs. JKD could modulate or even dampen activities of
281 the SHR-SCR complexes, since JKD and SHR-SCR exert opposite effects on meristem size.

282 The SHR-SCR-JKD complex triggers cell division in lateral organ primordia by 283 regulating *CYCD6;1* expression

284 Lateral organ initiation in the SAM periphery is controlled by *CYCLIN* genes, which are key
285 regulators of cell division (Dewitte *et al.*, 2003). We examined the expression patterns of
286 *pCYCD1;1:GFP, pCYCD2;1:GFP, pCYCD3;2:GFP, pCYCD3;3:GFP, pCYCD5;1:GFP,*
287 *pCYCD6;1:GFP, pCYCD7;1:GFP* and *pCYCB1;1:CYCB1;1-GFP (Ubeda-Tomás et al., 2009).*
288 Amongst these, only *CYCD1;1*, *CYCD3;2*, *CYCD3;3*, *CYCD6;1* and *CYCB1;1* were visibly
289 expressed in the SAM (Fig. 7A; Suppl Fig. 4A-D and G). *CYCD1;1*, *CYCD3;2* and *CYCB1;1*
290 exhibited a patchy expression pattern in sepal primordia (Suppl Fig. 4A-B and D), while
291 *CYCD3;3* was more uniformly distributed with an enrichment in lateral organ primordia (Suppl
292 Fig. 4C). *pCYCD6;1:GFP* expression was detected in lateral organ primordia and floral organs
293 in sepal primordia from all stages, but not at the center of the SAM (Fig. 7A,C,E,L and O).
294 Notably, *pCYCD6;1:GFP* was predominantly expressed in the region where expression of
295 SHR, SCR and JKD overlapped (Fig. 7J-O; Suppl Fig. 4E-S). We tested if expression of
296 *pCYCD6;1:GFP* is affected when *SHR* function is compromised, and observed a strong
297 reduction in *pCYCD6;1:GFP* expression level in the sepal primordia of *shr-2* and its complete
298 absence from lateral organ primordia in the *shr-2* mutant, while *pCYCD6;1:GFP* was detected
299 in the L3 of WT lateral organ primordia (Fig. 7A-F). In the root meristem, *CYCD6;1* specifically
300 controls periclinal cell divisions and the formation of new tissue layers (Long et al., 2015b). We
301 found that the number of cell layers in the L3 of lateral organ primordia is strongly reduced in
302 *shr-2* mutants compared to WT (Fig. 7G-I), consistent with the SHR-SCR-JKD complex acting
303 through *CYCD6* to inducte periclinal cell divisions in the SAM.

304 Auxin induces *SHR* and *SCR* expression in the SAM

305 Since we observed that *SHR* and *SCR* control SAM size and lateral organ initiation which is
306 triggered by local auxin accumulation, we investigated SHR-SCR interaction with auxin
307 distribution and/or signaling. We wanted to first examine if *SHR* and *SCR* expression patterns
308 correlated with that of auxin distribution using the functional *pPIN1:PIN1-GFP* reporter (Heisler
309 et al., 2005). PIN1 is an auxin efflux transporter which controls the flow and the distribution of
310 auxin across the SAM (Benková et al., 2003) (Suppl Fig. 6C and F). The expression patterns
311 of *SHR* and *SCR* in primordia strongly overlapped with that of *PIN1* during primordia initiation
312 and development (Fig. 3A-D; Suppl Fig. 6A-F). This indicates that *SHR* and *SCR* might act

313 downstream in response to auxin signaling. *In silico* analysis of the *SHR* promoter sequence
314 revealed the presence of two putative auxin-response element (AuxRE) core motifs (TGTCTC)
315 (Fig. 10A). These motives are thought to be sufficient for recruitment of ARF transcription
316 factors (Schlereth *et al.*, 2010, Zhao *et al.*, 2010, Ulmasov *et al.*, 1999), which are the
317 downstream TFs released after auxin dependent degradation of IAAs (Paque & Weijers, 2016).
318 This suggests that *SHR* might be induced by ARF upon auxin signaling. We then tested if auxin
319 regulates expression of *SHR* and *SCR* in the SAM and treated WT inflorescences with 10µM
320 indole-3-acetic acid (IAA). Within 12h of hormone application, the expression levels of both
321 *SHR* and *SCR* increased to about 300% of untreated control levels. *SHR* expression increased
322 slightly earlier than that of *SCR*, further supporting our previous observation that *SHR* activates
323 *SCR* expression (Fig. 8A). To uncover the spatial distribution of *SHR* and *SCR* in response to
324 exogenous auxin application, we analyzed SAMs expressing *pSHR:SHR-YFP* and
325 *pSCR:SCR-YFP* after treatment with 10µM of the synthetic auxin analogue 2,4D, a form of
326 auxin that can diffuse into cells. We found that expression visibly increased within 2-5h after
327 the start of the hormone treatment (Fig. 8B-G). Importantly, the expression patterns of both
328 *SHR* and *SCR* were not strongly altered. Since we observed an overlap of auxin accumulation
329 domains with those of *SHR* and *SCR,* and also established that auxin induces *SHR* and *SCR*
330 expression, we tested if changes in auxin transport and local distribution in turn affected *SHR*
331 and *SCR* expression patterns. We inhibited polar auxin transport and hence its distribution in
332 tissues using N-1-naphthylphthalamic acid (NPA). The mock control SAMs expressing
333 *pPIN1:PIN1-GFP* showed a wide distribution of *PIN1-GFP*, which relocated into a ring shaped
334 domain in deeper regions of the meristem 3d after treatment with 100µM NPA (Fig. 8P-S).
335 Concomitantly, the expression pattern of *SHR-YFP* changed from being associated with
336 primordia into a ring shaped domain, reflecting the rearrangement of the *PIN1* expression
337 domain (Fig. 8H-K). Similar changes in expression pattern were found for *SCR* upon NPA
338 treatment (Fig. 8L-O). In addition, NPA treatment resulted in enlarged expression domains for
339 *pCYCD6;1:GFP*, a key target gene of the SHR-SCR-JKD complex (Suppl Fig. 5A-D). Based
340 on all these observations, we conclude that, in the SAM, *SHR* and *SCR* levels and expression
341 pattern are to a large extent coordinated by auxin levels and distribution.

342 MONOPTEROS regulates *SHR* and *SCR* expression in the SAM

343 We have shown that auxin regulates *SHR* expression likely through ARFs (Fig 8A). The ARF
344 MONOPTEROS (MP) is required to promote expression of *SHR* and *SCR* in the early embryo
345 (Möller et al., 2017). In the SAM, the expression patterns of *MP, SCR* and *SHR* partially overlap
346 in the primordia (Fig. 3D and E; Suppl Fig. 6A-B and D-E). We then analyzed the expression
347 of *pSHR:ntdTomato* in *mp-B4149,* a loss-of-function mutant for *MP*. In WT vegetative
348 meristems at 7 DAG, *SHR* was expressed in the deeper region of the young leaf primordia,

349 where the vasculature will eventually develop. *SHR* was expressed in a similar pattern in the
350 *mp-B4149* mutants, albeit at lower levels (Fig. 9A- B), indicating that *MP* is required for normal
351 *SHR* expression levels post embryogenesis. Since *mp-B4149* mutants fail to develop beyond
352 the early seedling stage, we used the hypomorphic allele *mp-S319* to study later stages of
353 development. *mp-S319* mutants display weaker phenotypes than *mpB-4149* null mutants and
354 initiate an inflorescence meristem with, occasionally, some flower primordia. We used the
355 transcriptional reporter *pSHR:ntdTOMATO* and the translational reporter *pSHR:SHR-YFP* to
356 distinguish between effects of auxin on *SHR* promoter activity and posttranscriptional effects
357 leading to altered protein localization. Compared to WT, *pSHR:ntdTOMATO* expression was
358 strongly reduced in *mp-S319* inflorescences (Fig. 9C-F). Similar results were observed for the
359 translational reporter *pSHR:SHR-YFP*, and weak expression in a ring-shaped domain was
360 found in cross sections through the inflorescence stem (Fig. 9K-N). Similarly, using
361 *pSCR:SCR-RFP*, we observed reduced expression of *SCR* in the meristem periphery in *mp-*
362 *S319*, which now overall resembled the *SHR* expression pattern (Fig. 9G-J). We therefore
363 conclude that *MP* is required for maintaining normal expression of *SHR* and *SCR* expression
364 in the meristem periphery and primordia. We then tested whether *MP* could promote *SHR*
365 expression throughout the meristem, using an inducible MP-GR fusion protein expressed from
366 the *Ubiquitin10* promoter (*pUBQ10:MP-GR*). Treatment of these plants with dexamethasone
367 (DEX) allows the nuclear entry of MP-GR. Within 4 h of DEX treatment, ubiquitously expressed
368 MP resulted in increased expression levels of *pSHR:SHR-YFP* and *pSHR:ntdTOMATO* while
369 retaining its WT expression domain (Fig. 9O-P; Suppl Fig. 10Q and R), indicating that MP can
370 increase *SHR* expression levels, but is not sufficient to control the precise expression pattern
371 in the absence of additional auxin. Thus, MP exerts a quantitative regulatory control over *SHR*
372 expression. To better understand the distinct roles of *SHR* and *MP* in organ initiation, we
373 generated double mutants of *mp-S319* and *shr-2*. Unlike *mp-S319* that forms only fewer flower
374 primordia than WT, the phenotype of the double mutant *mp-S319; shr-2* was more severe with
375 naked inflorescences that lacked all organ primordia (Suppl Fig. 7A-D''). We conclude that MP
376 acts through SHR to promote lateral organ initiation.

377 **AuxRE motifs in the *SHR* promoter control its activity**

378 We showed that *SHR* expression is induced by the ARF MP (Fig. 9A-F and K-P; Suppl Fig.
379 10Q and R). To test if MP can directly activate *SHR* expression, we analyzed two candidate
380 AuxREs (AuxRE1 and AuxRE2) in the *SHR* promoter. We tested the ability of the *SHR*
381 promoter, with or without these AuxREs, to control the expression of the reporters mVenus or
382 Luciferase upon Agrobacterium-mediated transient expression in *Nicotiana benthamiana*
383 leaves. mVenus under control of the WT *SHR* promoter was co-infiltrated with *p35S:MP*, or
384 *p35S:GUS* as a negative control. We observed strong *mVenus* expression from the WT *SHR*

385 promoter in the presence of *p35S:MP*, which was about 6 fold higher than upon coexpression
386 of *p35S:GUS* (Suppl Fig. 8B). Mutating AuxRE1 from “GAGACA” to “GAGCCA” (mAuxRE1)
387 or “GTGCTC” (mAuxRE1-2) and AuxRE2 from “TGTCTC” to “TGGCTC“ (mAuxRE2) or
388 "TGGAGA" (mAuxRE2-2) by site directed mutagenesis drastically reduced the response to
389 *p35S:MP* coexpression, and mutating both AuxREs had an additive effect, resulting in no
390 significant response to overexpression of *MP* (Suppl Fig. 8A-J and Suppl Fig. 9A-J). Similar
391 results were obtained using a Luciferase assay system (Suppl Fig. 10A-H), indicating that MP
392 interacts with these two AuxRE elements in the *SHR* promoter to regulate *SHR* expression. To
393 investigate if these elements also contribute to *SHR* expression in Arabidopsis, we generated
394 transgenic plants using either the WT *SHR* promoter, or the mutant versions carrying base
395 changes in one or both AuxREs. At least ten independent transgenic lines were analyzed for
396 each promoter construct. Expression of the WT *pSHR:mVenus-NLS* produced a strong
397 expression in lateral organ primordia and floral meristems. However, mutations in AuxRE1
398 (mAuxRE1 or mAuxRE1-2) or AuxRE2 (mAuxRE2 or mAuxRE2-2) led to decreased mVenus
399 expression in all organ primordia stages and the floral meristem (Fig. 10B-D; Suppl Fig 9K-M).
400 When both AuxREs (mAuxRE1+2 or mAuxRE1-2+2-2) were mutated, mVenus expression was
401 barely detectable (Fig. 10E; Suppl Fig 9N). We concluded that both AuxRE motifs function in
402 an additive manner during ARF-dependent activation of *SHR* expression in the SAM. Notably,
403 consistent with the expression in the SAM, mutations in AuxREs motifs in the *SHR* promoter
404 also led to a decreased *mVenus* expression in the RAM compared to the WT *pSHR:mVenus-*
405 *NLS,* where *SHR* and *MP* expression overlap (Suppl Fig. 11A-H).

406 ## ***SHR* regulates *LFY* expression in the SAM**

407 It has been previously shown that MP directly activates *LFY* expression to confer floral identity
408 to organ primordia (Yamaguchi et al., 2013). Since MP induces also *SHR* expression, we
409 asked how *SHR* and *LFY* activities are coordinated. In WT, *SHR* and *SCR* were expressed
410 two plastochrons prior to *LFY* in the primordia (Suppl Fig. 12A), and we hypothesized that *SHR*
411 might mediate MP-dependent *LFY* expression. We first tested whether *LFY* expression was
412 altered in *shr-2* mutants. mRNA quantification via qRT-PCR from SAM and flower primordia
413 up to stage 5 revealed that *LFY* RNA levels were downregulated by approximately 60% in *shr-*
414 *2* compared to WT (Suppl Fig. 12D). We further tested the LFY protein level and expression
415 pattern using *pLFY:GFP-LFY* reporter (previously named *pLFY::GLFY*) (Wu *et al.*, 2003). In
416 WT, *LFY* was not expressed in the SAM, but in flower primordia from stage 3 onwards. At later
417 stages, *LFY* remained expressed in the adaxial side of sepals, and in the 2nd and 3rd floral
418 whorls. In *shr-2* mutants, LFY-GFP fluorescence was barely visible at early stages and strongly
419 decreased at later stages, compared to WT (Suppl Fig. 12B-C). This indicates that *SHR*
420 function is required for normal *LFY* expression patterns. However, analysis of *SHR* and *SCR*

421 expression in *lfy-12* mutants revealed no obvious differences compared to WT (Suppl Fig. 13A-
422 D), and we therefore conclude that *LFY* does not feed-back to the *SHR-SCR* module. In the
423 *lfy-12* null-mutant, leaf-like bracts are generated from the inflorescence meristem and
424 formation of flower meristems is delayed. Most floral organs are leaf-like and not arranged in
425 regular whorls. Double mutants of *lfy-12; shr-2* were strongly retarded in growth and displayed
426 dramatically enhanced floral primordium initiation defects (Suppl Fig. 12E-L). We conclude
427 from this analysis that the *SHR-SCR* module promotes *LFY* expression, and that it also
428 promotes floral meristem development in a *LFY*-independent manner.

429 *SCL23* genetically interacts with the *SHR-SCR* pathway and contributes to SAM 430 size maintenance

431 The closest homologue of SCR is the GRAS-family TF SCARECROW-LIKE23 (SCL23). We
432 investigated the expression pattern of *SCL23* in the SAM using the transcriptional reporter
433 *pSCL23:H2B-YFP*, and the functional translational reporter line *pSCL23:SCL23-YFP (Long et*
434 *al., 2015a)*. *pSCL23:H2B-YFP* was expressed in the L3 of the SAM and floral meristems, and
435 in floral organ primordia (Fig. 11A and C). The translational reporter *pSCL23:SCL23-YFP*
436 showed a wider expression pattern than the transcriptional reporter (Fig. 11B and D), which
437 was suggestive of SCL23 protein mobility. To test if the wider expression pattern of the
438 translational reporter line is due to the presence of additional transcriptional control regions
439 within the coding sequence of *SCL23*, we expressed SCL23-mVenus under the *CLV3*
440 promoter, which confines the expression exclusively to the CZ. We observed SCL23 spreading
441 from the expression domain in the CZ into the surrounding cells, consistent with high SCL23
442 protein mobility in the SAM (Fig. 11E and F). We then analysed co-expression of SCL23 and
443 SCR to investigate the regulatory dynamics among *SCL23*, *SCR* and *SHR*. A dual reporter line
444 with *pSCR:SCR-RFP* and *pSCL23:SCL23-YFP* revealed that the expression patterns of both
445 genes are in most cases mutually exclusive, with SCL23 in a central domain of the SAM and
446 in the inner cell layers of primordia, while SCR is confined to the PZ, the L1 of the CZ and the
447 outer cell layers of lateral organ primordia (Fig. 11G, I and K). Some cells expressing both
448 SCL23 and SCR were located deep inside lateral organ primordia (Fig. 11I and K (yellow
449 arrowheads)). A similar coexpression analysis of *pSCL23:SCL23-YFP* with *pSHR:mScarlet-*
450 *SHR* indicated an overlap of expression in the deep cell layers of lateral organ primordia (Fig.
451 11H, J and L(yellow arrowheads)). In *shr-2* mutants, *pSCL23:SCL23-YFP* remains only weakly
452 expressed in the meristem centre (Fig. 11M and N), indicating that SHR is required to promote
453 expression of *SCL23* in the SAM periphery. We then performed genetic interaction studies to
454 understand the relationship between *SCL23*, *SCR* and *SHR* in the SAM. In *scl23-2* mutants,
455 SAM size is significantly decreased compared to WT, or to the complemented line
456 *pSCL23:SCL23-YFP/scl23-2* (Fig. 11O-R). Using the PlaCCI marker to analyze cell division

457 patterns, we found that similar to *shr-2* and *scr-3* or *scr-4* mutants, the percentage of cells in
458 G1 phase increased, indicating an extended G1 phase and delayed cell divisions in the SAM
459 (Fig.11S-U). Genetic analyses showed that *shr* mutants are epistatic to *scl23* mutants in double
460 mutant combinations, and that *scr-3; scl23-2* double mutants and *shr-2; scr-3; scl23-2* triple
461 mutants were additive with smaller plant rosettes and reduced plant stature (Suppl Fig. 14A-
462 H') (Yoon *et al.*, 2016). To further analyse *SCL23* function, we generated transgenic
463 Arabidopsis plants overexpressing *SCL23* from the *pUBIQ10* (*pUBIQ10:SCL23-mVenus*) or
464 *pRPS5A* (*pRPS5A*:*SCL23-mVenus*) promoter. Both *UBIQ10* and *RPS5A* promoters drive
465 high-level and widespread expression of the fused reporter gene. However, we observed
466 SCL23-mVenus fluorescence confined to the lateral organ primordia and not in the meristem
467 center, where endogenous SCL23 is normally expressed (Suppl Fig. 15C-D). We found a
468 similar scenario when we tried to overexpress *SHR* or *SCR* in the SAM (Suppl Fig. 15A-B),
469 implying tight regulatory controls acting in the different domains in the SAM preventing
470 excessive protein accumulation. However, excessive accumulation of these transcription
471 factors was observed outside their normal expression domains (Suppl Fig. 15A-E). We
472 propose that SCL23, SHR and SCR are under translational or post-translational control, for
473 example due to the localised presence of miRNAs (Llave *et al.*, 2002), and that meristem cells
474 can therefore express only a set maximum amount of these GRAS proteins. We also conclude
475 that SHR controls expression of both SCL23 and SCR in the periphery of the SAM.

476 **SCL23 acts together with WUS to maintain stem cell homeostasis in the SAM**

477 The *GRAS* family transcription factors HAM1 and HAM2 were shown to physically interact with
478 WUS to promote shoot stem cell proliferation and repress *CLV3* expression in the OC (Zhou
479 *et al.*, 2015). Since *SCL23* and *WUS* expression strongly overlap in the OC and rib meristem
480 (Fig. 12A-B and D-E), we asked if SCL23, like HAM1/2, could also interact with WUS. We
481 tested via FRET for *in vivo* interactions of WUS-FP and SCL23-FP fusions after inducible
482 transient expression in *Nicotiana benthamiana* leaves. SCL23-mVenus interacted with WUS-
483 mCherry with a FRET efficiency similar to the FRET-positive control, a nuclear localized
484 mVenus-mCherry fusion protein (Fig. 12C). SCL23 showed only a weak tendency to form
485 homomers, assayed by measuring FRET between SCL23-mVenus and SCL23-mCherry (Fig.
486 12C). SCL23-mVenus with the unrelated transcription factor AS2-mCherry served as negative
487 control (Fig. 12C). Given its interaction with WUS and its developmental role in the SAM, we
488 asked if SCL23 expression is also subject to regulation by the *CLV* signaling pathway. We first
489 observed the expression pattern of *SCL23* and *CLV3*. A dual reporter line with *pSCL23:SCL23-*
490 *YFP* and *pCLV3:NLS-mCherry* showed that *SCL23* and *CLV3* were expressed in largely
491 complementary patterns in the SAM (Fig. 12A-B and D-E). SCL23 was expressed in the rib
492 meristem, but absent from L1 and L2 layers in the meristem center, while *CLV3* is highly

493 expressed in the L1 and L2 layers and to a lesser level in the L3 layer (Fig. 12D-E). When
494 introduced into the *clv3-9* mutant background, *pSCL23:SCL23-YFP* expression was strongly
495 expanded and extended throughout the enlarged and sometimes fasciated meristems, similar
496 to the altered expression domain of *WUS* in strong *clv*-mutants (Fig. 12F-I). This supports the
497 hypothesis that *SCL23* expression is, like *WUS*, negatively regulated by the *CLV* signalling
498 pathway. To study the developmental role of *SCL23* and *WUS* interaction, we conducted
499 genetic interaction studies. While the SAM of *scl23-2* single mutant was smaller than WT (Fig.
500 11R), the null allele *wus-am* had terminated SAM development at an early seedling stage, but
501 continued to initiate new shoot meristems from axillary positions (Suppl Fig. 16C). The *wus-*
502 *am; scl23-2* double mutants showed an enhanced phenotype with earlier arrest of SAM
503 development (Suppl Fig. 16D). Hypomorphic *wus-7* mutants form inflorescence meristems
504 similar to WT (Suppl Fig. 16E,E',E'',F,F',F'',G,G' and G'') (Zhou et al., 2015), while *wus-7;*
505 *scl23-2* double mutants display premature termination of floral meristems (Fig. 15I- I'-I''). These
506 genetic data support our hypothesis that SCL23 and WUS function together in shoot meristem
507 stem cell maintenance. Taken together, the colocalization and interaction between SCL23 and
508 WUS along with the genetic data strongly suggest that SCL23 and WUS function as partners
509 in SAM maintenance.

510 ## Discussion

511 To better understand the mechanisms that form and maintain the multiple functional domains
512 within the SAM, we asked if the well-characterized SHR-SCR-SCL23-JKD gene regulatory
513 network responsible for ground tissue patterning in the RAM plays a similar role in the SAM.
514 (Scheres et al., 1995, Long et al., 2015a, Long et al., 2015b). Using quantitative live-cell
515 imaging together with molecular and genetic approaches, we found that all four TFs are
516 expressed in the SAM and together their expression covers all functional domains of the SAM
517 in a combination of complementary and overlapping domains. Auxin-triggered primordia
518 initiation in the peripheral zone of the SAM activates the SHR network, which promotes cell
519 cycle progression and, at the same time, communicates with the stem cell regulatory system
520 at the center of the meristem through direct interaction with the WUS-CLV3 feedback loop.

521 ### SHR, SCR, SCL23 and JKD control SAM size and organ primordia initiation.

522 Plants mutated in the three GRAS genes (*SHR*, *SCR* or *SCL23*) had smaller SAMs than the
523 WT caused by a decrease in cell proliferation (Fig. 1E-H, I-L and L-P; Fig. 11O-U). *shr* and *scr*
524 mutants also displayed a delay in primordia formation suggesting that the *SHR, SCR* and
525 *SCL23* genes promote proliferation of stem cells within the central zone and primordia initiation
526 at the peripheral zone (Fig. 1M; Suppl Fig. 1A'-D'). These findings are consistent with the
527 growth-promoting activities of *SHR* and *SCR* in leaves and roots (Dhondt *et al.*, 2010, Long et
528 al., 2015a, Scheres et al., 1995). In contrast, *jkd* mutants showed an increase in the SAM size
529 indicating that JKD might restrict growth in the shoot by interfering with the SHR-SCR
530 complexes, similar to what had been previously shown in roots (Fig. 6A-D) (Long et al., 2015b,
531 Welch et al., 2007).

532 ### Transcriptional profiles and interdependencies of SCR, SCL23 and JKD in the
533 SAM

534 Analysis of expression patterns showed that SHR, SCR, SCL23 and JKD are distributed across
535 all functional domains of the SAM, and mutant analyses suggest that the SHR network is
536 required for SAM function and organogenesis. We found both SHR and SCL23 to be mobile
537 in the SAM with SCL23 exhibiting hypermobility, moving from the center to the periphery of the
538 SAM, similar to what was previously shown in the RAM (Fig. 3C-D; Fig. 11A-F). SCL23 could
539 thereby mediate communication between the CZ and PZ, and coordinate stem cell proliferation
540 in the center with lateral organ formation at the periphery via the conserved SHR signalling
541 pathway. SHR acts as master regulator in the network, since all combinations between *shr,*
542 *scr* and *scl23* mutants displayed the *shr* phenotype (Suppl Fig. 14A-H') (Yoon et al., 2016).
543 Previous studies had shown that SCR and SCL23 restrict the mobility of SHR, probably by

544 complex formation, and both SCR and SCL23 are transcriptionally regulated by SHR in the
545 RAM. Similarly, we found here that the expression of *SCR* and *SCL23* was down-regulated in
546 the *shr* mutant organ primordia (Fig. 5D-E and H-I; Fig. 11M-N) and SHR is more restricted to
547 the nucleus in the presence of SCR compared to its absence (Fig. 5A, 5A inset and F). This
548 could be explained by the nuclear retention of SHR through its interaction with SCR to restrict
549 SHR movement and activate SCR expression. Together, these results suggest that SHR
550 regulates the expression of SCR and SCL23, which in turn restrict SHR mobility. SCL23 and
551 SCR have been previously shown to function in a mutually antagonistic manner in the RAM
552 and act redundantly to specify endodermal cell fate (Kim et al., 2017, Long et al., 2015a). Our
553 data also showed that the expression patterns of SCL23 and SCR are complementary in the
554 center of the SAM, but overlap in the primordia where SHR and JKD are also expressed (Fig.
555 6I; Fig. 11G- K).

556 **SHR, SCR, SCL23 and JKD interact to form protein complexes in the SAM**

557 In root CEI, a SHR-SCR-JKD complex controls the expression of CYCD6;1 (Suppl Fig. 17A-G
558 arrow heads) and triggers an asymmetric cell division that leads to the formation of endodermis
559 and cortex (Cui et al., 2007, Sozzani *et al.*, 2010, Long et al., 2015b, Long et al., 2017). Using
560 *in vivo* FRET-FLIM, we now showed that SHR, SCR and JKD physically interact in the SAM
561 (Fig. 4E-F; Fig. 6H). Furthermore, expression analysis of targets of the SHR-SCR-JKD
562 complex demonstrates that CYCD6;1 expression perfectly overlaps with that of SHR, SCR and
563 JKD in the inner cells of the lateral primordia (Fig. 7J-L). *shr* mutants showed a down-regulation
564 of *CYCD6;1* and a decrease in the number of cell layers at the PZ (Fig. 7A-I). We conclude
565 that the SHR-SCR-SCL23-JKD complex acts as a positive regulator of cell proliferation within
566 the PZ leading to lateral organ initiation and outgrowth.

567 **SHR regulates the initiation of flower primordia in an auxin dependent manner**

568 The expression patterns of SHR closely resemble that of PIN1 and MP during organ primordia
569 development, and also in the RAM (Fig. 3C; Suppl Fig. 6A-C and E-F). We now show that SHR
570 expression responds to changes in auxin distribution in the SAM and that the addition of
571 exogenous synthetic auxin enhances its expression (Fig. 8A-D and H-K). Moreover, we found
572 that MP-mediated auxin signalling positively regulates *SHR* expression (Fig. 9A-F and K-P).
573 SHR has been previously proposed to be a putative downstream target of MP, as SHR
574 expression was found to be down regulated in *mp* mutant embryo (Möller et al., 2017). Our
575 genetic and expression analysis now revealed that MP is a direct regulator of SHR expression.
576 The two AuxRE motifs in the *SHR* promoter were found to be essential for the response to MP
577 in our transient expression experiments (Suppl Fig. 8A-J; Suppl Fig. 9A-J; Suppl Fig.10A-H).

578 These results suggest that the AuxRE motifs enable auxin-mediated regulation of *SHR*
579 expression and both motifs have roughly equal contribution in this transcriptional regulation.
580 Thus, the SHR network regulates organogenesis in the SAM downstream of MP in response
581 to auxin accumulation at the meristem periphery, and thereby plays a crucial role for lateral
582 organ formation. Moreover, the altered expression of both *pDR5v2:3xYFP-N7* and R2D2 auxin
583 reporters in *shr* and *scr* mutants (Fig. 2A-G) with fewer auxin maxima indicates that *SHR* and
584 *SCR* contribute to a positive feed-back loop with auxin.

585 **A WUS-SCL23 heteromeric complex maintains the stem cell niche in the SAM**

586 Unlike the other genes in the SHR network, *SCL23* was expressed in a broad pattern in the
587 OC, PZ and in lateral organ primordia (Fig. 11A-D). SCL23 overlapped with WUS expression
588 in the OC, but is excluded from the CZ (Fig. 12D-E). WUS protein migrates from the OC to the
589 CZ where stem cells are located and activates the expression of its negative regulator CLV3
590 (Daum et al., 2014, Yadav et al., 2011). The resulting WUS-CLV3 negative feedback loop
591 maintains the balance between stem cell numbers at the CZ and differentiation rates of stem
592 cell descendents at the PZ (Daum et al., 2014). Null mutations in *WUS* cause premature
593 termination of the SAM (Suppl Fig. 16C) (Laux et al., 1996). Two GRAS TFs, HAM1 and HAM2,
594 are expressed in the OC, physically interact with WUS and inhibit WUS from activating *CLV3*
595 expression in the OC. At the meristem tip and in the CZ, *HAM1* and *HAM2* transcripts are
596 downregulated due to miRNA171, which is expressed from the L1 and diffuses downward into
597 deeper meristem layers. In consequence, WUS lacks its binding partners HAM1 and HAM2
598 only in the top layers of the meristem where miRNA171 levels are high, and WUS can then
599 promote stem cell fate and activate CLV3 expression (Zhou et al., 2015, Zhou et al., 2018).
600 SCL23 physically interacts with WUS, and SAMs lacking SCL23 activity are smaller, indicating
601 that the SCL23-WUS complexes promote stem cell activity (Fig. 11R and Fig. 12C;). However,
602 SCL23 appears to lack the recognition sequences for regulation by miRNA171, but is itself
603 transcriptionally regulated by CLV3 signalling. Thus, two types of GRAS transcription factors
604 modulate WUS activity: (i) the HAMs, due to their regulation by miRNA171, position the domain
605 of WUS activity relative to the SAM surface (L1); (ii) SCL23 sets the WUS domain in relation
606 to the CLV3 domain and, since SCL23 is regulated by the auxin-controlled SHR network, in
607 relation to lateral organ primordia formation in the PZ.
608

609 **A SHR-SCR-SCL23-JKD regulatory network coordinates SAM activities**

610 We propose that a gene regulatory network consisting of mobile transcription factors, together
611 with auxin, controls SAM functions (Fig. 13A-B). *SCL23* gene expression is confined by CLV3

signalling to the OC, where SCL23 forms a complex with WUS to maintain stem cell homeostasis. SCL23 might work in a similar way as its closest homologues, the HAM proteins, which act as WUS partners to control shoot stem cell proliferation. The hypermobile SCL23 protein acts as a signal from the OC to the PZ (Fig. 13B). In the PZ, auxin promotes SHR expression via MP. SHR then physically interacts with SCR, SCL23 and JKD to activate the expression of *CYCD6;1* and promote cell division, leading to lateral organ primordia outgrowth.

Acknowledgements

We thank Jan Lohmann, Dolf Weijers, Francois Parcy and Doris Wagner for providing seeds. We are also grateful to the CAi team at HHU, especially Sebastian Hänsch for support with imaging methods, and Patrick Blümke, Jan Maika, Jenia Schlegel, Maike Breiden, Meik Thiele, Karine Gustavo Pinto, Svenja Augustin, Carin Theres, Silke Winters, Vivien Strotmann, Rebecca Drisch, Madhumita Narasimhan, Vicky Howe, Pavithran Narayanan and Cornelia Gieseler for diverse contributions.

Research in the lab of R.Simon is supported by the DFG through the Cluster of Excellence on Plant Sciences (CEPLAS, EXC2048), CRC1208 and RTG CSCS.

Research in the lab of Crisanto Gutierrez is supported by the Grant ERC-2018-AdG_833617 (European Union, H2020) and Grant RTI2018-094793-B-I00 (from Spanish Ministry of Science and Innovation, and FEDER).

632 **References**

633 Barbier de Reuille, P., Routier-Kierzkowska, A. L., Kierzkowski, D., Bassel, G. W., Schüpbach,
634 T., Tauriello, G.*, et al.* (2015) MorphoGraphX: A platform for quantifying morphogenesis
635 in 4D. *Elife,* **4,** 05864.
636 Benková, E., Michniewicz, M., Sauer, M., Teichmann, T., Seifertová, D., Jürgens, G.*, et al.*
637 (2003) Local, efflux-dependent auxin gradients as a common module for plant organ
638 formation. *Cell,* **115,** 591-602.
639 Berleth, T. and Jürgens, G. (1993) The role of the monopteros gene in organising the basal
640 body region of the Arabidopsis embryo. *Development,* **118,** 575-587.
641 Bhatia, N., Bozorg, B., Larsson, A., Ohno, C., Jönsson, H. and Heisler, M. G. (2016) Auxin
642 Acts through MONOPTEROS to Regulate Plant Cell Polarity and Pattern Phyllotaxis.
643 *Curr Biol,* **26,** 3202-3208.
644 Bleckmann, A. and Simon, R. (2009) Interdomain signaling in stem cell maintenance of plant
645 shoot meristems. *Mol Cells,* **27,** 615-620.
646 Boer, D. R., Freire-Rios, A., van den Berg, W. A., Saaki, T., Manfield, I. W., Kepinski, S.*, et al.*
647 (2014) Structural basis for DNA binding specificity by the auxin-dependent ARF
648 transcription factors. *Cell,* **156,** 577-589.
649 Brand, U., Fletcher, J. C., Hobe, M., Meyerowitz, E. M. and Simon, R. (2000) Dependence of
650 stem cell fate in Arabidopsis on a feedback loop regulated by CLV3 activity. *Science,*
651 **289,** 617-619.
652 Clark, S. E., Williams, R. W. and Meyerowitz, E. M. (1997) The CLAVATA1 gene encodes a
653 putative receptor kinase that controls shoot and floral meristem size in Arabidopsis.
654 *Cell,* **89,** 575-585.
655 Clough, S. J. and Bent, A. F. (1998) Floral dip: a simplified method for Agrobacterium-mediated
656 transformation of Arabidopsis thaliana. *Plant J,* **16,** 735-743.
657 Cui, H., Kong, D., Liu, X. and Hao, Y. (2014) SCARECROW, SCR-LIKE 23 and SHORT-ROOT
658 control bundle sheath cell fate and function in Arabidopsis thaliana. *Plant J,* **78,** 319-
659 327.
660 Cui, H., Levesque, M. P., Vernoux, T., Jung, J. W., Paquette, A. J., Gallagher, K. L.*, et al.*
661 (2007) An evolutionarily conserved mechanism delimiting SHR movement defines a
662 single layer of endodermis in plants. *Science,* **316,** 421-425.
663 Czechowski, T., Stitt, M., Altmann, T., Udvardi, M. K. and Scheible, W. R. (2005) Genome-
664 wide identification and testing of superior reference genes for transcript normalization
665 in Arabidopsis. *Plant Physiol,* **139,** 5-17.
666 Daum, G., Medzihradszky, A., Suzaki, T. and Lohmann, J. U. (2014) A mechanistic framework
667 for noncell autonomous stem cell induction in Arabidopsis. *Proc Natl Acad Sci U S A,*
668 **111,** 14619-14624.

669 Desvoyes, B., Arana-Echarri, A., Barea, M. D. and Gutierrez, C. (2020) A comprehensive
670 fluorescent sensor for spatiotemporal cell cycle analysis in Arabidopsis. *Nat Plants,* **6,**
671 1330-1334.
672 Dewitte, W., Riou-Khamlichi, C., Scofield, S., Healy, J. M., Jacqmard, A., Kilby, N. J.*, et al.*
673 (2003) Altered cell cycle distribution, hyperplasia, and inhibited differentiation in
674 Arabidopsis caused by the D-type cyclin CYCD3. *Plant Cell,* **15,** 79-92.
675 Dhondt, S., Coppens, F., De Winter, F., Swarup, K., Merks, R. M., Inzé, D.*, et al.* (2010)
676 SHORT-ROOT and SCARECROW regulate leaf growth in Arabidopsis by stimulating
677 S-phase progression of the cell cycle. *Plant Physiol,* **154,** 1183-1195.
678 Di Laurenzio, L., Wysocka-Diller, J., Malamy, J. E., Pysh, L., Helariutta, Y., Freshour, G.*, et al.*
679 (1996) The SCARECROW gene regulates an asymmetric cell division that is essential
680 for generating the radial organization of the Arabidopsis root. *Cell,* **86,** 423-433.
681 Fletcher, J. C., Brand, U., Running, M. P., Simon, R. and Meyerowitz, E. M. (1999) Signaling
682 of cell fate decisions by CLAVATA3 in Arabidopsis shoot meristems. *Science,* **283,**
683 1911-1914.
684 Friml, J., Yang, X., Michniewicz, M., Weijers, D., Quint, A., Tietz, O.*, et al.* (2004) A PINOID-
685 dependent binary switch in apical-basal PIN polar targeting directs auxin efflux.
686 *Science,* **306,** 862-865.
687 Fukaki, H., Wysocka-Diller, J., Kato, T., Fujisawa, H., Benfey, P. N. and Tasaka, M. (1998)
688 Genetic evidence that the endodermis is essential for shoot gravitropism in Arabidopsis
689 thaliana. *Plant J,* **14,** 425-430.
690 Gälweiler, L., Guan, C., Müller, A., Wisman, E., Mendgen, K., Yephremov, A.*, et al.* (1998)
691 Regulation of polar auxin transport by AtPIN1 in Arabidopsis vascular tissue. *Science,*
692 **282,** 2226-2230.
693 Gardiner, J., Donner, T. J. and Scarpella, E. (2011) Simultaneous activation of SHR and
694 ATHB8 expression defines switch to preprocambial cell state in Arabidopsis leaf
695 development. *Dev Dyn,* **240,** 261-270.
696 Graf, P., Dolzblasz, A., Würschum, T., Lenhard, M., Pfreundt, U. and Laux, T. (2010) MGOUN1
697 encodes an Arabidopsis type IB DNA topoisomerase required in stem cell regulation
698 and to maintain developmentally regulated gene silencing. *Plant Cell,* **22,** 716-728.
699 Han, H., Geng, Y., Guo, L., Yan, A., Meyerowitz, E. M., Liu, X.*, et al.* (2020) The Overlapping
700 and Distinct Roles of HAM Family Genes in Arabidopsis Shoot Meristems. *Front Plant*
701 *Sci,* **11,** 541968.
702 Hardtke, C. S. and Berleth, T. (1998) The Arabidopsis gene MONOPTEROS encodes a
703 transcription factor mediating embryo axis formation and vascular development. *Embo*
704 *j,* **17,** 1405-1411.

705 Heisler, M. G., Ohno, C., Das, P., Sieber, P., Reddy, G. V., Long, J. A.*, et al.* (2005) Patterns
706 of auxin transport and gene expression during primordium development revealed by
707 live imaging of the Arabidopsis inflorescence meristem. *Curr Biol,* **15,** 1899-1911.
708 Helariutta, Y., Fukaki, H., Wysocka-Diller, J., Nakajima, K., Jung, J., Sena, G.*, et al.* (2000)
709 The SHORT-ROOT gene controls radial patterning of the Arabidopsis root through
710 radial signaling. *Cell,* **101,** 555-567.
711 Lampropoulos, A., Sutikovic, Z., Wenzl, C., Maegele, I., Lohmann, J. U. and Forner, J. (2013)
712 GreenGate---a novel, versatile, and efficient cloning system for plant transgenesis.
713 *PLoS One,* **8,** e83043.
714 Laux, T., Mayer, K. F., Berger, J. and Jürgens, G. (1996) The WUSCHEL gene is required for
715 shoot and floral meristem integrity in Arabidopsis. *Development,* **122,** 87-96.
716 Lee, M. H., Kim, B., Song, S. K., Heo, J. O., Yu, N. I., Lee, S. A.*, et al.* (2008) Large-scale
717 analysis of the GRAS gene family in Arabidopsis thaliana. *Plant Mol Biol,* **67,** 659-670.
718 Liao, C. Y., Smet, W., Brunoud, G., Yoshida, S., Vernoux, T. and Weijers, D. (2015) Reporters
719 for sensitive and quantitative measurement of auxin response. *Nat Methods,* **12,** 207-
720 210, 202 p following 210.
721 Llave, C., Xie, Z., Kasschau, K. D. and Carrington, J. C. (2002) Cleavage of Scarecrow-like
722 mRNA targets directed by a class of Arabidopsis miRNA. *Science,* **297,** 2053-2056.
723 Long, Y., Goedhart, J., Schneijderberg, M., Terpstra, I., Shimotohno, A., Bouchet, B. P.*, et al.*
724 (2015a) SCARECROW-LIKE23 and SCARECROW jointly specify endodermal cell fate
725 but distinctly control SHORT-ROOT movement. *Plant J,* **84,** 773-784.
726 Long, Y., Smet, W., Cruz-Ramírez, A., Castelijns, B., de Jonge, W., Mähönen, A. P.*, et al.*
727 (2015b) Arabidopsis BIRD Zinc Finger Proteins Jointly Stabilize Tissue Boundaries by
728 Confining the Cell Fate Regulator SHORT-ROOT and Contributing to Fate
729 Specification. *Plant Cell,* **27,** 1185-1199.
730 Long, Y., Stahl, Y., Weidtkamp-Peters, S., Postma, M., Zhou, W., Goedhart, J.*, et al.* (2017)
731 In vivo FRET-FLIM reveals cell-type-specific protein interactions in Arabidopsis roots.
732 *Nature,* **548,** 97-102.
733 Mayer, K. F., Schoof, H., Haecker, A., Lenhard, M., Jürgens, G. and Laux, T. (1998) Role of
734 WUSCHEL in regulating stem cell fate in the Arabidopsis shoot meristem. *Cell,* **95,** 805-
735 815.
736 Mockaitis, K. and Estelle, M. (2008) Auxin receptors and plant development: a new signaling
737 paradigm. *Annu Rev Cell Dev Biol,* **24,** 55-80.
738 Möller, B. K., Ten Hove, C. A., Xiang, D., Williams, N., López, L. G., Yoshida, S.*, et al.* (2017)
739 Auxin response cell-autonomously controls ground tissue initiation in the early
740 Arabidopsis embryo. *Proc Natl Acad Sci U S A,* **114,** E2533-e2539.

741 Nakajima, K., Sena, G., Nawy, T. and Benfey, P. N. (2001) Intercellular movement of the
742 putative transcription factor SHR in root patterning. *Nature,* **413,** 307-311.
743 Nimchuk, Z. L., Zhou, Y., Tarr, P. T., Peterson, B. A. and Meyerowitz, E. M. (2015) Plant stem
744 cell maintenance by transcriptional cross-regulation of related receptor kinases.
745 *Development,* **142,** 1043-1049.
746 Ohyama, K., Shinohara, H., Ogawa-Ohnishi, M. and Matsubayashi, Y. (2009) A glycopeptide
747 regulating stem cell fate in Arabidopsis thaliana. *Nat Chem Biol,* **5,** 578-580.
748 Paque, S. and Weijers, D. (2016) Q&A: Auxin: the plant molecule that influences almost
749 anything. *BMC Biol,* **14,** 67.
750 Pfaffl, M. W. (2001) A new mathematical model for relative quantification in real-time RT-PCR.
751 *Nucleic Acids Res,* **29,** e45.
752 Pysh, L. D., Wysocka-Diller, J. W., Camilleri, C., Bouchez, D. and Benfey, P. N. (1999) The
753 GRAS gene family in Arabidopsis: sequence characterization and basic expression
754 analysis of the SCARECROW-LIKE genes. *Plant J,* **18,** 111-119.
755 Reddy, G. V., Heisler, M. G., Ehrhardt, D. W. and Meyerowitz, E. M. (2004) Real-time lineage
756 analysis reveals oriented cell divisions associated with morphogenesis at the shoot
757 apex of Arabidopsis thaliana. *Development,* **131,** 4225-4237.
758 Scheres, B., Di Laurenzio, L., Willemsen, V., Hauser, M.-T., Janmaat, K., Weisbeek, P.*, et al.*
759 (1995) Mutations affecting the radial organisation of the Arabidopsis root display
760 specific defects throughout the embryonic axis. *Development,* **121,** 53-62.
761 Schlegel, J., Denay, G., Wink, R. H., Pinto, K. G., Stahl, Y., Schmid, J.*, et al.* (2021) Control of
762 Arabidopsis shoot stem cell homeostasis by two antagonistic CLE peptide signalling
763 pathways. *Elife,* **10**.
764 Schlereth, A., Möller, B., Liu, W., Kientz, M., Flipse, J., Rademacher, E. H.*, et al.* (2010)
765 MONOPTEROS controls embryonic root initiation by regulating a mobile transcription
766 factor. *Nature,* **464,** 913-916.
767 Schneider, C. A., Rasband, W. S. and Eliceiri, K. W. (2012) NIH Image to ImageJ: 25 years of
768 image analysis. *Nat Methods,* **9,** 671-675.
769 Schoof, H., Lenhard, M., Haecker, A., Mayer, K. F., Jürgens, G. and Laux, T. (2000) The stem
770 cell population of Arabidopsis shoot meristems in maintained by a regulatory loop
771 between the CLAVATA and WUSCHEL genes. *Cell,* **100,** 635-644.
772 Schultz, E. A. and Haughn, G. W. (1991) LEAFY, a Homeotic Gene That Regulates
773 Inflorescence Development in Arabidopsis. *Plant Cell,* **3,** 771-781.
774 Sozzani, R., Cui, H., Moreno-Risueno, M. A., Busch, W., Van Norman, J. M., Vernoux, T.*, et*
775 *al.* (2010) Spatiotemporal regulation of cell-cycle genes by SHORTROOT links
776 patterning and growth. *Nature,* **466,** 128-132.

Ubeda-Tomás, S., Federici, F., Casimiro, I., Beemster, G. T., Bhalerao, R., Swarup, R.*, et al.* (2009) Gibberellin signaling in the endodermis controls Arabidopsis root meristem size. *Curr Biol,* **19,** 1194-1199.

Ulmasov, T., Hagen, G. and Guilfoyle, T. J. (1999) Dimerization and DNA binding of auxin response factors. *Plant J,* **19,** 309-319.

Vernoux, T., Brunoud, G., Farcot, E., Morin, V., Van den Daele, H., Legrand, J.*, et al.* (2011a) The auxin signalling network translates dynamic input into robust patterning at the shoot apex. *Molecular systems biology,* **7,** 508.

Vernoux, T., Brunoud, G., Farcot, E., Morin, V., Van den Daele, H., Legrand, J.*, et al.* (2011b) The auxin signalling network translates dynamic input into robust patterning at the shoot apex. *Mol Syst Biol,* **7,** 508.

Wang, J., Andersson-Gunnerås, S., Gaboreanu, I., Hertzberg, M., Tucker, M. R., Zheng, B.*, et al.* (2011) Reduced expression of the SHORT-ROOT gene increases the rates of growth and development in hybrid poplar and Arabidopsis. *PLoS One,* **6,** e28878.

Weigel, D., Alvarez, J., Smyth, D. R., Yanofsky, M. F. and Meyerowitz, E. M. (1992) LEAFY controls floral meristem identity in Arabidopsis. *Cell,* **69,** 843-859.

Welch, D., Hassan, H., Blilou, I., Immink, R., Heidstra, R. and Scheres, B. (2007) Arabidopsis JACKDAW and MAGPIE zinc finger proteins delimit asymmetric cell division and stabilize tissue boundaries by restricting SHORT-ROOT action. *Genes Dev,* **21,** 2196-2204.

Wu, M. F., Yamaguchi, N., Xiao, J., Bargmann, B., Estelle, M., Sang, Y.*, et al.* (2015) Auxin-regulated chromatin switch directs acquisition of flower primordium founder fate. *Elife,* **4,** e09269.

Wu, X., Dinneny, J. R., Crawford, K. M., Rhee, Y., Citovsky, V., Zambryski, P. C.*, et al.* (2003) Modes of intercellular transcription factor movement in the Arabidopsis apex. *Development,* **130,** 3735-3745.

Wysocka-Diller, J. W., Helariutta, Y., Fukaki, H., Malamy, J. E. and Benfey, P. N. (2000) Molecular analysis of SCARECROW function reveals a radial patterning mechanism common to root and shoot. *Development,* **127,** 595-603.

Xu, J., Hofhuis, H., Heidstra, R., Sauer, M., Friml, J. and Scheres, B. (2006) A molecular framework for plant regeneration. *Science,* **311,** 385-388.

Yadav, R. K., Perales, M., Gruel, J., Girke, T., Jönsson, H. and Reddy, G. V. (2011) WUSCHEL protein movement mediates stem cell homeostasis in the Arabidopsis shoot apex. *Genes Dev,* **25,** 2025-2030.

Yamaguchi, N., Wu, M. F., Winter, C. M., Berns, M. C., Nole-Wilson, S., Yamaguchi, A.*, et al.* (2013) A molecular framework for auxin-mediated initiation of flower primordia. *Dev Cell,* **24,** 271-282.

814 Yoon, E. K., Dhar, S., Lee, M. H., Song, J. H., Lee, S. A., Kim, G.*, et al.* (2016) Conservation
815 and Diversification of the SHR-SCR-SCL23 Regulatory Network in the Development of
816 the Functional Endodermis in Arabidopsis Shoots. *Mol Plant,* **9,** 1197-1209.
817 Zhang, Z., Tucker, E., Hermann, M. and Laux, T. (2017) A Molecular Framework for the
818 Embryonic Initiation of Shoot Meristem Stem Cells. *Dev Cell,* **40,** 264-277.e264.
819 Zhao, Z., Andersen, S. U., Ljung, K., Dolezal, K., Miotk, A., Schultheiss, S. J.*, et al.* (2010)
820 Hormonal control of the shoot stem-cell niche. *Nature,* **465,** 1089-1092.
821 Zhou, Y., Liu, X., Engstrom, E. M., Nimchuk, Z. L., Pruneda-Paz, J. L., Tarr, P. T.*, et al.* (2015)
822 Control of plant stem cell function by conserved interacting transcriptional regulators.
823 *Nature,* **517,** 377-380.
824 Zhou, Y., Yan, A., Han, H., Li, T., Geng, Y., Liu, X.*, et al.* (2018) HAIRY MERISTEM with
825 WUSCHEL confines CLAVATA3 expression to the outer apical meristem layers.
826 *Science,* **361,** 502-506.

827

828

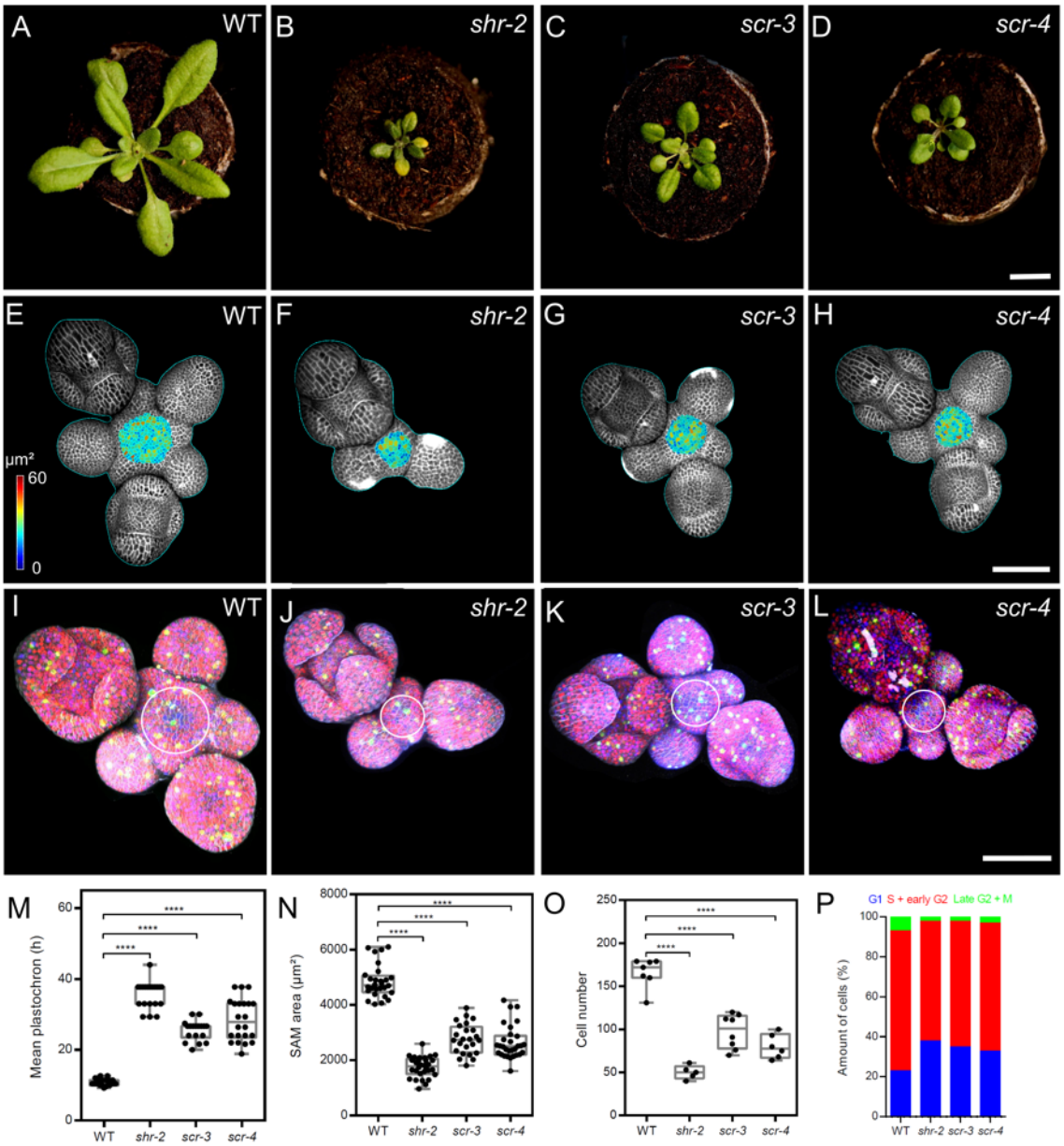

Fig. 1: The *shr* and *scr* mutant phenotypes

(A-D) Top view of 21-day-old rosettes from WT (col-0) **(A)**, *shr-2* mutant **(B)**, *scr-3* mutant **(C)** and *scr-4* mutant **(D)**. Scale bar represents 1cm. **(E-H)** Heat-map quantification of the cell area in the meristem region at 5 weeks after germination from WT (n=7) **(E)**, *shr-2* mutant (n=5) **(F)**, *scr-3* mutant (n=8) **(G)** and *scr-4* mutant (n=6) **(G)**. Cell walls were stained with PI (gray). Scale bar represents 50 µm. **(I-L)** Representative 3D projection of shoot apical meristems at 5 weeks after germination expressing the three PlaCCI markers: *pCDT1a:CDT1a-eCFP* (blUE), *pHTR13:pHTR13-mCherry* (red), and *pCYCB1;1:NCYCB1;1-YFP* (green) in WT (n=11) **(I)**, *shr-2* mutant (n=4) **(J)**, *scr-3* mutant (n=7) **(K)** and *scr-4* mutant (n=6) **(L)**. White circles in **(I)**, **(J)**, **(K)** and **(L)** mark the meristem region. Cell walls were stained with DAPI (gray). Scale bar represents 50 µm. **(M)** Quantification of shoot apical meristem size at 5 weeks after

germination from WT (n=28), *shr-2* mutant (n=30), *scr-3* mutant (n=24) and *scr-4* mutant (n=30). **(N)** Mean inflorescence plastochron in WT (n=21), *shr-2* mutant (n=20), *scr-3* mutant (n=18), and *scr-4* mutant (n=22). **(O)** Quantification of epidermal cell number in the meristem region of WT (n=11), *shr-2* mutant (n=4), *scr-3* mutant (n=7) and *scr-4* mutant (n=6). **(P)** Quantification of cells in different cell cycle phases in the meristem region (area surrounded by white circles in **(I)**, **(J)**, **(K)** and **(L)**) of WT (n=11), *shr-2* mutant (n=4), *scr-3* mutant (n=7) and *scr-4* mutant (n=6). Asterisks indicate a significant difference (****$p < 0.0001$: Statistically significant differences were determined by Student's *t*-test).

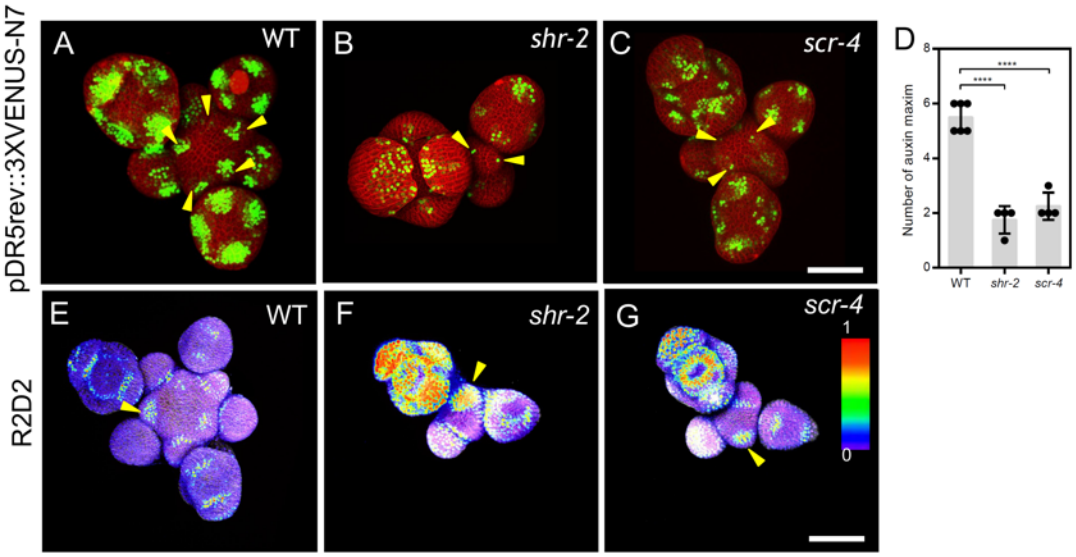

850

851 **Fig. 2: SHR and SCR functions modulate auxin signalling in the shoot apical meristem**

852 **(A-C)** Representative 3D projection of shoot apical meristems at 5 weeks after germination
853 expressing the auxin response reporter *pDR5rev:3XVENUS-N7* in WT (Col-0) (n=6) **(A)**, *shr-*
854 *2* mutant (n=4) **(B)** and *scr-4* mutant (n=4) **(C)**. Yellow arrowheads in **(A)**, **(B)** and **(C)** show
855 primordia with pDR5rev:3XVENUS-N7 expression. Cell walls were stained with PI (red). Scale
856 bar represents 50 µm. **(D)** Quantification of auxin maxima in WT (n=6), *shr-2* mutant (n=4) and
857 *scr-4* mutant (n=4). **(E-G)** Representative 3D projection of shoot apical meristems at 5 weeks
858 after germination expressing the auxin input sensor R2D2 showing DII/mDII ratio intensity in
859 WT (Col-0) (n=11) **(E)**, *shr-2* mutant (n=9) **(F)** and *scr-4* mutant (n=6) **(G)**. Yellow arrowheads
860 in **(E)**, **(F)** and **(G)** show primordia with low auxin. Cell walls were stained with DAPI (gray).
861 Scale bars represents 50 µm. Asterisks indicate a significant difference (****$p < 0.0001$:
862 Statistically significant differences were determined by Student's *t*-test). Error bars display SD.

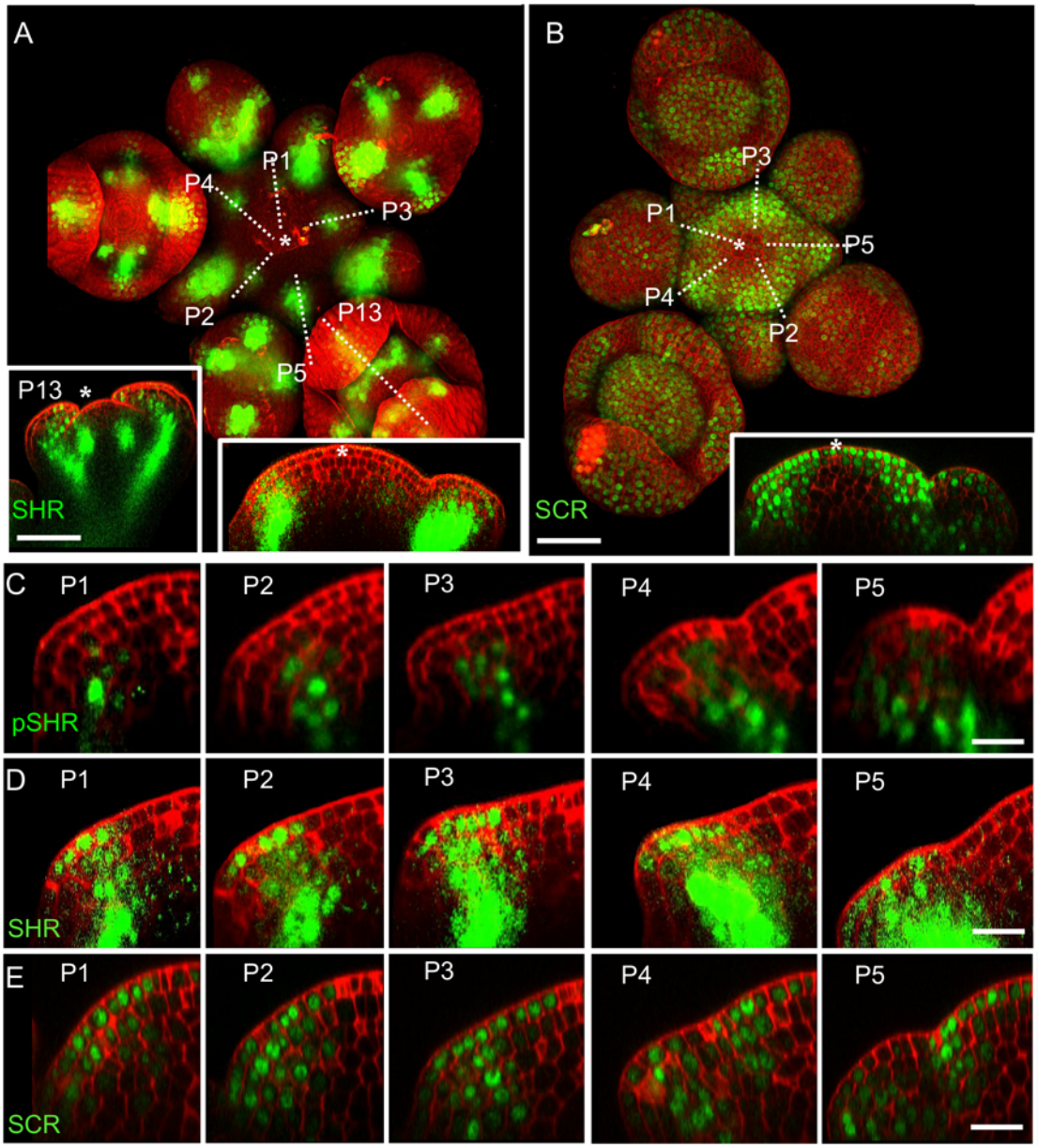

Fig. 3: Expression patterns of SHR and SCR in the shoot apical meristem

(A) Representative 3D projection of SAM at 5 weeks after germination expressing *pSHR:YFP-SHR* reporter (green) (n=30). The lower right inset shows a longitudinal optical section through the middle of the SAM. The lower left inset shows a longitudinal optical section through the middle of primordia 13 (representative section orientation shown by dotted line). Cell walls were stained with DAPI (red). Scale bar represents 50 µm. **(B)** Representative 3D projection of SAM at 5 weeks after germination expressing *pSCR:SCR-YFP* reporter (green) (n=25). The lower right inset shows longitudinal optical section through the middle of the SAM. Cell walls were stained with PI (red). Scale bars represent 50 µm. **(C)** Longitudinal optical sections through the middle of five successive primordia expressing *pSHR:ntdTomato* reporter (green) (representative section orientation shown by dotted line in Suppl Fig. 2A). Cell walls were

875 stained with DAPI (red). Scale bar represents 20 µm. **(D and E)** Longitudinal optical sections
876 through the middle of five successive primordia expressing *pSHR:YFP-SHR* reporter (green)
877 **(C)** and *pSCR:SCR-YFP* reporter (green) **(D)** (representative section orientation shown by
878 dotted line in **(A)** and **(B)**, respectively). Scale bars represent 20 µm. P= Primordium.
879

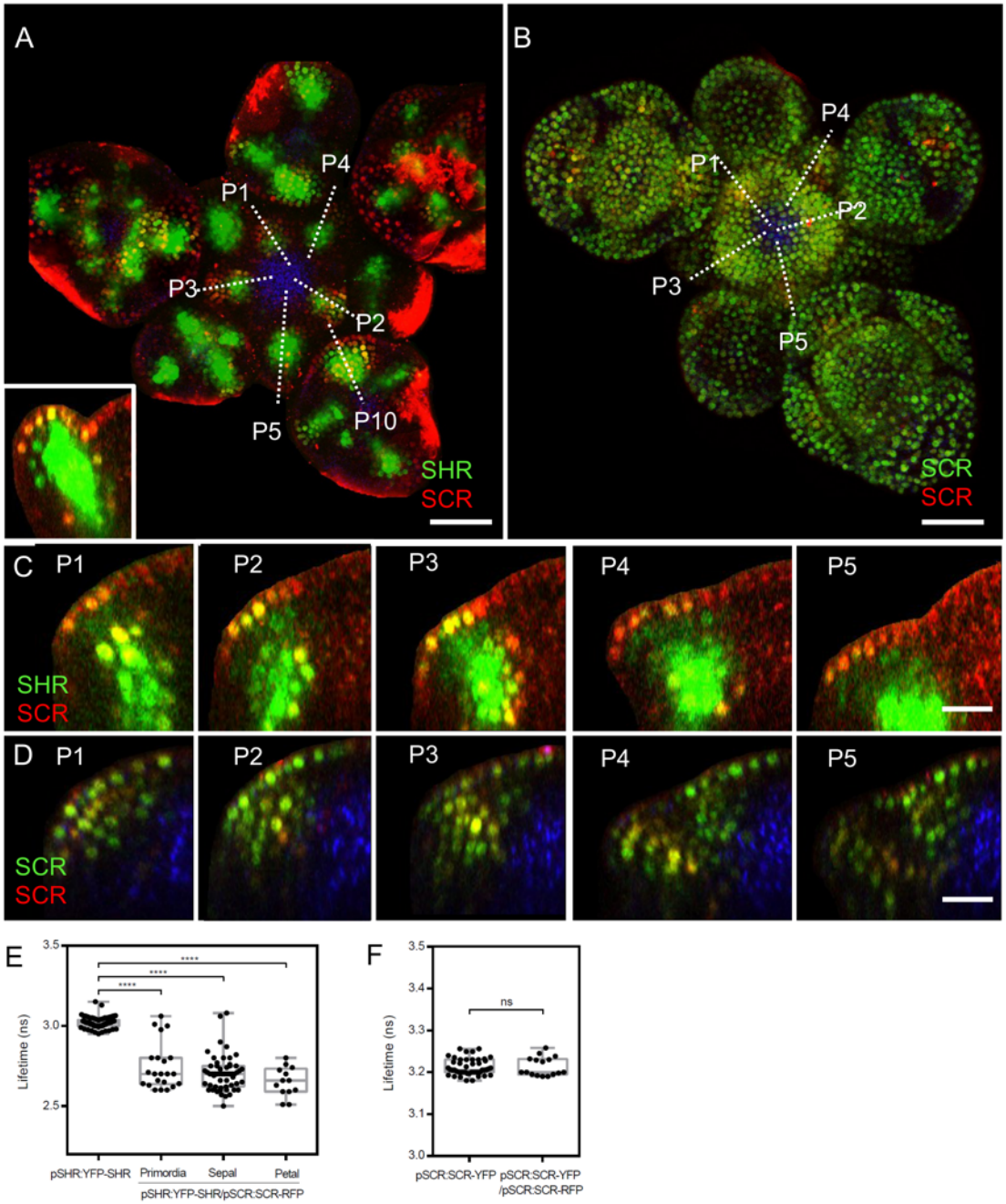

Fig. 4: *In vivo* FRET–FLIM quantification of SHR-SCR association in the SAM

(A-B) Representative 3D projection of SAM at 5 weeks after germination coexpressing *pSHR:YFP-SHR* reporter (green) and *pSCR:SCR-RFP* reporter (red) (n=17) **(A)** (the lower left inset shows a longitudinal optical section through the middle of primordia 10; representative section orientation shown by dotted line) and *pSCR::SCR:YFP* reporter (green) and *pSCR::SCR:RFP* reporter (red) (n=11) **(B)**. Chlorophyll (blue). Scale bars represent 50 µm. **(C-D)** Longitudinal optical sections through the middle of five successive primordia coexpressing *pSHR:YFP-SHR* reporter (green) and *pSCR:SCR-RFP* reporter (red) **(C)**, and

890 *pSCR::SCR:YFP* reporter (green) and *pSCR::SCR:RFP* reporter (red) **(D)** (representative
891 section orientation shown by dotted line in **(A)** and **(B)** respectively). Chlorophyll (blue). Scale
892 bars represent 20 µm. **(E)** Average lifetime of YFP-SHR when expressed alone (pSHR:YFP-
893 SHR (*n* =75)), or coexpressed together with SCR-RFP (pSHR:YFP-SHR/pSCR:SCR-RFP) in
894 lateral organ primordia (n=22), sepal primordia (n=55) and petal primordia (n=13). **(F)** Average
895 lifetime of SCR-YFP when expressed alone (pSCR:SCR-YFP), or coexpressed together with
896 SCR-RFP (pSCR:SCR-YFP/pSCR:SCR-RFP). Asterisks indicate a significant difference (****p
897 < 0.0001: Statistically significant differences were determined by Student's *t*-test, ns= no
898 significant difference). P= primordium.

899

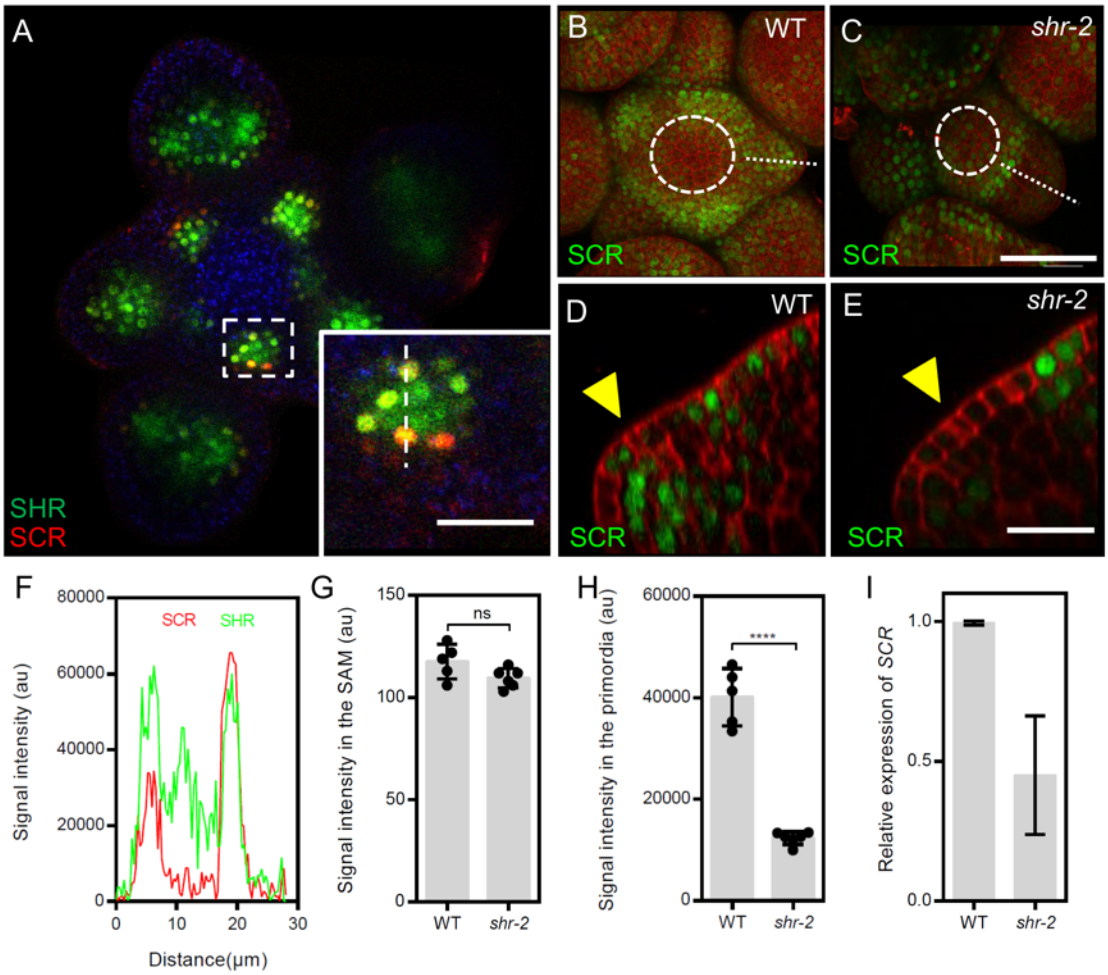

Fig. 5: SHR regulates *SCR* expression in the SAM

(A) Representative transversal confocal image of SAM at 5 weeks after germination coexpressing the *pSHR:SHR-YFP* reporter (green) and the *pSCR:SCR-RFP* reporter (red) (n=5). Chlorophyll (blue). The lower right inset shows an optical section view with high magnification of the area surrounded by white dashed rectangle in **(A)**. Scale bar represents 50 μm. **(B and C)** Representative 3D projection of SAM at 5 weeks after germination expressing the *pSCR:SCR-YFP* reporter (green) in WT (n=16) **(B)** and *shr-2* mutant (n=10) **(C)**. Cell walls were stained with PI (red). Scale bar represents 50 μm. **(D and E)** Longitudinal optical sections through the middle of primordia shown by dotted line in **(B)** and **(C)** respectively. Yellow arrowheads in **(D)** and **(E)** show primordia with SCR-YFP expression. Scale bar represents 20 μm. **(F)** Intensity plot profile of SHR-YFP (green) signal and the SCR-RFP (red) signal in the area crossed by white dashed line in **(A)** inset. **(G and H)** Quantification of SCR-YPF signal intensity in the meristem center (area surrounded by white dashed circles in **(B)** and **(C)**) **(G)** and in the primordia **(H)**. **(I)** Quantitative real-time reverse transcriptase

916 PCR analysis showing the relative expression levels of *SCR* in WT and *shr-2* mutant SAMs.
917 The expression level in Col-0 is set to 1. Expression levels were normalized using AT4G34270
918 and AT2G28390. Asterisks indicate a significant difference (****$p < 0.0001$: Statistically
919 significant differences were determined by Student's *t*-test, ns= no significant difference). Error
920 bars display SD.

921

922

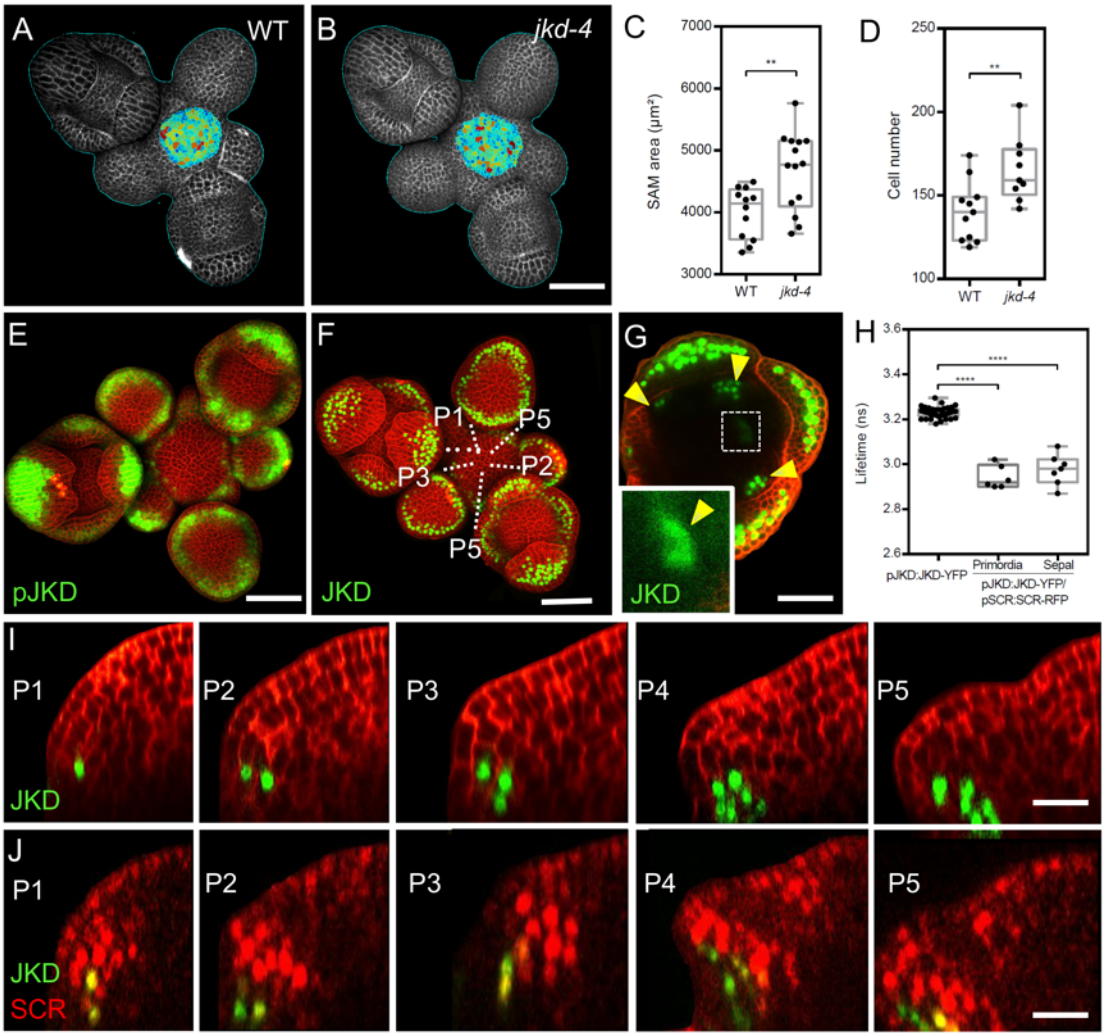

923

924 **Fig. 6: JKD functions and expression pattern in the SAM**

925 **(A and B)** Heat-map quantification of the cell area in the meristem region at 5 weeks after
926 germination from WT **(A)** (n=10) and *jkd-4* mutant **(B)** (n=10). Cell walls were stained with PI
927 (gray). Scale bar represents 50 µm. **(C)** Quantification of SAM size at 34 days after germination
928 (DAG) from WT (n=12) and *jkd-4* mutant (n=14). **(D)** Quantification of epidermal cell number
929 in the meristem region of WT **(A)** (n=10) and *jkd-4* mutant **(B)** (n=10). **(E and F)** Representative
930 3D projection of SAM at 5 weeks after germination expressing *pJKD:YFP-RFP* reporter (green)
931 (n=9) **(E)** and *pJKD:JKD-YFP* reporter (green) (n=24) **(F)**. Cell walls were stained with PI (red).
932 Scale bars represent 50 µm. **(G)** Transversal optical through the primordium 16 from an
933 inflorescence apex. Yellow arrowheads show petal primordia with *pJKD:JKD-YFP* expression
934 (green). The lower left inset shows an optical view with high magnification of the area
935 surrounded by a white dashed rectangle. Cell walls were stained with PI (red). **(H)** Average
936 lifetime of JKD-YFP when expressed alone (*pJKD:JKD-YFP* (n =38)), or coexpressed together

with SCR-RFP (*pJKD:JKD-YFP/pSCR:SCR-RFP*) in lateral organ primordia (n=6) and sepal primordia (n=7). **(I)** Longitudinal optical sections through the middle of five successive primordia (representative section orientation shown by dotted line in **(A)**) expressing *pJKD:JKD-YFP* reporter (green). Cell walls were stained with PI (red). Scale bar represents 20 µm. **(J)** Longitudinal optical sections through the middle of five successive primordia (representative section orientation shown by dotted line in Suppl Fig. 4F) coexpressing *pJKD:JKD-YFP* reporter (green) and *pSCR:SCR-RFP* reporter (red) (n=7). Scale bar represents 20 µm. Asterisks indicate a significant difference (****$p < 0.0001$; **$p < 0.001$: Statistically significant differences were determined by Student's *t*-test). P= primordium.

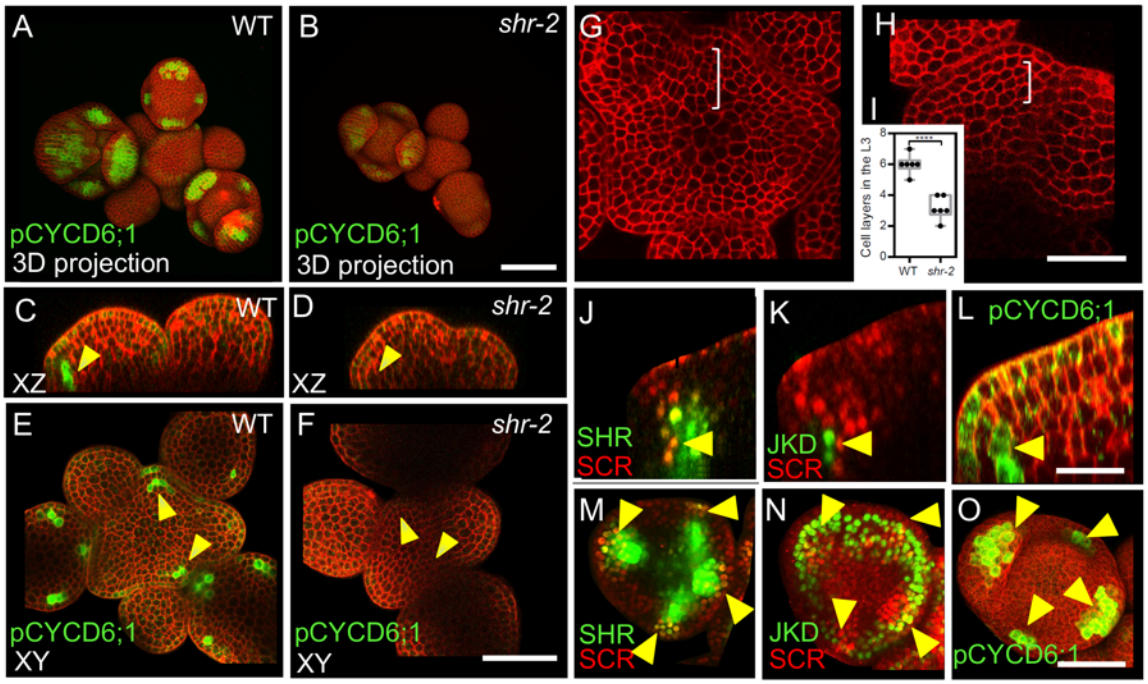

Fig. 7: SHR regulates *CYCD6;1* expression in the SAM

(A and B) Representative 3D projection of SAM at 5 weeks after germination expressing *pCYCD6;1:GFP* reporter (green) in WT (n=11) **(A)** and *shr-2* mutant (n=6) **(B)**. Cell walls were stained with PI (red). Scale bar represents 50 µm. **(C and D)** Longitudinal optical sections of **(A)** and **(B)** respectively. **(E and F)** Transversal optical sections of **(A)** and **(B)** respectively. Scale bar represents 50 µm. **(G and H)** Transversal optical sections of the inflorescence apex at 5 weeks after germination from WT **(G)** and *shr-2* mutant **(H)**. **(I)** Quantitative comparison of cell files within the L3 in optical sections of the inflorescence apex from WT (n=6) and *shr-2* mutant (n=6). **(J-L)** lateral organ primordia showing coexpression of *pSHR:SHR-YFP* reporter (green) and *pSCR:SCR-RFP* reporter (red) **(J)**, *pJKD:JKD-YFP* reporter (green) and *pSCR:SCR-RFP* reporter (red) **(K)** and *pCYCD6;1:GFP* reporter (green) **(L)**. Scale bar represents 20 µm. **(M-O)** Florescence meristem stage 4 of flower development showing coexpression of *pSHR:SHR-YFP* reporter (green) and *pSCR::SCR-RFP* reporter (red) **(M)**, *pJKD:JKD-YFP* reporter (green) and *pSCR::SCR-RFP* reporter (red) **(N)** and *pCYCD6;1:GFP* reporter (green) **(O)**. Scale bar represents 20 µm. Asterisks indicate a significant difference (****$p < 0.0001$; analyzed by Student's t test).

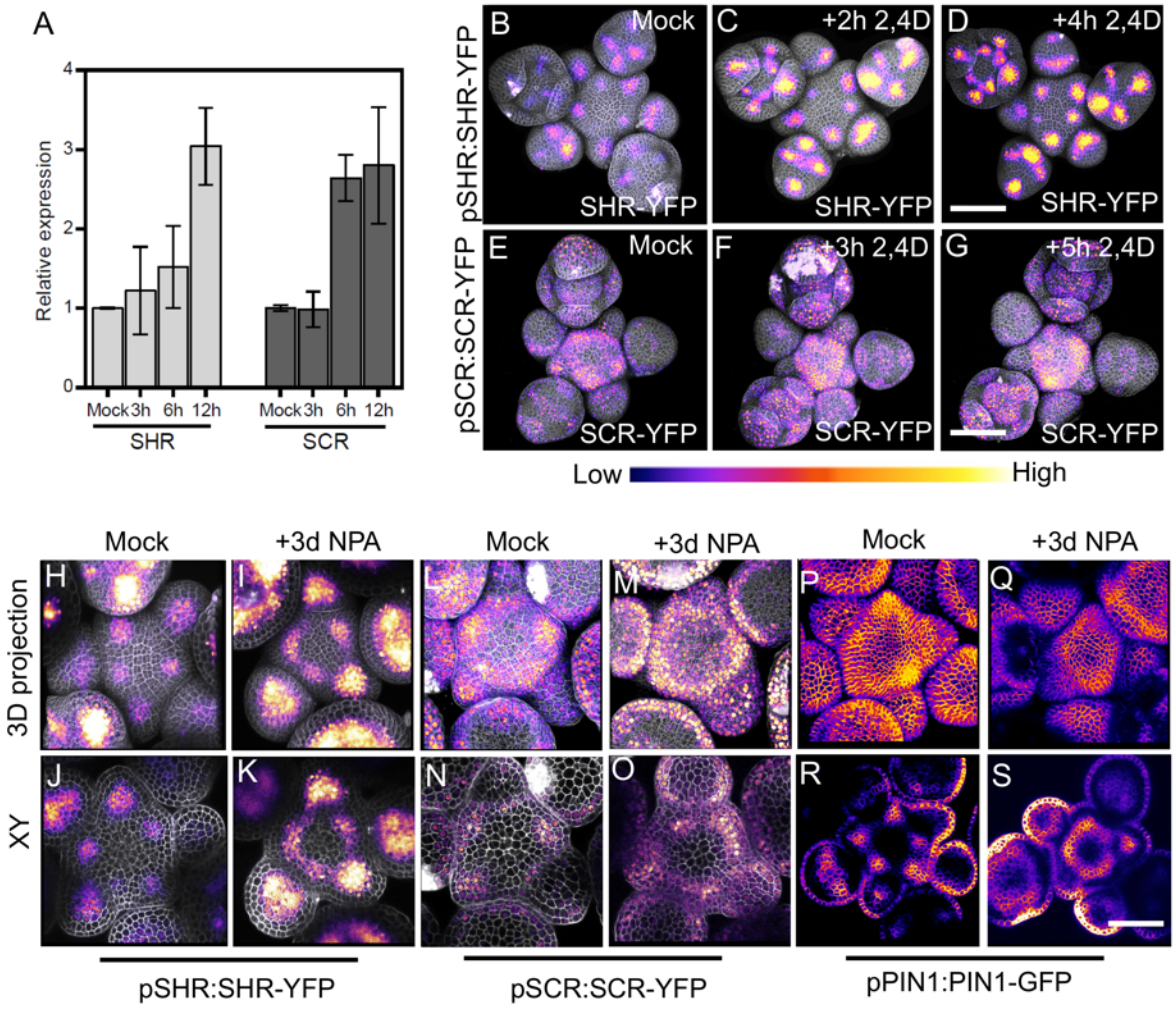

Fig. 8: SHR and SCR expressions respond to auxin

(A) Quantitative real-time reverse transcriptase PCR analysis showing the relative expression levels of *SHR* and *SCR* expression in response to auxin (10 µm IAA) in WT SAMs. The expression level in Col-0 is set to 1 and error bars show standard deviation. Expression levels were normalized using AT4G34270 and AT2G28390. **(B-D)** Representative 3D projection of SAMs at 5 weeks after germination expressing *pSHR:SHR-YFP* reporter (magenta) in mock **(B)** (n=18), or after 2h (n=12) **(C)** or 4h 10µM 2,4D treatment (n=8) **(D)**. Fluorescence intensities were coded blue to yellow corresponding to increasing intensity. Scale bar represents 50 µm. **(E-G)** Representative 3D projection of SAMs at 5 weeks after germination expressing *pSCR:SCR-YFP* reporter (magenta) mock **(E)** (n=11), after 3h (n=6) **(F)** or after 5h 10µM 2,4D treatment (n=7) **(G)**. Fluorescence intensities were coded blue to yellow corresponding to increasing intensity. Scale bar represents 50 µm. **(H and I)** Representative 3D projection of SAMs at 5 weeks after germination expressing *pSHR:SHR-YFP* reporter (magenta) three days after mock (n≥40) **(H)** or 100µM NPA treatment (n≥60) **(I)**. **(J and K)** Transversal optical sections of **(H)** and **(I)** respectively. **(L and M)** Representative 3D projection

979 of SAMs at 5 weeks after germination expressing *pSCR:SCR-YFP* reporter (magenta) three
980 days after mock (n=5) **(L)** or 100µM NPA treatment (n=10) **(M)**. **(N and O)** Transversal optical
981 sections of **(L)** and **(M)** respectively. **(P and Q)** Representative 3D projection of SAMs at 5
982 weeks after germination expressing *pPIN1:PIN1-GFP* reporter (magenta) three days after
983 mock (n=9) **(P)** or 100µM NPA treatment (n=16) **(Q)**. **(R and S)** Transversal optical sections of
984 **(P)** and **(Q)** respectively.

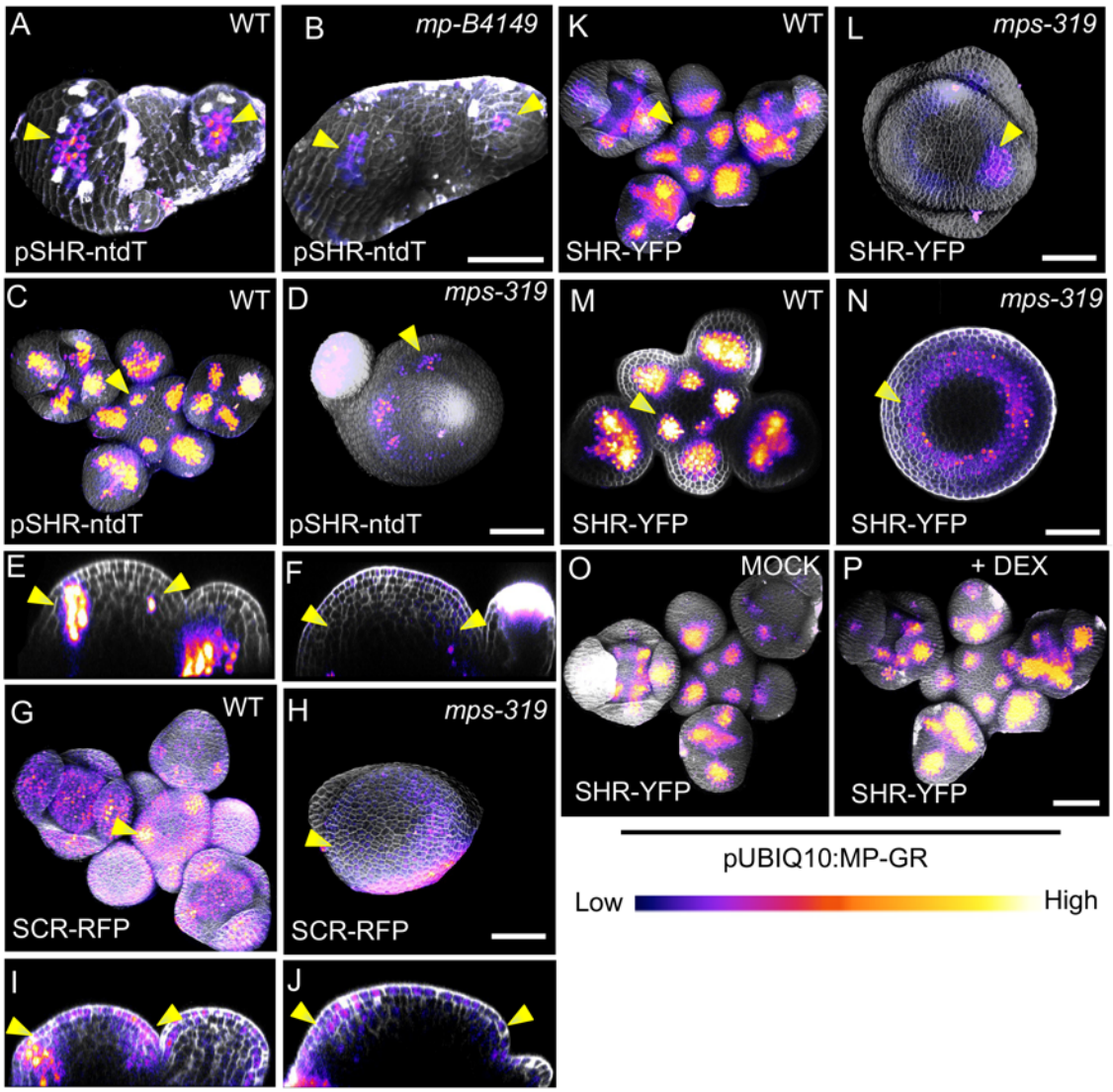

Fig. 9: SHR and SCR act downstream of MP in the SAM

(A and B) Representative 3D projection of SAMs at 5 days after germination expressing *pSHR:ntdTomato* reporter (magenta) in WT (n=8) **(A)** and *mp-B4149* (n=5) **(B)** mutant vegetative meristems. Yellow arrowheads in **(A)** and **(B)** indicate the region where flower primordia initiate and *pSHR:ntdTomato* expression. Scale bar represents 50 µm. **(C and D)** Representative 3D projection of SAMs at 5 weeks after germination expressing *pSHR:ntdTomato* reporter (magenta) in WT (n=10) **(C)** and *mps-319* mutant (n=15) **(D)**. **(E and F)** Longitudinal optical section of **(C)** and **(D)** respectively. Yellow arrowheads in **(C)**, **(D)**, **(E)** and **(F)** indicate the region where flower primordia initiate and *pSHR:ntdTomato* expression. Scale bar represents 50 µm. **(G and H)** Representative 3D projection of SAMs at 5 weeks after germination expressing *pSCR:SCR-RFP* reporter (magenta) in WT (n=12) **(G)** and *mps-319* mutant (n=4) **(H)**. **(I and J)** Longitudinal optical section of **(G)** and **(H)** respectively. Yellow arrowheads in **(G)**, **(H)**; **(I)** and **(J)** indicate the region where flower primordia initiate and *pSCR:SCR-RFP* expression. Scale bar represents 50 µm. **(K and L)**

1000 Representative 3D projection of SAMs at 5 weeks after germination expressing *pSHR:SHR-*
1001 *YFP* reporter (magenta) in WT (n=9) **(K)** and *mps-319* mutant (n=6) **(L)**. **(M and N)** Transversal
1002 optical section of **(K)** and **(L)** respectively. Yellow arrowheads in **(K)**, **(L)**; **(M)** and **(N)** indicate
1003 the region where flower primordia initiate and *pSHR:SHR-YFP* expression. Scale bar
1004 represents 50 µm. **(O and P)** Representative 3D projection of shoot apical meristems at 5
1005 weeks after germination expressing *pSHR:SHR-YFP* reporter (magenta) in *pUBIQ10:MP-GR*
1006 plants 4hr after mock (n=5) **(O)** or 4hr after DEX treatment (n=7) **(P)**. Fluorescence intensities
1007 were coded blue to yellow corresponding to increasing intensity. Scale bar represents 50 µm.

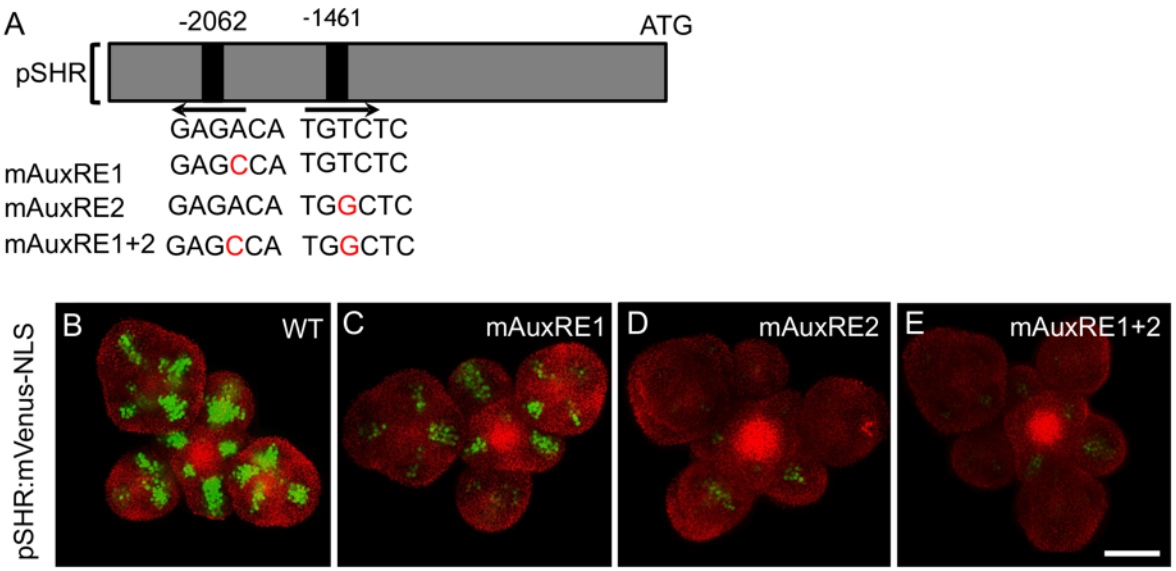

Fig. 10: MP Regulates *SHR* expression in the SAM

(A) Schematic representation of the *SHR* promoter. The positions of two auxin response elements are shown. Overview of mutated promoter versions of *pSHR*. AuxREs were mutated and multiple combinations of these mutated motifs were combined into a single promoter. The original AuxRE sequence GAGACA was mutated to GAGCCA (mAuxRE1), the original AuxRE sequence TGTCTC was mutated to TGGCTC (mAuxRE2). **(B–E)** Representative 3D projection of SAMs at 5 weeks after germination expressing mVenus-NLS under the control of the wild-type *SHR* promoter (n=12) **(B)**, and under the control of the *SHR* promoter with mutations in AuxRE motifs mAuxRE1 (n=7) **(C)** mAuxRE2 (n=5) **(D)** and mAuxRE1+2 (n=11) **(E)**; Chlorophyll (red). Scale bar represents 50 µm.

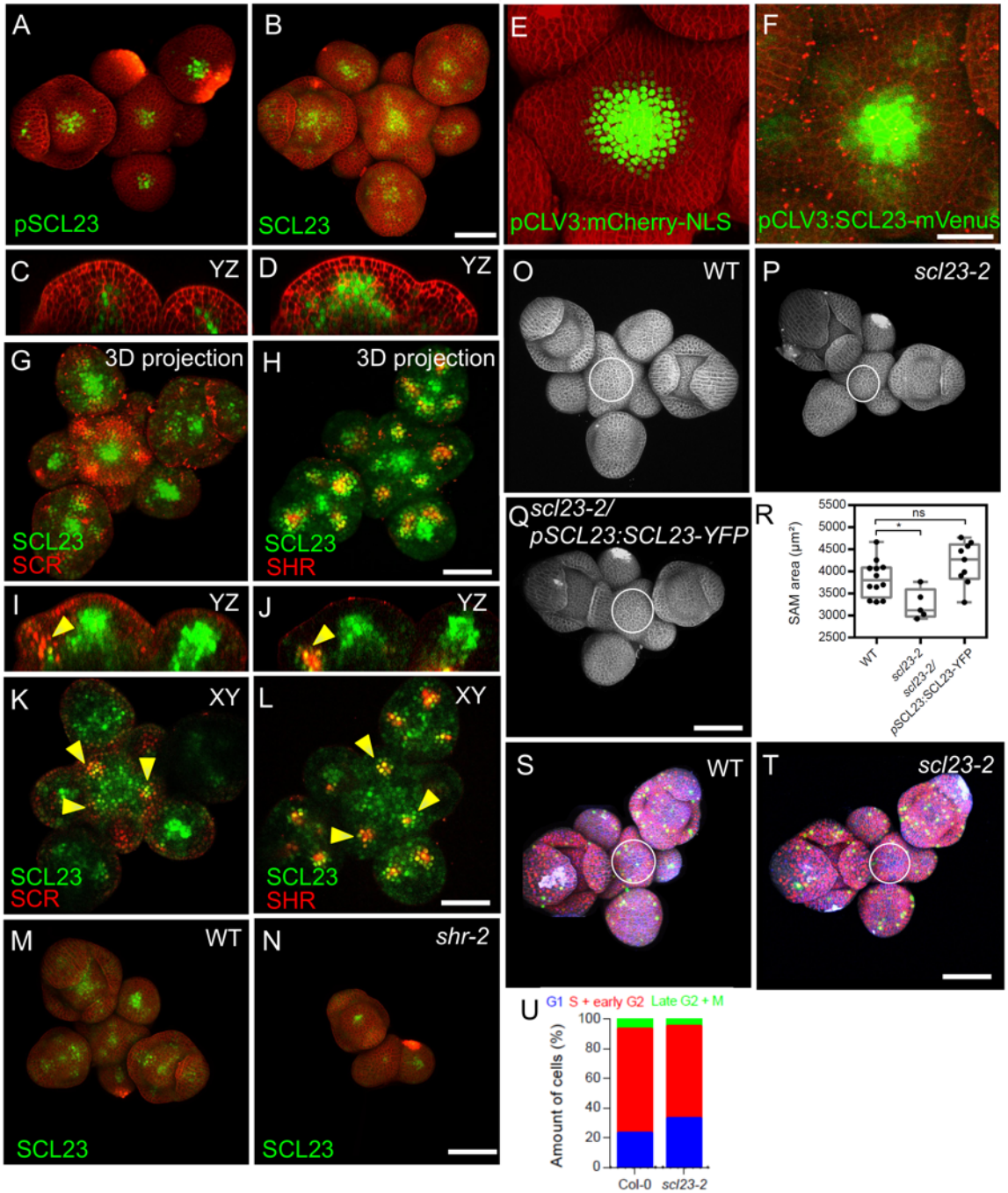

Fig. 11: SCL23, SCR and SHR proteins show spatially different patterns but perform similar functions in the SAM

(A and B) Representative 3D projection of SAMs at 5 weeks after germination expressing *pSCL23:H2B-YFP* reporter (green) (n=5) **(A)** and *pSCL23:SCL23-YFP* reporter (green) (n=25) **(B)**. Cell walls were stained with PI (red). Scale bar represents 50 µm. **(C and D)** Longitudinal optical sections of **(A)** and **(B)** respectively. **(E and F)** Representative 3D projection of SAMs at 5 weeks after germination expressing *pCLV3:mCherry-NLS* reporter (green) (n=4) **(E)** and the *pCLV3:SCL23-mVenus* reporter (green) (n=13) **(F)**. Cell walls were stained with PI (red).

Scale bar represents 50 µm. **(G and H)** Representative 3D projection of SAMs at 5 weeks after germination meristems coexpressing *pSCL23:SCL23-YFP* reporter (green) and *pSCR:SCR-RFP* reporter (red) (n=6) **(G)** and *pSCL23:SCL23-YFP* reporter (green) and *pSHR:mScarlet-RFP* reporter (red) (n=7) **(H)**. Scale bar represents 50 µm. **(I and J)** Longitudinal optical sections of **(G)** and **(H)** respectively. **(K and L)** Transversal optical sections of **(G)** and **(H)** respectively. Yellow arrowheads in **(I)** and **(K)** indicates the region where both *pSCL23:SCL23-YFP* reporter (green) and *pSCR:SCR-RFP* reporter (red) expression overlap. Yellow arrowheads in **(J)** and **(L)** indicates the region where both *pSCL23:SCL23-YFP* reporter (green) and *pSHR:mScarlet-SHR* reporter (red) expression overlap. **(M and N)** Representative 3D projection of SAMs at 5 weeks after germination expressing *pSCL23:SCL23-YFP* reporter (green) in WT (n=14) **(M)** and *shr-2* mutant (n=4) **(N)**. Cell walls were stained with PI (red). Scale bar represents 50 µm. **(O-Q)** Representative 3D projection of SAMs at 5 weeks after germination from WT (n=12) **(O)**, *scl23-2* mutant (n=5) **(P)** and *scl23-2/pSCL23:SCL23-YFP* (n=9) **(Q)**. **(R)** Quantification of SAM size at 5 weeks after germination from Col-0 (n=12), *scl23-2* mutant (n=5) and *scl23-2/pSCL23:SCL23-YFP* (n=9). Cell walls were stained with PI (gray). Scale bar represents 50 µm. **(S and T)** Representative 3D projection of SAMs at 5 weeks after germination from WT (n=11) **(S)** and *scl23-2* (n=5) **(T)** coexpressing the three PlaCCI markers. *pCDT1a:CDT1a-eCFP* reporter (blue), *pHTR13:pHTR13-mCherry* reporter (red) and *pCYCB1;1:NCYCB1;1-YFP* reporter (green). Cell walls were stained with DAPI (gray). Scale bar represents 50 µm. **(U)** Quantification of different cell cycle phases of SAM expressing PlaCCI in WT (n=6) and *scl23-2* (n=5). Asterisks indicate a significant difference (*$p < 0.01$: Statistically significant differences were determined by Student's *t*-test, ns= no significant difference).

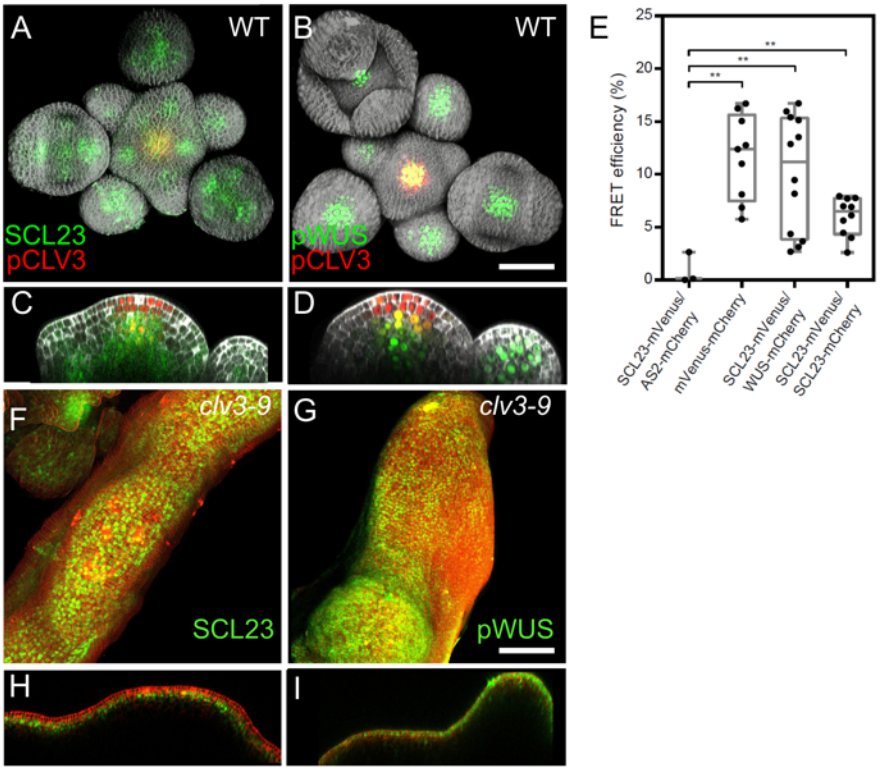

Fig. 12: SCL23 and WUS physically interact and are negatively regulated by CLV signalling

(A and B) Representative 3D projection of SAMs at 5 weeks after germination coexpressing *pSCL23:SCL23-YFP* (green) and *pCLV3:mCherry-NLS* reporter (red) (n=3) **(A)** and *pWUS:3xVenus-NLS* reporter (green) and *pCLV3:mCherry-NLS* reporter (red) (n=6) **(B)**. Cell walls were stained with DAPI (gray). Scale bar represents 50 µm. **(C and D)** Longitudinal optical sections of **(A)** and **(B)** respectively. **(E)** FRET efficiency measured in epidermis cells of *N. benthamiana* between SCL23-mVenus and WUS-mCherry (n=12) or SCL23-mCherry (n=10), compared with the negative control SCL23-mVenus and AS2-mCherry (n=3) and positive control mVenus-mCherry (n=9). **(F and G)** Representative 3D projection of shoot apical meristems at 5 weeks after germination expressing *pSCL23:SCL23-YFP* reporter (green) in *clv3-9* mutant (n=3) **(F)** and *pWUS:3xVenus-NLS* reporter (green) in *clv3-9* mutant (n=3) **(G)**. Cell walls were stained with PI (red). Scale bar represents 50 µm. **(H and I)** Longitudinal optical sections of **(F)** and **(G)** respectively. Asterisks indicate a significant difference (**$p < 0.001$: Statistically significant differences were determined by Student's *t*-test).

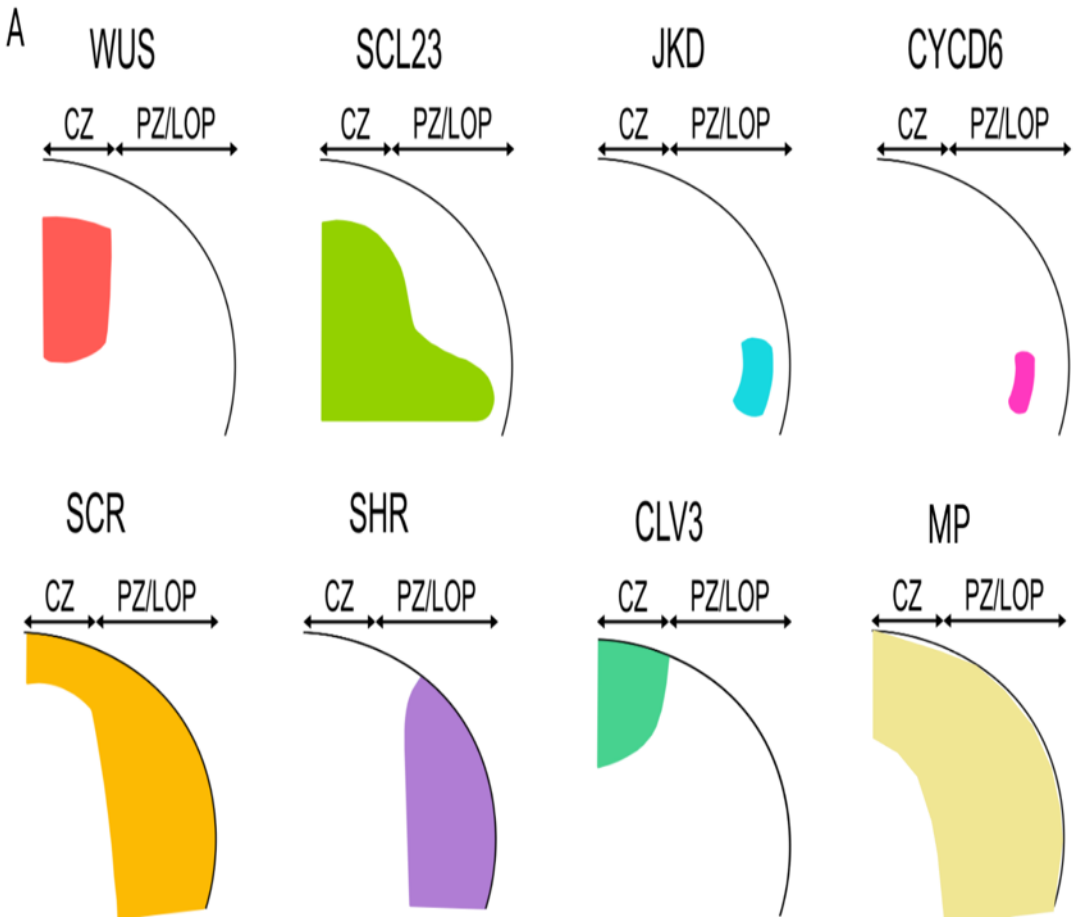

Fig. 13: Proposed model for SHR-SCR-SCL23-JKD regulatory network function in the SAM

(A) Schematic representation of observed expression patterns of *WUS*, *SCL23, JKD, SCR, SHR, CLV3*, *MP* and *LFY* showing typical expression domains in the SAM. **(B)** Schematic molecular models for SHR-SCR-SCL23-JKD gene regulatory network function in the SAM, genes with genetic and/or biochemical interactions are indicated. Lines with arrows depict positive regulation, and with bars depict negative regulation. Dashed lines with arrows depict intercellular protein movement. Overlap between circles describe protein–protein interactions. In the organizing center (OC), SCL23 interacts with WUS to maintain stem cell homeostasis in the central zone (CZ). Like WUS, SCL23 is subject to regulation by CLV3 signalling. SCL23 is hypermobile and moves to the peripheral zone (PZ), where *SHR* transcription is promoted by auxin through MP. In the PZ, SHR activates *SCR* transcription. The SHR-SCR-SCL23-JKD protein complex promotes cell cycle progeression and induces periclinal cell divisions that lead to the outgrowth of lateral organ primordia through the activation of *CYCD6;1*. SHR also regulates the expression of *LFY* within the corpus in the PZ/LOP leading to lateral organ initiation. CZ=Central zone, OC=Organizing center, PZ/LOP=Peripheral zone/lateral organ primordia.

1085 ## Materials and methods

1086 ### Plant material and growth conditions

1087 *Arabidopsis thaliana* plants were grown on soil in climate chambers under long day (LD)
1088 conditions (16 h light / 8 h dark) at 21 °C. Most plants used in this study were in the Columbia
1089 (Col-0) background, except for: *scr-4* (WS) (Fukaki *et al.*, 1998) and *wus*-7 (Graf *et al.*, 2010)
1090 in the *Landsberg erecta* (L.er.) background (Tab. 8 and 9).

1091 ### Plasmid construction and plant transformation

1092 The entry plasmids in this study (Tab. 5) were generated by gDNA or cDNA sequences that
1093 were amplified with Phusion High-Fidelity PCR polymerase using primers described in Tab. 1.
1094 All destination vectors in this study (Tab. 6 and Tab. 7) were generated using the GreenGate
1095 cloning system (Lampropoulos *et al.*, 2013). Entry plasmid containing SHR promoter sequence
1096 (2.5 KB) was used as a template to create different promoter mutants using the QuikChange
1097 II kit according to manufacturer's protocol (Agilent Technologies). Mutagenic mismatch primers
1098 are listed in Tab. 2. all the clones were confirmed by sequencing. *Arabidopsis thaliana* wildtype
1099 (Col-0) plants were transformed with *Agrobacterium tumefaciens* (strain GV3101 pMP90
1100 pSoup) containing the respective destination vectors using the floral dipping method (Clough
1101 & Bent, 1998). Transgenic plants were initially selected on the appropriate antibiotic in the T1
1102 generation. Homozygous T2 plants were identified through confirmation in the T3 generation.
1103 Several independent lines were analysed and a representative line was selected for further
1104 work. *Nicotiana benthamiana* plants were grown 4 – 5 weeks in the greenhouse and
1105 subsequently used for transient leaf epidermis cell transformation.

1106 ### *Nicotiana benthamiana* infiltration

1107 *Agrobacterium tumefaciens* strains (strain GV3101 pMP90 pSoup) harbouring relevant
1108 reporter constructs were cultured overnight with shaking at 28 °C in 5 ml dYT (double Yeast
1109 Tryptone, 1.6 % w/v tryptone, 1 % w/v yeast extract, 0.5 % w/v NaCl) with appropriate
1110 antibiotics. Cell cultures were adjusted to an optical density (OD_{600}) of 0.3 and then harvested
1111 by centrifugation at 4000xg for 10 min. The pellet was resuspended in infiltration buffer (5%
1112 w/v sucrose, 150µM acetosyringone, 0.01% v/v Silwet) and incubated for 2h at 4°C. For
1113 coexpression of two transgenes, the corresponding transformed *A. tumefaciens* were mixed
1114 equally. The resuspensions were infiltrated into the abaxial leaf surface of the 3-4 weeks old
1115 *N. benthamiana* using a needle-less syringe. Plants transformed with constructs under the
1116 control of the 35S promotor were used for analyses 4 days after infiltration.

1117 **Chemical treatments**

1118 For hormone and dexamethasone treatments, plants were grown in soil. For RNA isolation
1119 experiments, *pSHR:SHR-YFP*, *pSCR:SCR-YFP* and *pCYCD6;1:GFP* expression analysis
1120 following auxin and auxin transport inhibitor treatment were performed by dipping 30-day-old
1121 plants inflorescence once in 10 µM (IAA or 2,4 D) once or with 100µM NPA twice (at 0h and 7
1122 h). For Dexamethasone treatment *pUBIQ1:MP-GR* inflorescence meristems were treated with
1123 10µM DEX only once and were imaged 5h after treatment.

1124 **Promoter mVenus activity in *Nicotiana benthamiana***

1125 *N. benthamiana* leaves were co-transformed with different *pSHR:mVenus-NLS* and the
1126 effector plasmids *p35S:GUS* or *p35S:MP* (Tab. 6). Four days after infiltration, the leaves were
1127 processed for further analysis using imaging with a Zeiss LSM780 using the same settings for
1128 all conditions.

1129 **Luciferase assay in *Nicotiana benthamiana***

1130 The different reporter constructs with firefly luciferase reporter (FLUC) under the control of the
1131 different versions of *SHR* promoter (Tab. 7) were co-infiltrated into *N. benthamiana* leaves
1132 together with the effector plasmids *p35S:GUS* or *p35S:MP* (Tab.6). Luciferase activities were
1133 measured four days after infiltration with the NightOwl luminescence system (Berthold). As
1134 substrate for the luciferase reaction, 5mM D-Luciferin potassium salt solution was used.

1135 **Image acquisition and analysis**

1136 All confocal images were obtained by using a Zeiss LSM780 confocal microscope (40x water
1137 immersion objective, Zeiss C-PlanApo, NA1.2). For time series analysis, settings were
1138 established in the beginning on mock samples and were kept standard during the experiment.
1139 Shoot meristems were manually dissected by cutting of the stem, removing the flowers, and
1140 were stained with 1mg/ml DAPI or 5mM propidium iodide (PI). Individual populations of 2 to 20
1141 plants were analyzed.

1142 Green fluorescence was excited with an argon laser at 488 nm and emission was detected at
1143 490 – 530nm, yellow was excited with an argon laser at 514 nm and emission was detected at
1144 520 – 550nm, and red was excited with Diode-pumped solid state (DPSS) lasers at 514nm
1145 and detected at 570 – 650nm. PI was excited at 561nm by DPSS lasers and detected by PMTs
1146 at 590 – 650nm. DAPI was excited at 405nm with a laser diode and detected at 410 – 480nm.

1147

1148 **FRET-Acceptor-Photobleaching (APB)**

1149 *N. benthamiana* leaf epidermal cells were examined using a Zeiss LSM780 confocal
1150 microscope (40x Water immersion objective, Zeiss C-PlanApo, NA1.2). FRET was measured
1151 via mVenus fluorescence intensity increase after photobleaching of the acceptor mCherry
1152 (Bleckmann et al., 2010). The percentage change of the mVenus intensity directly before and
1153 after bleaching was analyzed as E_{FRET}= (E_{FRET} = ($mVenus_{after}$ – $mVenus_{before}$)/$mVenus_{after}$ x 100.
1154 All photobleaching experiments were performed in the nucleus. The displayed data were
1155 obtained from at least 3 independent experiments.

1156 **FRET-FLIM interaction analysis in the SAM**

1157 In vivo FRET-FLIM experiments were measured using a Zeiss LSM780 confocal microscope
1158 (40x Water immersion objective, Zeiss C-PlanApo, NA1.2) equipped with a single-photon
1159 counting device (PicoQuant HydraHarp400) and a linear polarized diode laser (LDH-D-C-485).
1160 YFP donor fluorophores was excited with a 485nm (LDH-D-C-485, 32MHz) pulsed polarized
1161 diode laser. Excitation power was adjusted to 1,5µW. Emitted light was separated by a
1162 polarizing beam splitter and detected with a band-pass filter (520/35 AHF) by Tau-SPADs
1163 (PicoQuant).
1164 Images were acquired with a resolution of 256x256 pixel, zoom 8, a pixel size of 0.1µm and a
1165 dwell time of 12.6µs. For each measurement 100 frames were taken and the intensity-weighted
1166 mean lifetimes τ (ns) were calculated using PicoQuant SymPhoTime64 software applying a bi-
1167 exponential fit. The displayed data were obtained from at least 5 independent experiments.

1168 **Quantitative real time PCR**

1169 For qRT-PCR, RNA was isolated from dissected inflorescence meristems using RNeasyMini
1170 kit (Qiagen). First strand cDNA was synthesized with 1µg of RNA cDNA using the Superscript
1171 III Kit (Invitrogen). Quantitative real-time PCR was performed with 10-fold diluted cDNA using
1172 The SsoAdvancedTM Universal SYBR® Green Supermix (Bio-Rad). The mean and standard
1173 error were determined using three biological replicates with three technical replicates each.
1174 Expression levels were normalized to the references genes TIP41-like (At4g34270) and
1175 SAND-domain protein (AT2G28390) (Czechowski *et al.*, 2005). Primers used are listed in Tab.
1176 3. Calculation of the relative expression was performed according to Michael W. Pfaffl (Pfaffl,
1177 2001).

1178 **Phenotypic analyses**

1179 Rosettes and plants were analyzed by taking photographs using Canon EOS400D camera
1180 with an EF-S 60 mm Canon ZOOM lens) of plants growing on soil. Inflorescences were

analyzed by taking pictures using stereo microscope (Nikon SMZ25). The inflorescence plastochron was obtained by calculating the average time separating the emergence of 2 successive flower above stage 15 emerging after plant bolting. For SAM area measurement, 30DAG plants growing under LD conditions were used. The primary inflorescence was dissected and imaged using LSM780. The SAM area measurement was done by Fiji.

Software

Microsoft Word, Excel, and PowerPoint software was used to organize experimental data. Images were analyzed and processed with ImageJ v 1.53c (Schneider *et al.*, 2012) and Carl Zeiss ZEN2011. All images were adjusted in “Brightness and Contrast”. VectorNTI (InvitrogenTM) was used for vector maps and sequence analysis. Databank gene research were performed on The Arabidopsis Information Resource (TAIR), (http://www.arabidopsis.org/). Indigo was used for the luciferase assay imaging. Statistical analyses and box plots were realized with GraphPad Prism v 8. For visualization. Using the open-source software MorphoGraphX (MGX) software (https://morphographx.org/) (Barbier de Reuille *et al.*, 2015) the surface of the meristem was extracted and the PI signal of the cell wall from layer1 (L1) was projected and used for segmentation of the images to quantify number and size of cells. Cells were segmented manually. MorphographX analysis was performed according to standards defined in the user manual (Barbier de Reuille et al., 2015). The visualisation and counting of nuclei expressing PlaCCI (Desvoyes et al., 2020) was done with Imaris (version 9.1.2, Bitplane, Oxford Instruments plc). Ratios for R2D2 were calculated as described previously (Bhatia *et al.*, 2016). All Statistical analyses and data plotting were realized with GraphPad Prism v 8. All images for an experimental set were captured under identical microscope settings.

1204 **Supplemental data**

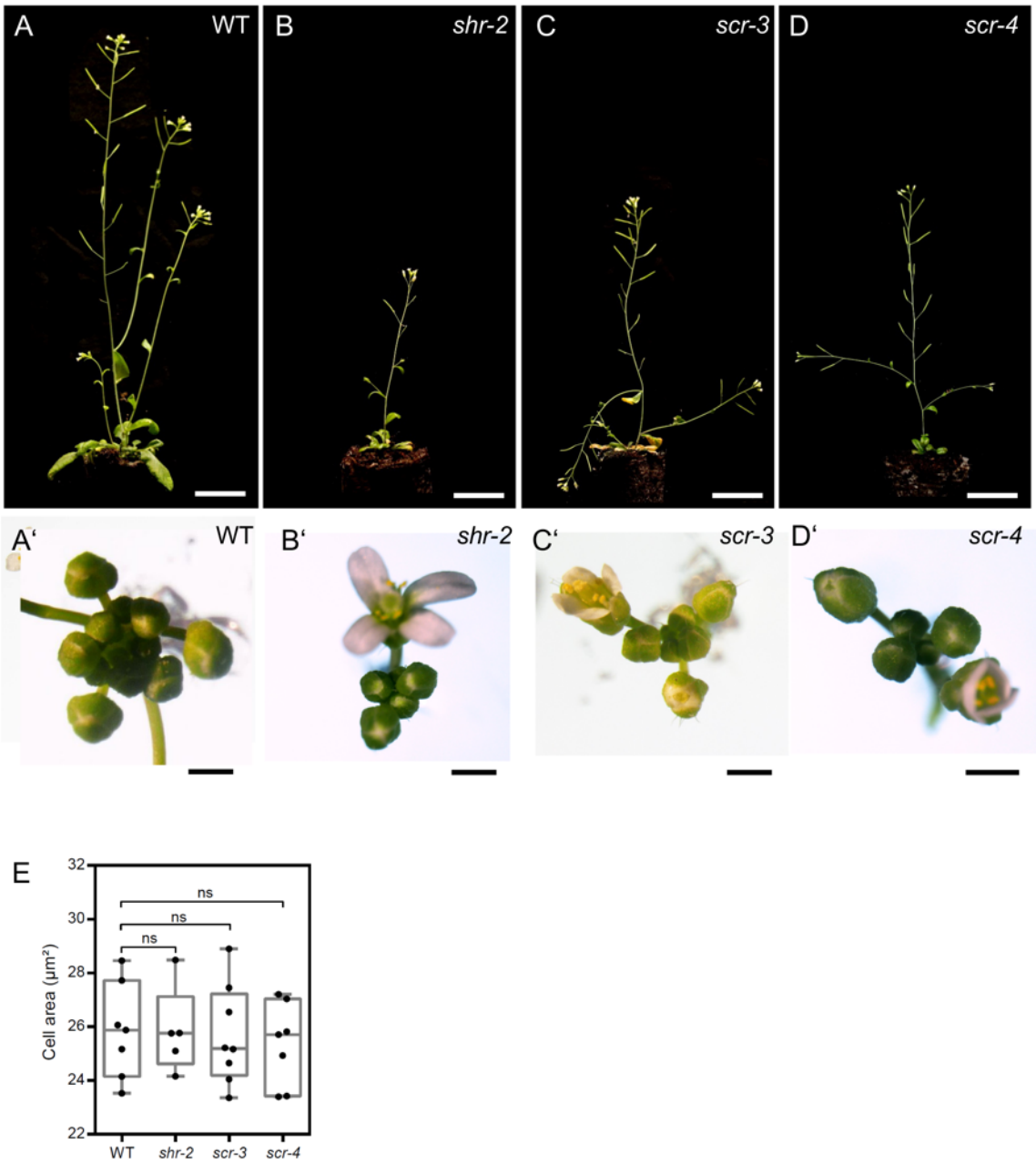

1205

1206 **Suppl Fig. 1: The *shr* and *scr* mutants phenotypes**

1207 **(A-D)** Plant phenotypes of 42-day-old WT (n> 30) **(A)**, *shr-2* mutant (n> 35) **(B)**, *scr-3* mutant
1208 (n> 30) **(C)** and *scr-4* mutant (n> 30) **(D)**. Scale bar represents 1cm. **(A'-D')** Top view of 31-
1209 day-old inflorescences of WT (n> 30) **(A')**, *shr-2* mutant (n> 35) **(B')**, *scr-3* mutant (n> 30) **(C')**
1210 and *scr-4* mutant (n> 30) **(D')**. Scale bars represent 2 mm. **(E)** Quantification of the epidermal
1211 cell area in the meristem region of WT (n=11), *shr-2* mutant (n=4), *scr-3* mutant (n=7) and *scr-*
1212 *4* mutant (n=6). Statistically significant differences were determined by Student's *t*-test, ns= no
1213 significant difference.

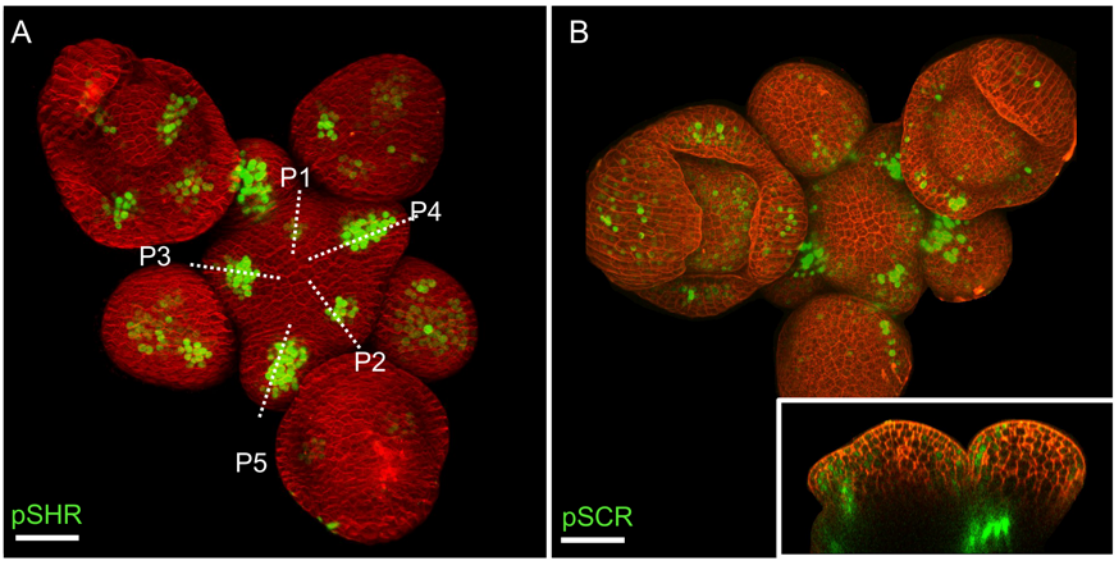

1214

1215 **Suppl Fig. 2: The expression pattern of SHR and SCR in the shoot apical meristem**

1216 **(A)** Representative 3D projection of shoot apical meristem at 5 weeks after germination
1217 expressing *pSHR:ntdTomato* reporter (green). Cell walls were stained with DAPI (red) (n≥5).
1218 Scale bar represents 50 µm. **(B)** Representative 3D projection of shoot apical meristem at 5
1219 weeks after germination expressing *pSCR:H2B-YFP* reporter (green). Cell walls were stained
1220 with PI (red) (n≥3). The lower right inset shows an optical longitudinal section through the
1221 middle of the SAM. Scale bar represents 50 µm.

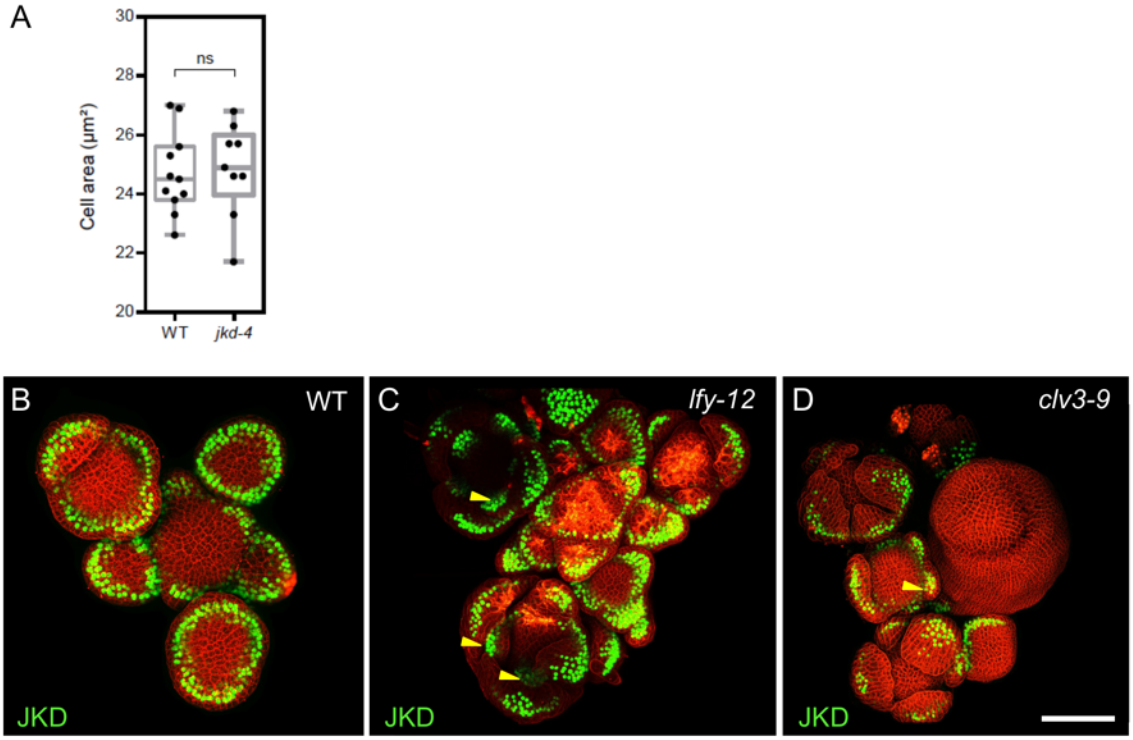

Suppl Fig. 3: The expression pattern of JKD in *lfy* and *clv3* mutants shoot apical meristem

(A) Quantification of the epidermal cell area in the meristem region of WT (n=10) and *jkd-4* mutant (n=10). **(B-D)** Representative 3D projection of shoot apical meristems at 5 weeks after germination expressing *pJKD:JKD-YFP* reporter (green) in WT **(B)**, *lfy-12* mutant **(C)** and *clv3-9* mutant **(D)**. Cell walls were stained with PI (red). Scale bar represents 50 µm. difference. Statistically significant differences were determined by Student's *t*-test, ns= no significant.

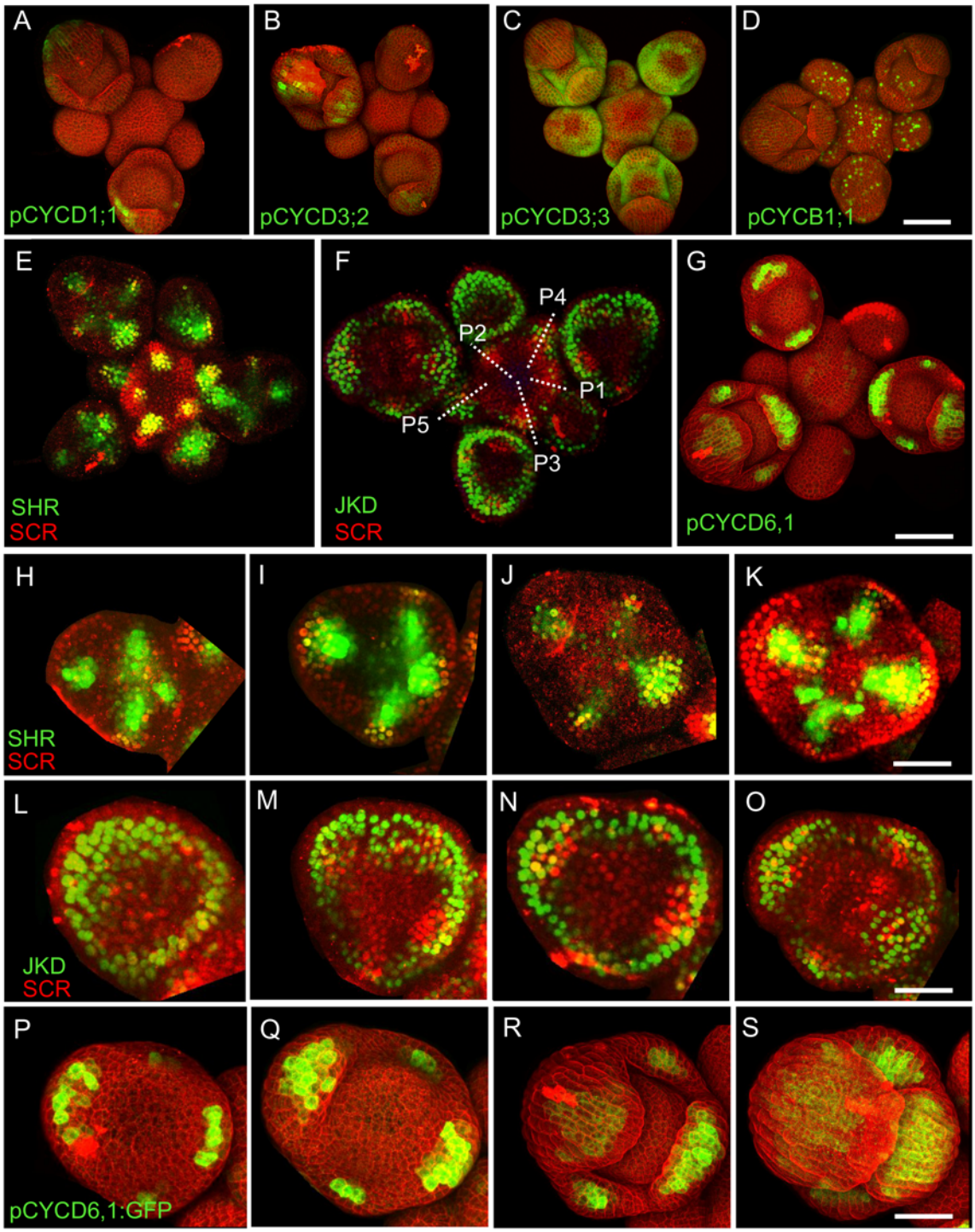

Suppl Fig. 4: The colocalization of the expression patterns of SHR, SCR, JKD and CYCD6;1 in the shoot apical meristem

(A-D) Representative 3D projection of shoot apical meristem at 5 weeks after germination expressing *pCYCD1;1-GFP* reporter (green) **(A)**, *pCYCD3;2-GFP* reporter (green) **(B)**, *pCYCD3;3-GFP* reporter (green) **(C)** and *pCYCB1;1:CYCB1;1-GFP* reporter (green) **(D)**. Cell walls were stained with PI (red). Scale bars, 50 µm. **(E and F)** Representative 3D projection of

shoot apical meristems at 5 weeks after germination coexpressing *pSHR:SHR-YFP* reporter (green) and *pSCR:SCR-RFP* reporter (red) (E) and *pJKD:JKD-YFP* reporter (green) and *pSCR:SCR-RFP* reporter (red) (F). Scale bar represents 50 µm. (G) Representative 3D projection of shoot apical meristems expressing *pCYCD6;1:GFP* (green) reporter (n≥5). Cell walls were stained with PI (red). Scale bar represents 50 µm. **(H-S)** Expression of SHR, SCR, JKD and *CYCD6;1* during early stages of flower development. expression is observed at the sepal primordia in the florescence meristem stage 3 **(H, L and P)**, stage 4 **(I, M and Q)**, stage 5 **(J, N and R)** and stage 6 **(K, O and S)**. Scale bar represents 20 µm.

1246

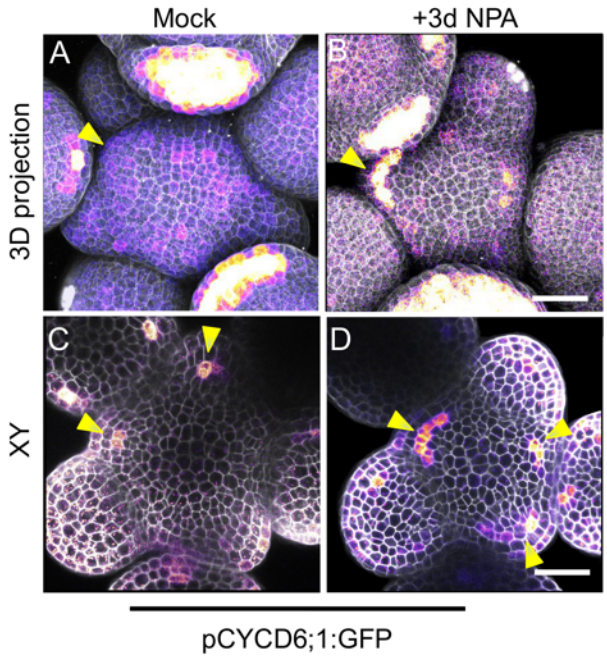

1247

1248 **Suppl Fig. 5: *CYCD6;1* expression responds to auxin**

1249 **(A and B)** Representative 3D projection of shoot apical meristems at 5 weeks after germination
1250 expressing *pCYCD6;1:GFP* reporter (magenta) three days after mock (n≥3) **(A)** or 100 µM
1251 NPA treatment (n≥6) **(B)**. **(C and D)** Transversal optical sections of **(A)** and **(B)** respectively.
1252 Yellow arrowheads in **(A)**, **(B)**, **(C)** and **(D)** show primordia with pCYCD6;1:GFP expression.
1253 Cell walls were stained with DAPI (gray). Scale bar represents 50 µm.

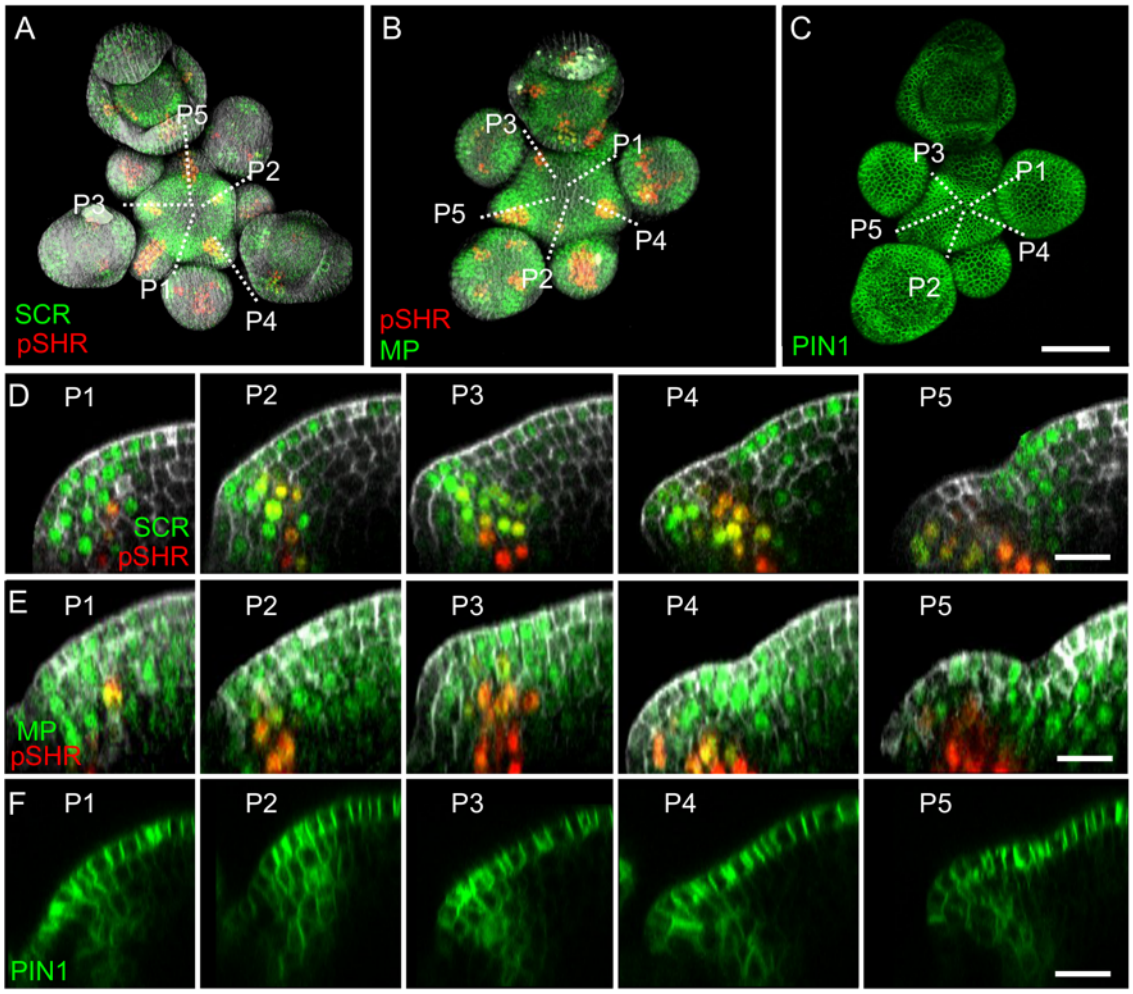

Suppl Fig. 6: The expression patterns of SHR, SCR, MP and PIN1 in the shoot apical meristem

(A and B) Representative 3D projection of shoot apical meristems at 5 weeks after germination coexpressing *pSCR:SCR-YFP* reporter (green) and *pSHR:ntdTomato* reporter (red) **(A)** and the *pMP:MP-GFP* (green) and *pSHR:ntdTomato* (red) reporters **(B)**. Cell walls were stained with DAPI (gray). Scale bar represents 50 µm. **(C)** Representative 3D projection of shoot apical meristems at 5 weeks after germination expressing *pPIN1:PIN1-GFP* reporter (green). Scale bar represents 50 µm. **(D-F)** Longitudinal optical sections through the middle of five successive primordia (representative section orientation shown by dotted line in **(A)**, **(B)** and **(C)** respectively). Scale bar represents 20 µm.

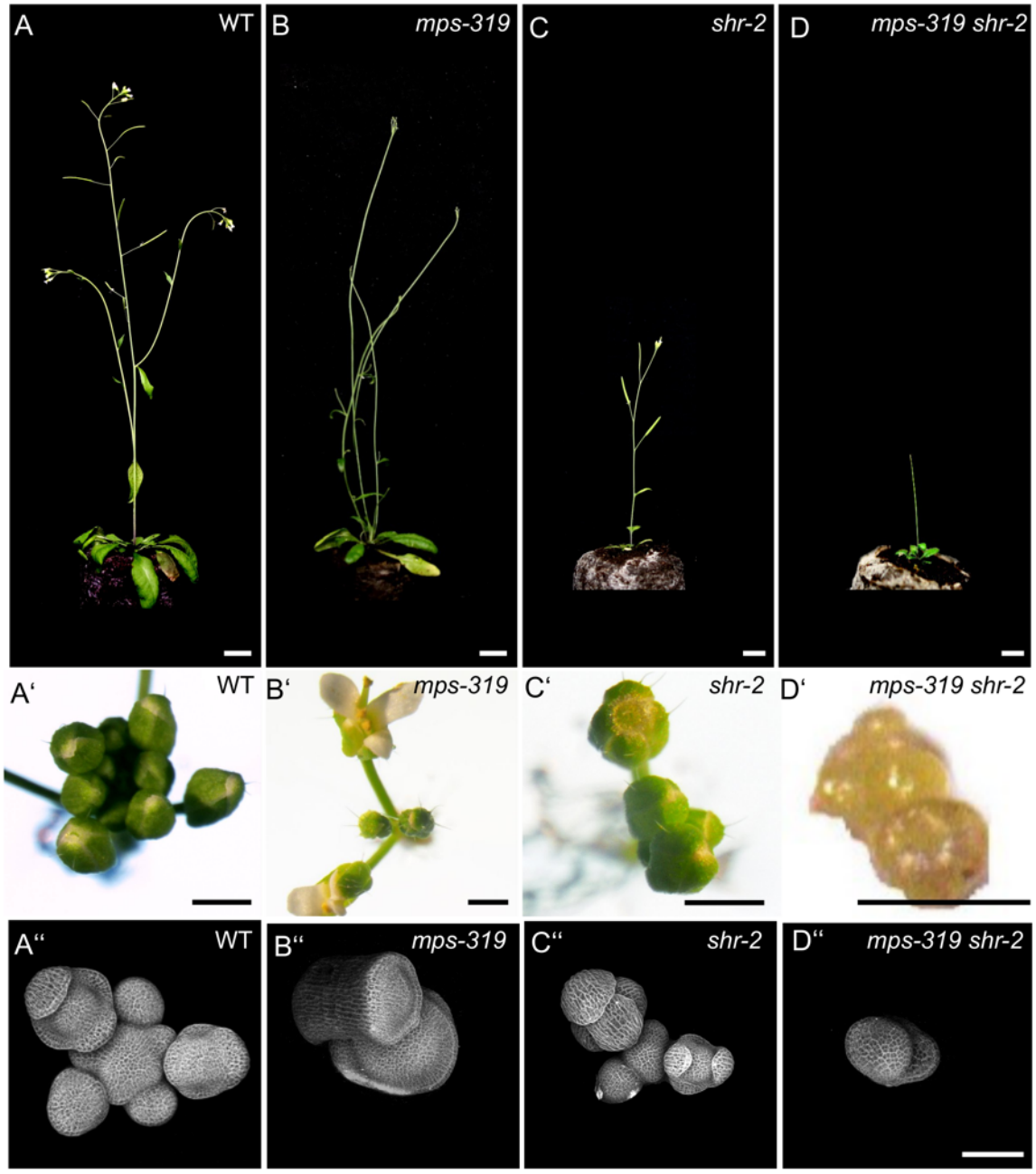

Suppl Fig. 7: *shr* mutant and *shr mps-319* double-mutant phenotypes

(A-D) Plant phenotypes of 42-day-old WT **(A)**, *mps-319* mutant **(B)**, *shr-2* mutant **(C)** and *mps-319 shr-2* double mutant **(D)**. Scale bar represents 1 cm. **(A'-D')** Top view of 31-day-old inflorescences of WT **(A')**, *mps-319* mutant **(B')**, *shr-2* mutant **(C')** and *mps-319 shr-2* double mutant **(D')**. Scale bars represent 2 mm. **(A''-D'')**. Representative 3D projection of shoot apical meristems at 5 weeks after germination from WT **(A'')**, *mps-319* mutant **(B'')**, *shr-2* mutant **(C'')** and *mps-319 shr-2* double mutant **(D'')**. Scale bar represents 50 µm.

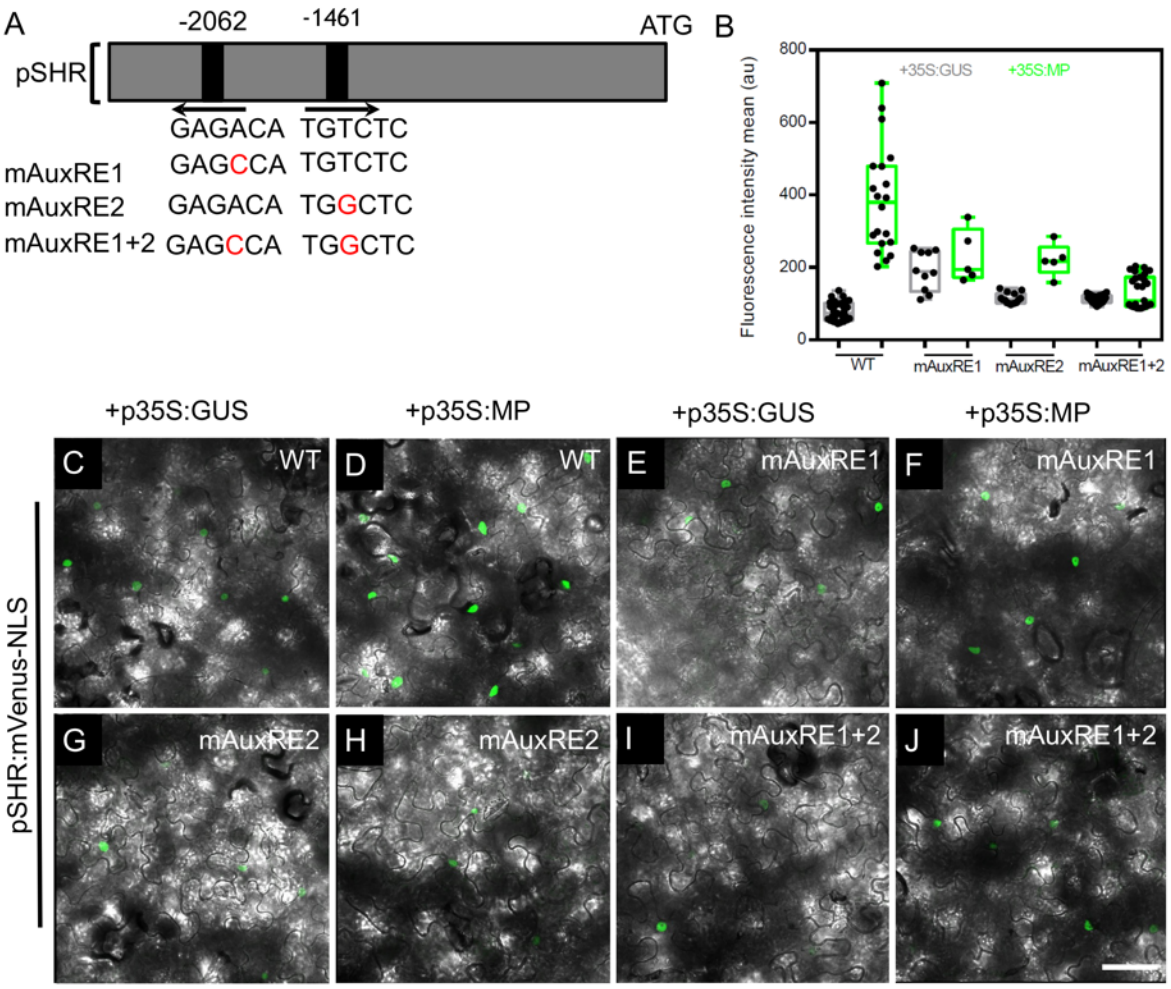

Suppl Fig. 8: MP Regulates *SHR* expression in the shoot apical meristem

(A) Schematic representation of the *SHR* promoter. The positions of two auxin response elements are shown. Overview of mutated promoter versions of *pSHR*. AuxREs were mutated and multiple combinations of these mutated motifs were combined into a single promoter. The original AuxRE sequence GAGACA was mutated to GAGCCA (mAuxRE1), the original AuxRE sequence TGTCTC was mutated to TGGCTC (mAuxRE2). **(B)** Quantification of mVenus fluorescence signal intensity from leaves transiently transformed with mVenus-NLS under the control of the wild-type SHR promoter or under the control of the SHR promoter with mutations in AuxRE motifs in the presence of *p35S:GUS* or *p35S:MP*. **(C-J)** Leaves transiently transformed with mVenus-NLS under the control of the wild-type SHR promoter **(C and D)** or under the control of the SHR promoter with mutations in AuxRE motifs, mAuxRE1 **(E and F)** mAuxRE2 **(G and H)** and mAuxRE1+2 **(I and J)** together with *p35S:MP* or *p35S:GUS*. mVenus fluorescence signals were detected by confocal microscopy. Scale bar represents 50 µm.

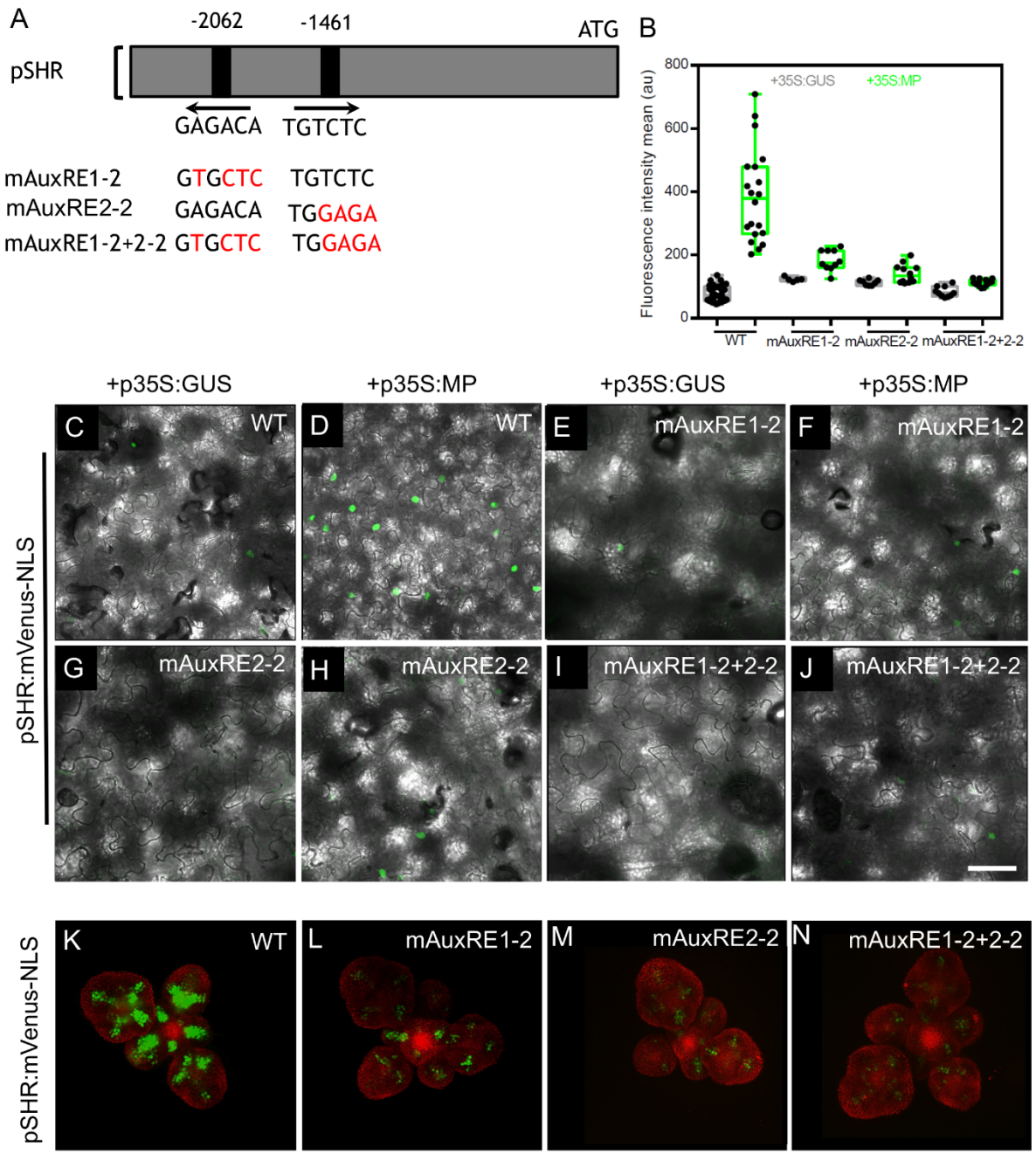

Suppl Fig. 9: MP Regulates *SHR* expression in the shoot apical meristem

(A) Schematic representation of the *SHR* promoter. The positions of two auxin response elements are shown. Overview of mutated promoter versions of *pSHR*. AuxREs were mutated and multiple combinations of these mutated motifs were combined into a single promoter. The original AuxRE sequence GAGACA was mutated to GTGCTC (mAuxRE1), the original AuxRE sequence TGTCTC was mutated to TGGAGA (mAuxRE2-2). **(B)** Quantification of mVenus fluorescence signal intensity from leaves transiently transformed with mVenus-NLS under the control of the wild-type SHR promoter or under the control of the SHR promoter with mutations in AuxRE motifs in the presence of *p35S:GUS* or *p35S:MP*. **(C-J)** Leaves transiently

1299 transformed with mVenus-NLS under the control of the wild-type SHR promoter **(C and D)** or
1300 under the control of the SHR promoter with mutations in AuxRE motifs, mAuxRE1-2 **(E and F)**
1301 mAuxRE2-2 **(G and H)** and mAuxRE1-2+2-2 **(I and J)** together with *p35S:MP* or *p35S:GUS*.
1302 mVenus fluorescence signals were detected by confocal microscopy. Scale bar represents 50
1303 µm. **(K–N)** Representative 3D projection of shoot apical meristems at 5 weeks after
1304 germination expressing mVenus-NLS under the control of the wild-type SHR promoter **(K)**, and
1305 under the control of the SHR promoter with mutations in AuxRE motifs mAuxRE1-2 **(L)**
1306 mAuxRE2-2 **(M)** and mAuxRE1-2+2-2 **(N)**; Chlorophyll (red). Scale bar represents 50 µm.

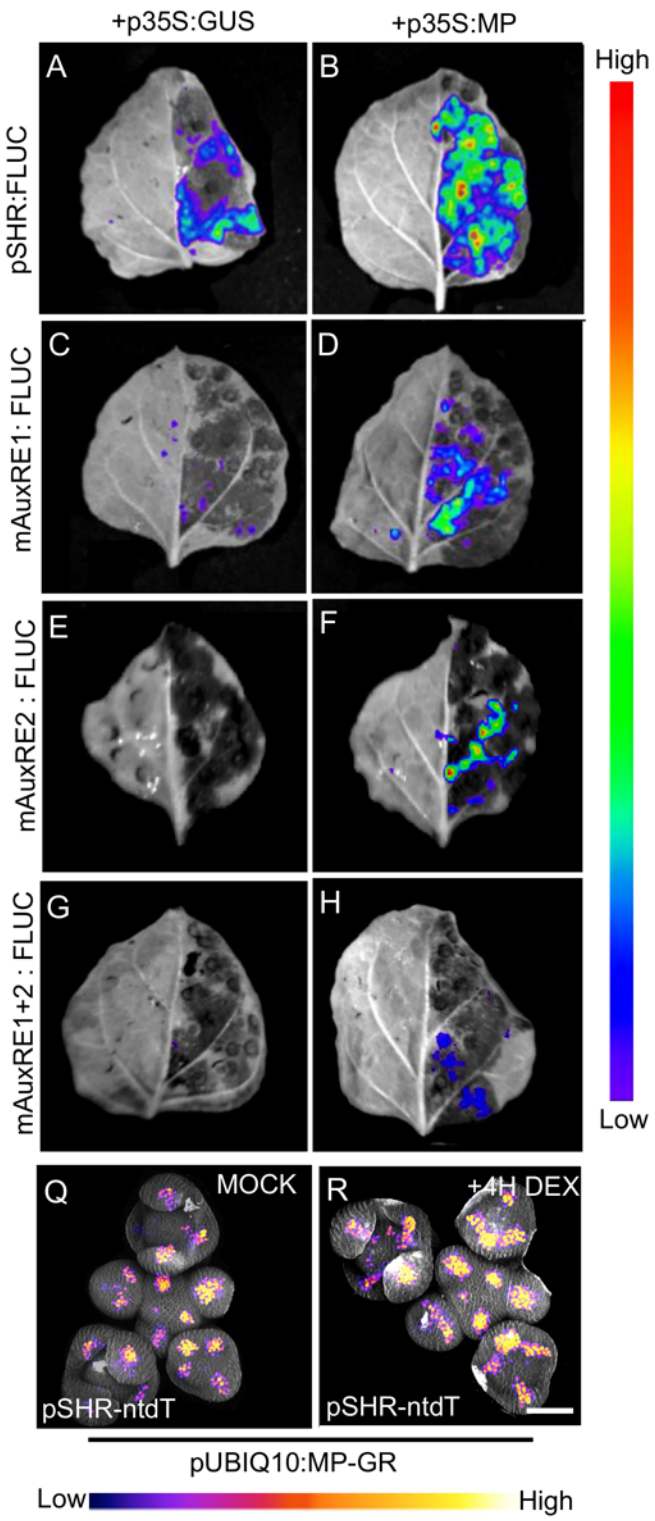

Suppl Fig. 10: MP induces the expression of SHR *in planta*

(A-H) Representative images of leaves transformed with pSHR variants (pSHR (A and B), mAuxRE1 **(C and D)**, mAuxRE2 **(E and F)** and mAuxRE1+2 **(G and H)** draving the reporter gene firefly luciferase (FLUC) together with *p35S:MP* or *p35S:GUS*. D-luciferin was used as the substrate of FLUC**.** No luminescence could be detected without the substrate D-Luciferin.

1314 Color code indicate relative signal intensities (red: high; violet: low). **(Q and R)** Representative
1315 3D projection of shoot apical meristems at 5 weeks after germination expressing
1316 *pSHR:ntdTomato* reporter (magenta) in *pUBIQ10:MP-GR* plants 4 hr after mock **(Q)** (n = 4)
1317 and 4 hr after DEX treatment **(P)** (n = 4). Cell walls were stained with DAPI (gray). Scale bar
1318 represents 50 μm.
1319

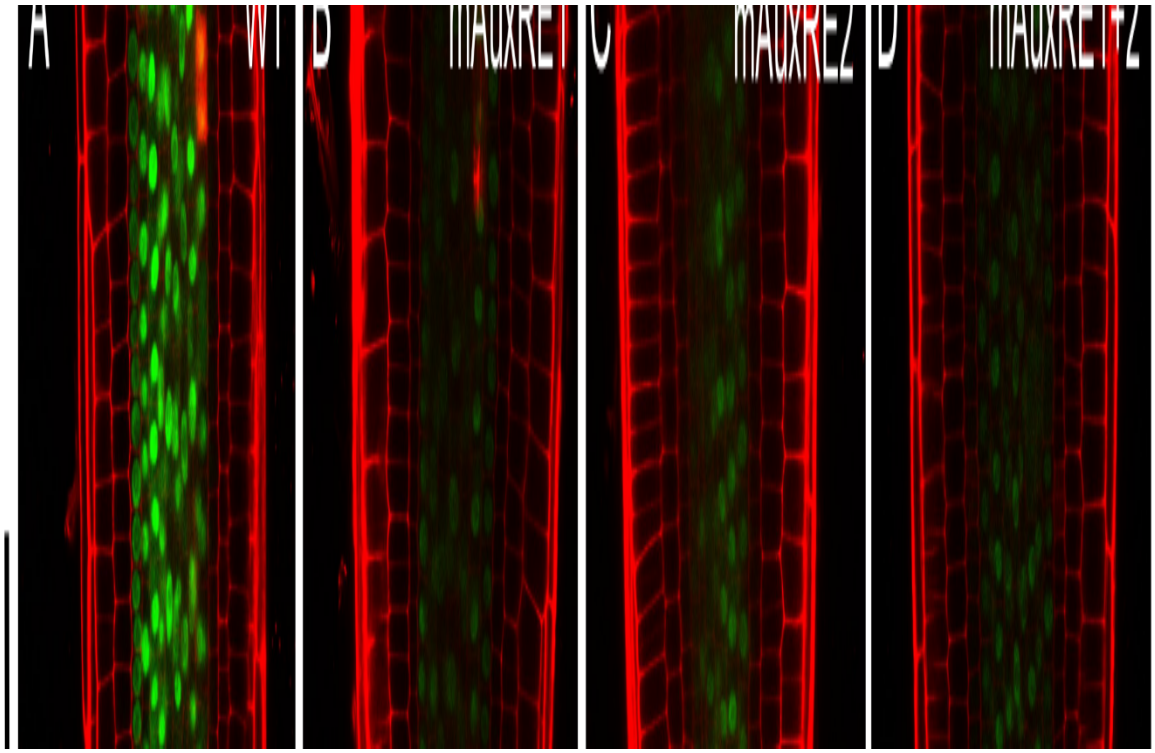

Suppl Fig. 11: The expression pattern of the different promoter versions of *SHR* in the root apical meristem

(A–G) Representative images of root apical meristem at 5 days after germination expressing mVenus-NLS driven by the wild-type SHR promoter **(A)**, and the SHR promoter with mutations in AuxRE motifs mAuxRE1 **(B)**, mAuxRE2 **(C)**, mAuxRE1+2 **(D)**, mAuxRE1-2 **(E)**, mAuxRE2-2 **(F)** and mAuxRE1-2+2-2 **(G)**. **(H)** Representative images of 5-d-old root tips that coexpressing the *pMP:MP-GFP* reporter (green) and *pSHR:ntdTomato* reporter (red). Cell walls were stained with PI (red). Scale bar represents 50 µm.

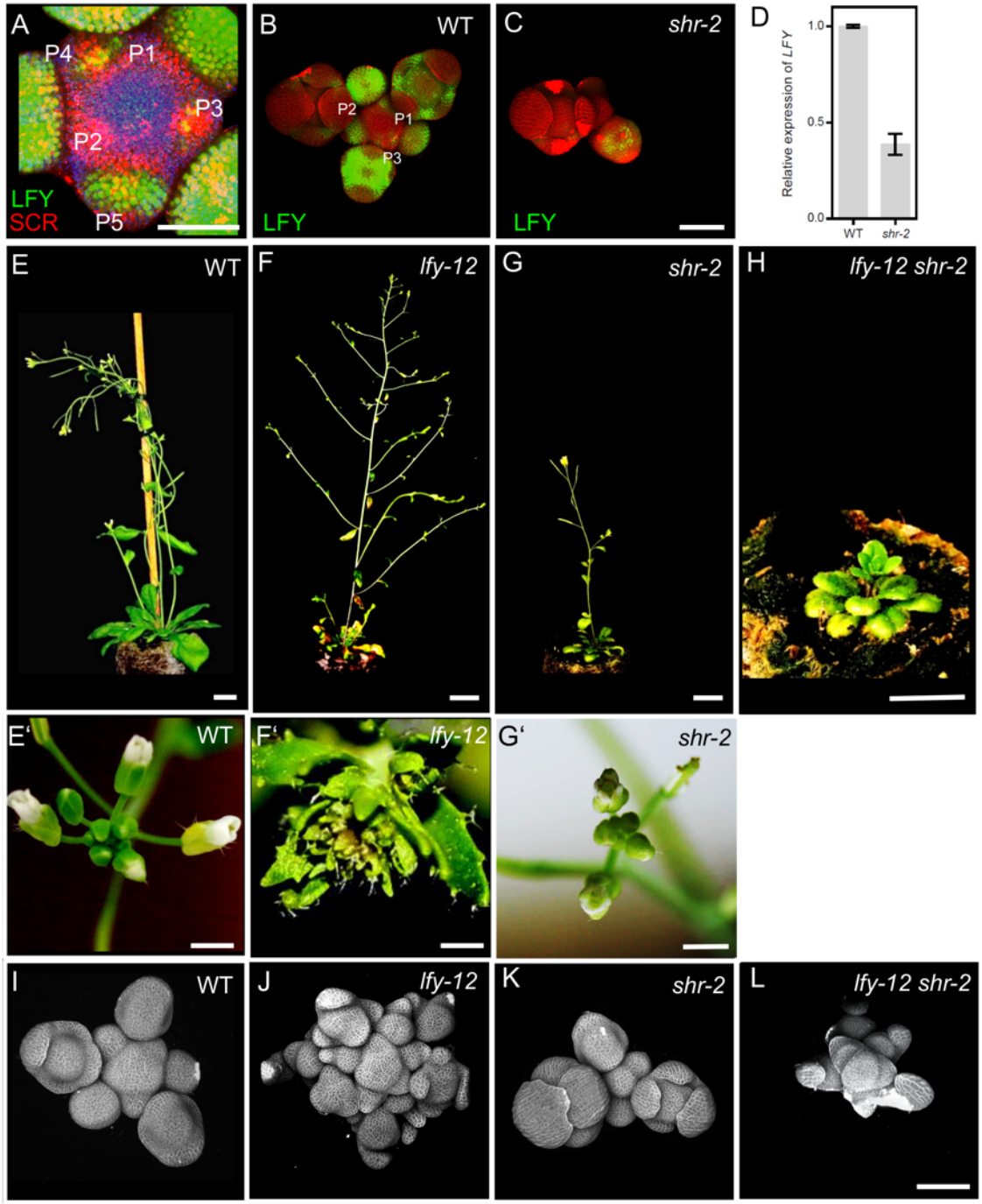

Suppl Fig. 12: *LFY* act downstream of SHR in the shoot apical meristem

(A) Representative 3D projection of shoot apical meristems at 5 weeks after germination coexpressing *pLFY:LFY-GFP* (green) and *pSCR:SCR-RFP* (red) reporters. Chlorophyll (blue). Scale bar represents 50 µm. **(B and C)** Representative 3D projection of shoot apical meristems expressing *pLFY:LFY-GFP* reporter (green) in WT(n≥3) **(L)** and *shr-2* mutant (n≥3) **(M)**. Cell walls were stained with PI (red). Scale bar represents 50 µm. **(D)** Quantitative real-time PCR analysis showing the relative expression levels of *LFY* in WT and *shr-2* mutant shoot apical

1337 meristems. The expression level in Col-0 is set to 1 and error bars show standard deviation.
1338 Expression levels were normalized using At4g34270 and AT2G28390. **(E-H)** Plant phenotypes
1339 of 45-day-old WT **(E)**, *lfy-12* mutant **(F)**, *shr-2* mutant **(G)** and *lfy-12 shr-2* double mutant **(H)**.
1340 Scale bar represents 1 cm. **(E'-G')** Top view of 31-day-old inflorescences of WT **(E')**, *lfy-12*
1341 **(F')** mutant and *shr-2* mutant **(G')**. Scale bar represents 2 mm. **(I-L)** Representative 3D
1342 constraction of shoot apical meristems at 5 weeks after germination from WT **(I)**, *lfy-12* mutant
1343 **(J)**, *shr-2* mutant **(K)** and *lfy-12 shr-2* double mutant **(L)**. Scale bar represents 50 μm.

1344

1345

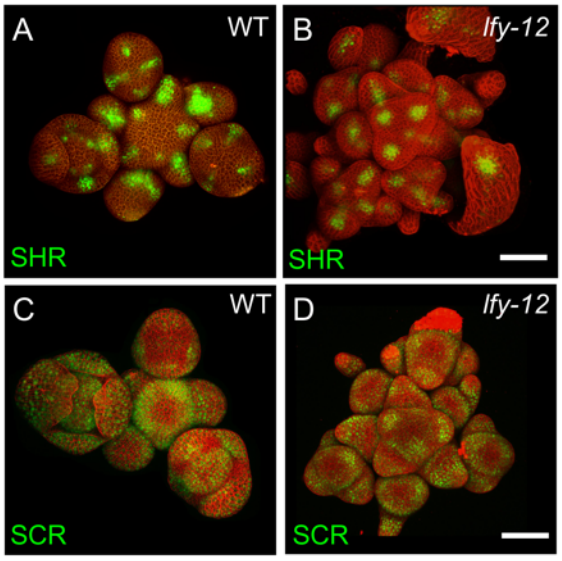

1346

1347 **Suppl Fig. 13: The expression pattern of SHR and SCR in *lfy* mutant shoot apical**
1348 **meristem**

1349 **(A and B)** Representative 3D projection of shoot apical meristems at 5 weeks after germination
1350 expressing *pSHR:SHR-YFP* reporter (green) in WT **(A)** and *lfy-12* mutant **(B)**. Cell walls were
1351 stained with PI (red). Scale bar represents 50 µm. **(C and D)** Representative 3D projection of
1352 shoot apical meristems expressing *pSCR:SCR-YFP* reporter (green) in WT **(C)** and *lfy-12*
1353 mutant **(D)**. Cell walls were stained with PI (red). Scale bar represents 50 µm.

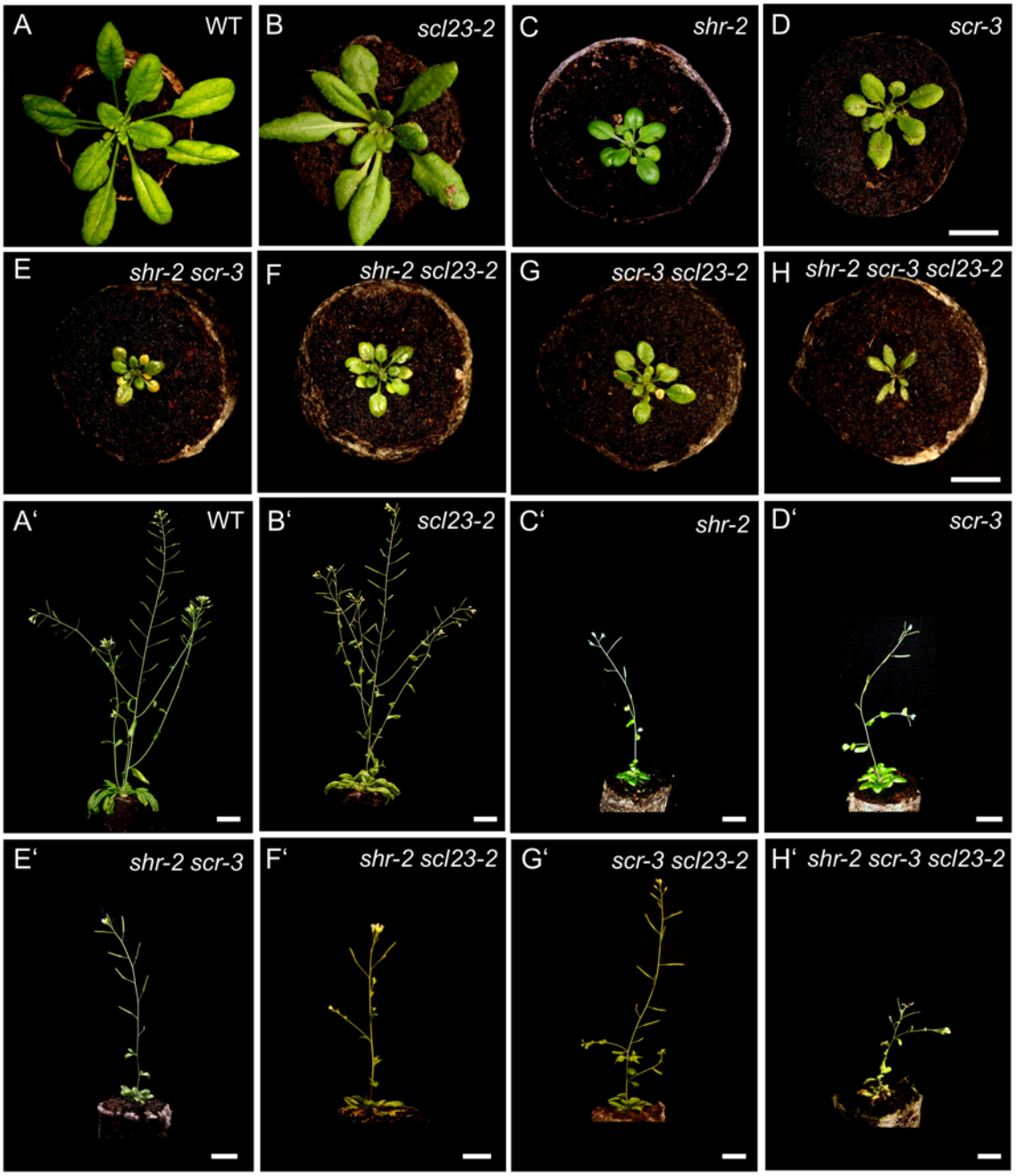

Suppl Fig. 14: Genetic combinations of *shr*, *scr* and *scl23*

(A-H) Top view of 21-day-old rosettes of WT **(A)**, *scl23-2* mutant **(B)**, *shr-2* mutant **(C)**, *scr-3* mutant **(D)**, *scr-3 shr-2* double mutant **(E)**, *scl23-2 shr-2* double mutant **(F)**, *scl23-2 scr-3* double mutant **(G)**, *scr-3 shr-2 scl23-2* triple mutant **(H)**. Scale bar represents 1 cm. **(A'-H')** Plant phenotypes of 6 weeks old WT **(A')**, *scl23-2* mutant **(B')**, *shr-2* mutant **(C')**, *scr-3* mutant **(D')**, *scr-3 shr-2* double mutant **(E')**, *scl23-2 shr-2* double mutant **(F')**, *scl23-2 scr-3* double mutant **(G')**, *scr-3 shr-2 scl23-2* triple mutant **(H')**. Scale bar represents: 2 cm **(A' and B')**, 1 cm **(C'-H')**.

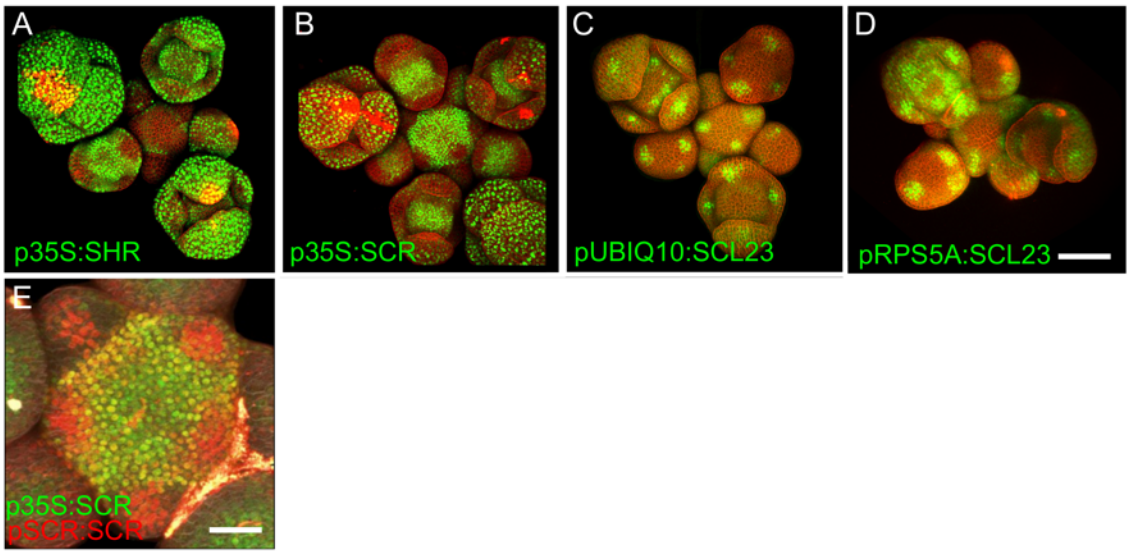

Suppl Fig. 15: The overexpression of SHR, SCR and SCL23 in the SAM

(A-D) Representative 3D projection of shoot apical meristems at 5 weeks after germination expressing *p35S:SHR-GFP* reporter (green) **(A)**, *p35S:SCR-GFP* reporter (green) **(B)**, *pUBIQ10:SCL23-mVenus* reporter (green) **(C)** and *pRPS5A:SCL23-mVenus* reporter (green) **(D)**. Cell walls were stained with PI (red). Scale bar represents 50 µm. **(E)** Top view of the inflorescence apex coexpressing the *p35S:SCR-GFP* reporter (green) and the *pSCR:SCR-RFP* reporter (red). Cell walls were stained with DAPI (gray). Scale bar represents 50 µm.

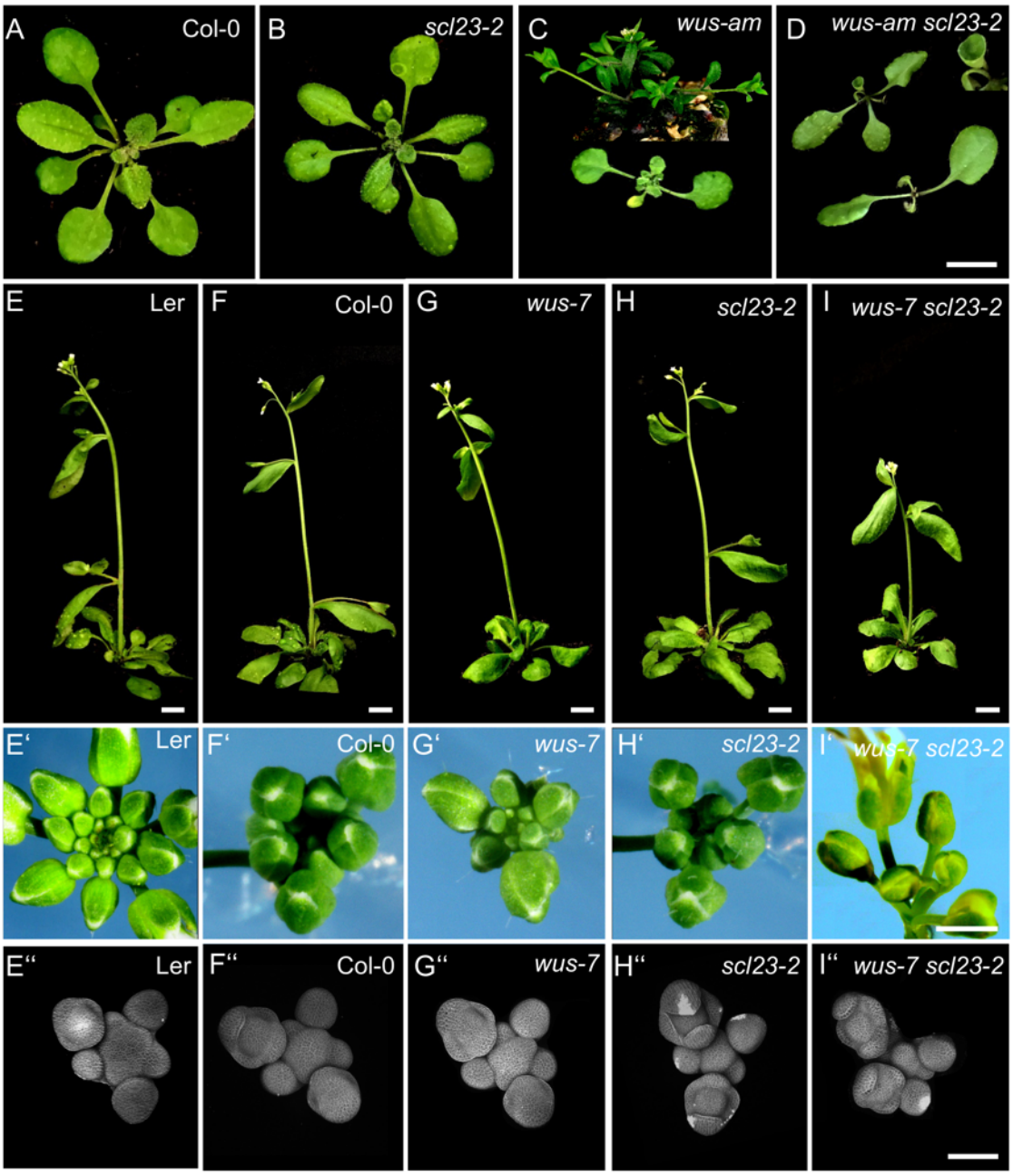

Suppl Fig. 16: WUS and SCL23 cooperatively control shoot stem cell homeostasis in the shoot apical meristem

(A-D) Top view of 21-day-old rosettes of Col-0 **(A)**, *scl23-2* mutant **(B)**, *wus-am* mutant **(C)** and *scl23-2 wus-am* double mutant **(D)**. Scale bar represents 1 cm. **(E-I)** plant phenotypes of 36 old L.er **(E)**, Col-0 **(F)**, *scl23-2* mutant **(G)**, *wus-7* mutant **(H)** and *scl23-2 wus-7* double mutant (I). Scale bar represents 1 cm. **(E'-I')** Top view of 35-day-old inflorescences of Ler **(E')**, Col-0(F'), *scl23-2* mutant **(G')**, *wus-7* mutant **(H')** and *scl23-2 wus-7* double mutant **(I')**. Scale bar represents 2 mm. **(E''-I'')** Representative 3D projection of shoot apical meristems at 5 weeks after germination from Ler **(E'')**, Col-0 **(F'')**, *scl23-2* mutant **(G'')**, *wus-7* mutant **(H'')** and *scl23-2 wus-7* double mutant (I''). Cell walls were stained with PI (gray). Scale bar represents 50 µm.

(A-D) Top view of 21-day-old rosettes of Col-0 **(A)**, *scl23-2* mutant **(B)**, *wus-am* mutant **(C)** and *scl23-2 wus-am* double mutant **(D)**. Scale bar represents 1 cm. **(E-I)** plant phenotypes of 36 old L.er **(E)**, Col-0 **(F)**, *scl23-2* mutant **(G)**, *wus-7* mutant **(H)** and *scl23-2 wus-7* double mutant **(I)**. Scale bar represents 1 cm. **(E'-I')** Top view of 35-day-old inflorescences of Ler **(E')**, Col-0(F'), *scl23-2* mutant **(G')**, *wus-7* mutant **(H')** and *scl23-2 wus-7* double mutant **(I')**. Scale bar represents 2 mm. **(E''-I'')** Representative 3D projection of shoot apical meristems at 5 weeks after germination from Ler **(E'')**, Col-0 **(F'')**, *scl23-2* mutant **(G'')**, *wus-7* mutant **(H'')** and *scl23-2 wus-7* double mutant (I''). Cell walls were stained with PI (gray). Scale bar represents 50 µm

1392

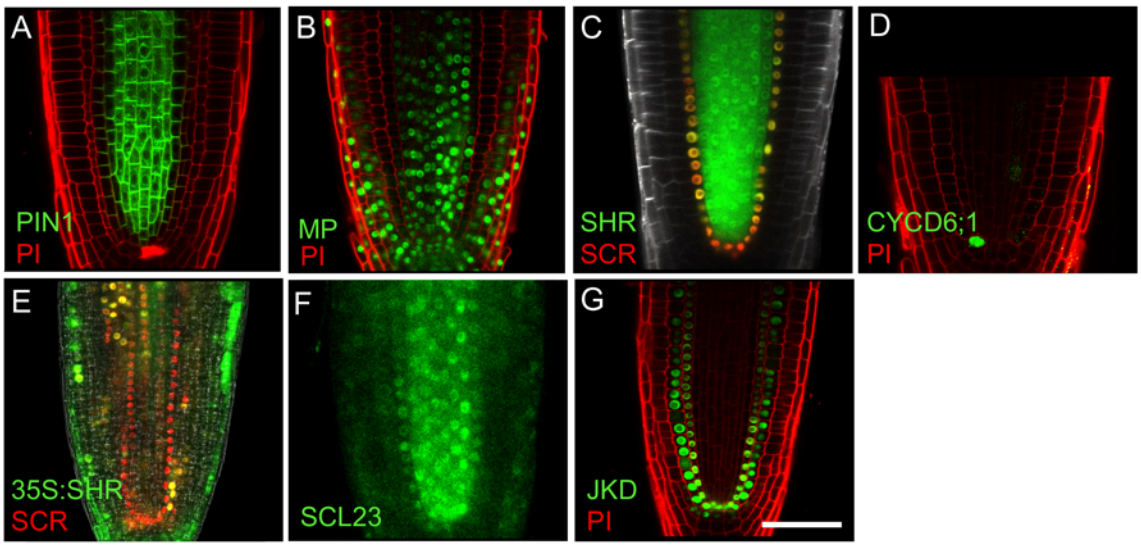

1393

1394 **Suppl Fig. 17: The overlapping expression pattern of PIN1, MP, SHR, SCR, *CYCD6;1*,**
1395 **SCL23 and JKD in the RAM**
1396 **(A-D)** Representative images of root apical meristem at 5 days after germination expressing,
1397 *pPIN1:PIN1-GFP* reporter (green) **(A)**, *pMP:MP-GFP* reporter (green) **(B)**, *pSHR:YFP-SHR*
1398 reporter (green) and *pSCR:SCR-RFP* reporters (red) **(C)**, *pCYCD6;1:GFP* reporter (green) **(D)**,
1399 *p35S:SHR-GFP* reporter (green) and *pSCR:SCR-RFP* reporter (red) **(E)**, *pSCL23:SCL23-YFP*
1400 reporter (green) **(F)** and *pJKD:JKD-YFP* reporter (green) **(G)**. Cell walls were stained with PI
1401 (red) in **(A) (B) (D) (G)** or DAPI (gray) in **(C)**. Scale bar represents 50 µm.
1402
1403
1404
1405

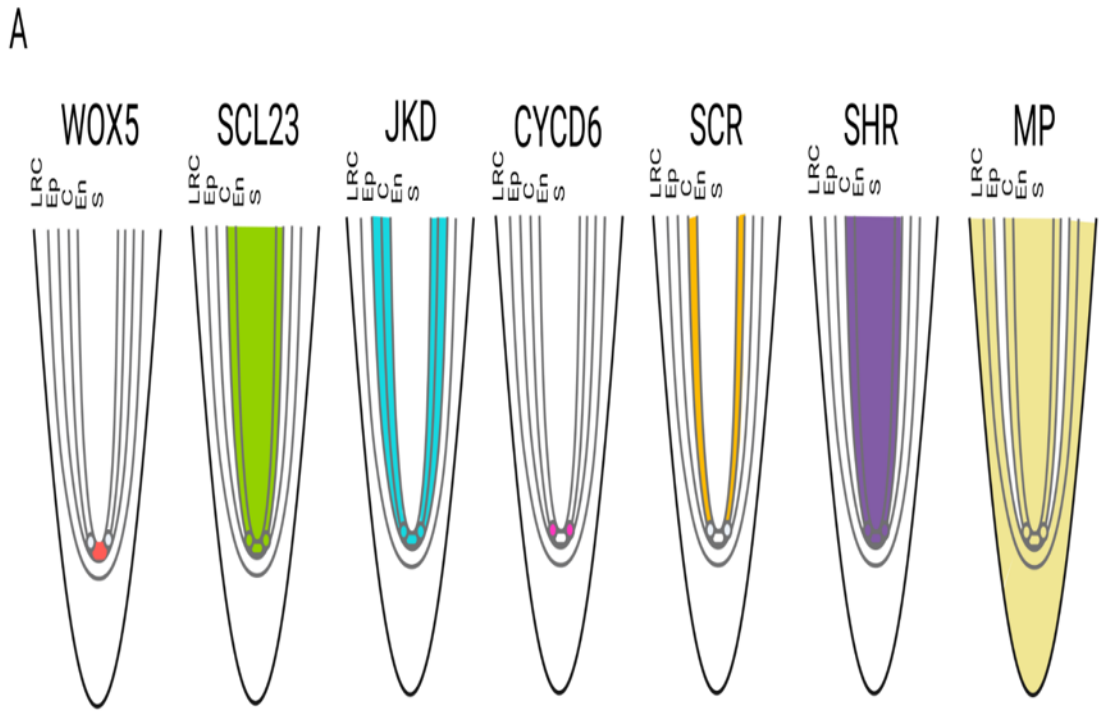

Suppl Fig. 18: Proposed model for SHR-SCR-SCL23-JKD regulatory network function in the RAM

(A) Schematic representation of observed expression patterns of *WOX5*, *SCL23*, *JKD, CYCD6, SCR, SHR* and *MP* showing typical expression domains in the RAM. **(B)** Schematic molecular models for SHR-SCR-SCL23-JKD gene regulatory network function in the RAM, genes with genetic and/or biochemical interactions are indicated. Lines with arrows depict positive regulation, and with bars depict negative regulation. Dashed lines with arrows depict intercellular protein movement. Overlap between circles describe protein–protein interactions. In the RAM, *SHR* is transcribed in the stele (S) in response to auxin-dependent activation of MP, and SHR protein moves to the CEI, where SHR activates *SCR*, *SCL23* and *JKD* expression. The multimeric protein complexes then induce formative division by activating expression of *CYCD6*. High levels of auxin in the CEI also contribute to *CYCD6* activation. In the QC, the SHR-SCR-SCL23-JKD protein complex positively regulates expression of *WOX5*. CEI= Cortex/endodermis initial, S=Stele, QC=Quiescent center.

1422 **Tab. 1: Enzymes used in this study**

Enzyme	Producer
BSA1 (ECORI)	Thermo Fisher Scientific, Braunschweig, Germany
Pfuμltra High-Fidelity DNA polymerase	Agilent, Santa Clara, USA
Phusion® High-Fidelity DNA Polymerase	Thermo Fisher Scientific, Braunschweig, Germany
T4-Ligase	Thermo Fisher Scientific, Braunschweig, Germany
Taq-DNA-Polymerase	Made in the lab according to (Pluthero, 1993)
Universal SYBR® Green Supermix	Bio-Rad

1423
1424

1425 **Tab. 2: Primers used for cloning**

Purpose	Primer	Sequence
SHR promoter cloning	EB-pSHR-F	AAAGGTCTCAACCTGAAGCAGAGCGTGGGGTTTC
	EB-pSHR-R	TTTGGTCTCATGTTTTTTAATGAATAAGAAAATGAATAGAAGAAAGGGGG
	EB-pSHR-BsaI-site-F	GTTCAAAAGTGGTCCCTTCTCTCTC
	EB-pSHR-BsaI-site-R	GAGAGAGAAGGGACCACTTTTGAAC
SHR CDS cloning	EB-SHR-CDS-F	AAAGGTCTCAGGCTTAATGGATACTCTCTTTAGACTAGTCAG
	EB-SHR-CDS-R	TTTGGTCTCACTGACGTTGGCCGCCACGCACTAG
SCR CDS cloning	EB-SCR-CDS-F	AAAGGTCTCAGGCTTAATGGCGGAATCCGGCGATTTC
	EB-SCR-CDS-R	TTTGGTCTCACTGAAGAACGAGGCGTCCAAGCTGAAG
	EB-SCR-CDS-BsaI-site-1-F	GCCATTATCAGGGACCTTATCC
	EB-SCR-CDS-BsaI-site-1-R	GGATAAGGTCCCTGATAATGGC
	EB-SCR-CDS-BsaI-site-2-F	GAAAATGGTATCTGCGTTTCAG
	EB-SCR-CDS-BsaI-site-2-R	CTGAAACGCAGATACCATTTTC
JKD CDS cloning	EB-JKD-CDS-F	AAAGGTCTCAGGCTTAATGCAGATGATTCCAGGAGATCC
	EB-JKD-CDS-R	TTTGGTCTCACTGAACCCAATGGAGCAAACCTTGCG
	EB-JKD-CDS-BsaI-site-F	GCCCTTGGTGACCTCACTGG
	EB-JKD-CDS-BsaI-site-R	CCAGTGAGGTCACCAAGGGC
SCL23 CDS cloning	EB-SCL23-F	AAAGGTCTCAGGCTTAATGACTACAAAACGCATAGACAG
	EB-SCL23-R	TTTGGTCTCACTGAATCGAACGGCTGAGATTTCC
MP CDS cloning	EB-MP-GG-F	AAAGGTCTCAGGCTTAATGATGGCTTCATTGTCTT
	EB-MP-GG-R	TTTGGTCTCACTGATGAAACAGAAGTCTTAAGATC
pSHR site-	EB-pSHRΔmAuxRE1-F	CTTTGTATCGAGCCAAACGAG

directed mutagen-esis	EB-pSHRΔmAuxRE1-R	CTCGTTTGGCTCGATACAAAG
	EB-pSHRΔmAuxRE2-F	TTCACATGGCTCTATGTTACTATG
	EB-pSHRΔmAuxRE1-R	CATAGTAACATAGAGCCATGTGAA
	EB-pSHRΔmAuxRE1-2-F	CTTTGTATCGAGCCAAACGAG
	EB-pSHRΔmAuxRE1-2-R	CTCGTTGTGCTCGATACAAAG
	EB-pSHRΔmAuxRE2-2-F	ATATTCACATGGGAGTATGTTACTATGTAAATG GTG ACC
	EB-pSHRΔmAuxRE2-2-R	GGTCACCATTTACATAGTAACATACTCCCATGTGA ATAT

1426

1427

1428 **Tab. 3: Primers used for qRT-PCR**

Primer name	Sequence
EB-RT-SHR-F	GATATCGAGTTTCCGACGGT
EB-RT-SHR-R	CGAAGCAAACCCTAAACCAT
EB-RT-SCR-F	GTAACCCAAATCTCGGTGCT
EB-RT-SCR-R	TTGCTGTTGTGGAGGAGAAG
EB-RT-JKD-F	ATCAACCTGGCACTCCAGA
EB-RT-JKD-R	GCAGATCTCGCACACGAAT
EB-RT-LFY-F	TGATGCTCTCTCCCAAGAAGA
EB-RT-LFY-R	CTTGACCTGCGTCCCAGTA
EB-SAND-F	AACTCTATGCAGCATTTGATCCACT
EB-SAND-R	TGATTGCATATCTTTATCGCCATC
EB-TIP41-F	GTGAAAACTGTTGGAGAGAAGCAA
EB-TIP41-R	TCAACTGGATACCCTTTCGCA

1429

1430

1431 **Tab. 4: Primers used for genotyping**

Primer name	Sequence
EB-scl23-2-LP	ATGACTACAAAACGCATAGACAG
EB-scl23-2-RP	TTTGGTCTCACTGAATCGAACGGC
LBb1.3	ATTTTGCCGATTTCGGAAC
mp-S319-LP	CCTGGAAACTGATGAGCTGAC
mp-S319-RP	CCTTCTTCACTCATCTGCTGG
LBb1.3	ATTTTGCCGATTTCGGAAC
jkd-4-F	GGATGAAAGCAATGCAAAACA
jkd-4-R	AATGTCGGGATGATGAACTCC
RB	TCAAACAGGATTTTCGCCTGCT
scr-4F	CTGCTTCACCTACTGTATGGG
scr-4R	GGGTCAGAGGAAGAGGAAGG
	Restriction enzyme: *Eco*57M which should not cut in the mutant
shr-2-R	AAATCGAACTTGCGAATTCCT
shr-2-L	CGCTCAACGAGCTCTCTTCT
shr-2ins	CAGCAAGACAAGATGGGTCA
wus-7-F	CCGACCAAGAAAGCGGCAACA
wus-7-R	AGACGTTCTTGCCCTGAATCTTT
	Restriction enzyme: *Xm*NI which should cut in the mutant

1432

1433

1434 **Tab. 5: Entry plasmids used in this study**

Name	Description	Backbone	Reference
pSHR	SHR promoter 2.5 Kb upstream from transcription start	pBlunt	This study
SHR CDS	SHR coding sequence	pGGC000	This study
SCL23 CDS	SCL23 coding sequence	pGGC000	This study
linker NLS (pGGD007)	NUCLEAR LOCALIZATION SIGNAL	pGGD000	Lampropoulos et al., 2013
mVenus (pRD43)	mVenus	pGGD000	Rebecca Burkhart
FLUC	Firefly luciferase	pGGC000	Greg Denay
mVenus (pRD42)	mVenus	pGGC000	Rebecca Burkhart
GUS (pGGC051)	E. coli ß-GLUCURONIDASE	pGGC000	Lampropoulos et al., 2013
MP CDS	MP coding sequence	pGGC000	This study
35S promoter (pGGA004)	Cauliflower mosaic virus 35S promoter	pGGA000	Lampropoulos et al., 2013
RPS5A promoter (pGGA012)	RIBOSOMAL PROTEIN 5A promoter	pGGA000	Lampropoulos et al., 2013
UBIQ10 promoter (pGGA006)	UBIQUITIN10 promoter	pGGA000	Lampropoulos et al., 2013
d-dummy (pGGD002)	d-dummy	pGGD000	Lampropoulos et al., 2013
tCLV3	CLV3 terminator 1257 bp downstream of transcription stop	pGGE000	Jenia Schlegel
UBQ10 terminator (pGGE009)	UBQ10 terminator	pGGE000	Lampropoulos et
BastaR (pGGF008)	pNOS:BastaR:tNOS	pGGF000	Lampropoulos et al., 2013
GR (pRD64)	Hormone-binding domain of the glucocorticoid receptor	pGGD000	Rebecca Burkhart
pCLV3	CLV3 promoter 1480 bp upstream from transcription start	pGGA000	Jenia Schlegel
omega-element (pGGB002)	Omega- element	pGGB000	Lampropoulos et al., 2013

1435

1436 **Tab. 6: Destination plasmids used in this study**

Name of construct	Promoter	N-Tag	CDS	C-Tag	Terminator	Resistance
pCLV3:SCL23-mVenus	pCLV3	Ω- element (pGGB002)	SCL23 CDS	mVenus	tCLV3	BastaR (pGGF008)
pRPS5A:SCL23-mVenus	pRPS5A	Ω- element (pGGB002)	SCL23 CDS	mVenus	tUBQ10 (pGGE009)	BastaR (pGGF008)
pUBIQ10:SCL23-mVenus	pUBIQ10	Ω- element (pGGB002)	SCL23 CDS	mVenus	tUBQ10 (pGGE009)	BastaR (pGGF008)
pUBIQ10:MP-GR	pUBIQ10	Ω- element (pGGB002)	MP CDS	GR	tUBQ10 (pGGE009)	BastaR (pGGF008)
p35S:GUS	p35S	Ω- element (pGGB002)	GUS	d-dummy (pGGD002)	tUBQ10 (pGGE009)	BastaR (pGGF008)
p35S:MP	p35S	Ω- element (pGGB002)	MP CDS	d-dummy (pGGD002)	tUBQ10 (pGGE009)	BastaR (pGGF008)
pSHR:mV-NLS	pSHR	Ω- element (pGGB002)	mVenus	linker NLS (pGGD007)	tUBQ10 (pGGE009)	BastaR (pGGF008)
pSHRΔmAuxRE1:mV-NLS	pSHRΔmAuxRE1	Ω- element (pGGB002)	mVenus	linker NLS (pGGD007)	tUBQ10 (pGGE009)	BastaR (pGGF008)
pSHRΔmAuxRE2:mV-NLS	pSHRΔmAuxRE2	Ω- element (pGGB002)	mVenus	linker NLS (pGGD007)	tUBQ10 (pGGE009)	BastaR (pGGF008)
pSHRΔmAuxRE1+2:mV-NLS	pSHRΔmAuxRE1+2	Ω- element (pGGB002)	mVenus	linker NLS (pGGD007)	tUBQ10 (pGGE009)	BastaR (pGGF008)
pSHRΔmAuxRE1-2:mV-NLS	pSHRΔmAuxRE1-2	Ω- element (pGGB002)	mVenus	linker NLS (pGGD007)	tUBQ10 (pGGE009)	BastaR (pGGF008)
pSHRΔmAuxRE2-2:mV-NLS	pSHRΔmAuxRE2-2	Ω- element (pGGB002)	mVenus	linker NLS (pGGD007)	tUBQ10 (pGGE009)	BastaR (pGGF008)
pSHRΔmAuxRE1-2+2-2:mV-NLS	pSHRΔmAuxRE1-2+2-2	Ω- element (pGGB002)	mVenus	linker NLS (pGGD007)	tUBQ10 (pGGE009)	BastaR (pGGF008)

1437

1438 **Tab. 7: Destination plasmids used for luciferase assay**

Name of construct	Promoter	N-Tag	CDS	C-Tag	Terminator	Resistance
pSHR:FLUC	pSHR	Ω- element (pGGB002)	FLUC	d-dummy (pGGD002)	tUBQ10 (pGGE009)	BastaR (pGGF008)
pSHRΔmAuxRE1:FLUC	pSHRΔmAuxRE1	Ω- element (pGGB002)	FLUC	d-dummy (pGGD002)	tUBQ10 (pGGE009)	BastaR (pGGF008)
pSHRΔmAuxRE2:FLUC	pSHRΔmAuxRE2	Ω- element (pGGB002)	FLUC	d-dummy (pGGD002)	tUBQ10 (pGGE009)	BastaR (pGGF008)
pSHRΔmAuxRE1+2:FLUC	pSHRΔmAuxRE1+2	Ω- element (pGGB002)	FLUC	d-dummy (pGGD002)	tUBQ10 (pGGE009)	BastaR (pGGF008)
pSHRΔmAuxRE1-2:FLUC	pSHRΔmAuxRE1-2	Ω- element (pGGB002)	FLUC	d-dummy (pGGD002)	tUBQ10 (pGGE009)	BastaR (pGGF008)
pSHRΔmAuxRE2-2:FLUC	pSHRΔmAuxRE2-2	Ω- element (pGGB002)	FLUC	d-dummy (pGGD002)	tUBQ10 (pGGE009)	BastaR (pGGF008)
pSHRΔmAuxRE1-2+2-2:FLUC	pSHRΔmAuxRE1-2+2-2	Ω- element (pGGB002)	FLUC	d-dummy (pGGD002)	tUBQ10 (pGGE009)	BastaR (pGGF008)

1439

1440 **Tab. 8: Mutants used in this study**

Lines	Reference
scr-4	Fukaki et al. 1998
jkd-4	Welch et al., 2007
scr-3	Fukaki et al., 1996b
shr-2	Nakajima et al. 2001
scl23-2	Lee et al.,2008
wus-7	Graf et al., 2010
wus-am	From Jan lohmann
mps-319	Schlereth et al., 2010
mp-b4149	Weijers et al., 2005
lfy-12	Huala and Sussex, 1992
clv3-9	Simon et al, 2003

1441

1442 **Tab. 9: Transgenic lines used in this study**

Lines	Plant Resistance	Reference
pSHR:mV-NLS	Basta	This study
pSHRΔmAuxRE1:mV-NLS	Basta	This study
pSHRΔmAuxRE2:mV-NLS	Basta	This study
pSHRΔmAuxRE1+2:mV-NLS	Basta	This study
pSHRΔmAuxRE1-2:mV-NLS	Basta	This study
pSHRΔmAuxRE2-2:mV-NLS	Basta	This study
pSHRΔmAuxRE1-2+2-2:mV-NLS	Basta	This study
pCLV3:SCL23-mVenus	Basta	This study
pRPS5A:SCL23-mVenus	Basta	This study
pUBIQ10:SCL23-mVenus	Basta	This study
pUBIQ10:MP-GR	Basta	This study
PlaCCI	Kanamycin	Desvoyes et al., 2020
pSHR:mScarlet-SHR	-	This study
pSHR:YFP-SHR	Basta	Long et al, 2017
pSCR:SCR-RFP	hyg	Long et al, 2017
pSCR:SCR-YFP	basta	Long et al, 2017
pSHR:SHR-YFP	Basta	Long et al, 2017
pJKD:mRFP-YFP	norf	Long et al, 2017
pJKD:JKD-YFP	Basta	Long et al, 2017
pSCL23:SCL23-YFP	Kanamycin	Long et al. 2015a
pSCL23:H2B-YFP	Kanamycin	Long et al. 2015a
pCYCD6;1:GFP	Basta	Sozzani et al., 2010
pSCR:H2B-YFP	Kanamycin	Heidstra et al, 2004
pPIN1:PIN1-GFP	Kanamycin	Benkova et al., 2003
pSHR:nTdTOMATO	-	Möller et al, 2017

pMP:MP-GFP	Kanamycin	Schlereth et al, 2010
pLFY:LFY-GFP	kanamycin	Wu et al., 2003
R2D2	kanamycin	Liao et al, 2015
pDR5v2:3xYFP-N7	Basta	Heisler et al, 2005
pWUS:3xVenus-NLS/pCLV3-mCherry-NLS	Kanamycin	Pfeiffer et al, 2016
pCYCD1,1-GFP	-	Forzani et al, 2014
pCYCD3,2-GFP	-	This study
pCYCD3,1-GFP	-	This study
pCYCD5,1-GFP	-	This study
pCYCD7,1-GFP	-	This study
pCYCD2,1-GFP	-	This study
pCYCD3,3-GFP	-	Forzani et al, 2014
pCYCB1;1:CYCB1;1-GFP	Kanamycin	Ubeda-Tomas et al., 2009

1443
1444
1445
1446
1447
1448
1449
1450
1451
1452
1453
1454
1455
1456
1457
1458

1459 **List of Figures**

1460 Fig. 10: The *shr* and *scr* mutant phenotypes

1461 Fig. 11: SHR and SCR functions modulate auxin signalling in the shoot apical meristem

1462 Fig. 12: Expression patterns of SHR and SCR in the shoot apical meristem

1463 Fig. 13: *In vivo* FRET–FLIM quantification of SHR-SCR association in the SAM

1464 Fig. 14: SHR regulates *SCR* expression in the SAM

1465 Fig. 15: JKD functions and expression pattern in the SAM

1466 Fig. 16: SHR regulates *CYCD6;1* expression in the SAM

1467 Fig. 17: SHR and SCR expressions respond to auxin

1468 Fig. 18: SHR and SCR act downstream of MP in the SAM

1469 Fig. 10: MP Regulates *SHR* expression in the SAM

1470 Fig. 11: SCL23, SCR and SHR proteins show spatially different patterns but perform similar
1471 functions in the SAM

1472 Fig. 12: SCL23 and WUS physically interact and are negatively regulated by CLV signalling

1473 Fig. 13: Proposed model for SHR-SCR-SCL23-JKD regulatory network function in the SAM

1474 **List of Supplementary Figures**

1475 Suppl Fig. 7: The *shr* and *scr* mutants phenotypes

1476 Suppl Fig. 8: The expression pattern of SHR and SCR in the shoot apical meristem

1477 Suppl Fig. 9: The expression pattern of JKD in *lfy* and *clv3* mutants shoot apical meristem

1478 Suppl Fig. 10: The colocalization of the expression patterns of SHR, SCR, JKD and CYCD6;1
1479 in the shoot apical meristem

1480 Suppl Fig. 11: *CYCD6;1* expression responds to auxin

1481 Suppl Fig. 12: The expression patterns of SHR, SCR, MP and PIN1 in the shoot apical
1482 meristem

1483 Suppl Fig. 7: *shr* mutant and *shr mps-319* double-mutant phenotypes

1484 Suppl Fig. 8: MP Regulates *SHR* expression in the shoot apical meristem

1485 Suppl Fig. 9: MP Regulates *SHR* expression in the shoot apical meristem

1486 Suppl Fig. 10: MP induces the expression of SHR *in planta*

1487 Suppl Fig. 11: The expression pattern of the different promoter versions of *SHR* in the root
1488 apical meristem

1489 Suppl Fig. 12: *LFY* act downstream of SHR in the shoot apical meristem

1490 Suppl Fig. 13: The expression pattern of SHR and SCR in *lfy* mutant shoot apical meristem

1491 Suppl Fig. 14: Genetic combinations of *shr*, *scr* and *scl23*

1492 Suppl Fig. 15: The overexpression of SHR, SCR and SCL23 in the SAM

1493 Suppl Fig. 16: WUS and SCL23 cooperatively control shoot stem cell homeostasis in the shoot
1494 apical meristem

1495 Suppl Fig. 17: The overlapping expression pattern of PIN1, MP, SHR, SCR, *CYCD6;1*, SCL23
1496 and JKD in the RAM

1497 Suppl Fig. 18: Proposed model for SHR-SCR-SCL23-JKD regulatory network function in the
1498 RAM

1499

1500

1501

1502

1503

1504

1505

1506

1507 **List of Tables**

1508 Tab. 10: Enzymes used in this study

1509 Tab. 11: Primers used for cloning

1510 Tab. 12: Primers used for qRT-PCR

1511 Tab. 13: Primers used for genotyping

1512 Tab. 14: Entry plasmids used in this study

1513 Tab. 15: Destination plasmids used in this study

1514 Tab. 16: Destination plasmids used for luciferase assay

1515 Tab. 17: Mutants used in this study

1516 Tab. 18: Transgenic lines used in this study

1517